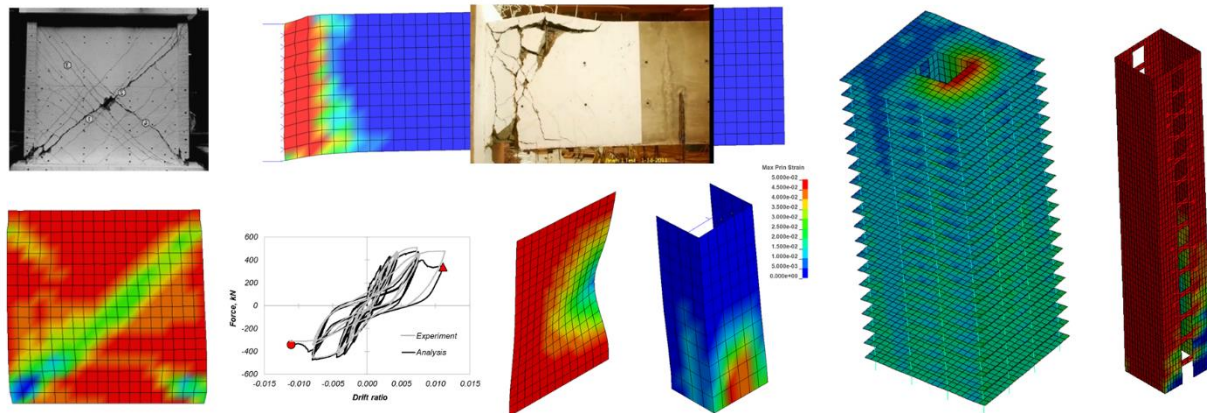


<https://www.school-of-earthquake-resilient-design.com/>

Los Angeles, California

Version 22.1 – June 20, 2022

Advanced and Practical Seismic Analysis of Reinforced Concrete Walls and Building Systems Using the *BTM-Shell Methodology* in the Program *FE-MultiPhys*



Marios Panagiotou, Ph.D., PE

Founder of the Online School of Earthquake Resilient Design

Senior Consultant at Nabih Youssef Associates

mp@school-of-earthquake-resilient-design.com

Ioannis Koutromanos, Ph.D.

Associate Professor of Structural Engineering, Virginia Tech

ikoutrom@vt.edu

Contents

| | | |
|-----|--|----|
| 1. | Abstract..... | 4 |
| 2. | Introduction | 5 |
| 3. | Behavior and Failure Modes of Reinforced Concrete Walls..... | 9 |
| 4. | Beam-Truss-Model for Reinforced Concrete Walls, Slabs, Beams, and Columns | 11 |
| 5. | Finite Element Program FE-MultiPhys and Installation | 18 |
| 6. | Overview of the Computational Framework | 19 |
| | Pre-Processing in LS-PrePost (.k file)..... | 20 |
| | FE-MultiPhys Input File (.txt file) | 20 |
| | Post-Processing in LS-PrePost (d3plot file) | 22 |
| 7. | Elements and Layered Sections Definition | 23 |
| | BTM-Shell Element (<i>SHEL2</i>) and Layered Sections | 23 |
| | Angle θ_d of Diagonals and Aspect Ratio of BTM-Shell Elements..... | 25 |
| | Nonlinear Out-of-Plane Shear Modeling in BTM-Shells..... | 30 |
| | Nonlinear Fiber-Section Three-Dimensional Beam Element (<i>BEAM2</i>) | 31 |
| 8. | Concrete, Reinforcing Steel, and Post-Tension Steel Materials..... | 33 |
| | Uniaxial Unconfined Concrete Material <i>CONWBET</i> | 33 |
| | Uniaxial Confined Concrete Material <i>CONWBET</i> | 34 |
| | Biaxial Concrete Material <i>CONWBET</i> for Diagonals | 35 |
| | Reinforcing Steel Material <i>STEELDR</i> | 37 |
| | Bilinear Steel Material (<i>STEEL01</i>) | 41 |
| | Modeling of Post-Tension via Initial Strain Material (<i>AUTOGENOUS</i>) | 42 |
| 9. | Mass and Body Forces..... | 43 |
| 10. | Load Pattern (<i>LOADPATTERN</i>) | 44 |
| 11. | Nonlinear Geometry Analysis Options | 45 |
| 12. | Solver Parameters for Modal and Nonlinear Analysis | 46 |

| | |
|---|----|
| Modal Analysis | 46 |
| Nonlinear Static Analysis | 46 |
| Nonlinear Dynamic Implicit Analysis and Transition from Static | 48 |
| Selection of Solver Parameters and Validation | 49 |
| 13. Parallel Processing..... | 50 |
| 14. Recorders and Post-Processing..... | 51 |
| Fiber Recorders - LAYSECTION | 51 |
| Section Cut Plane Recorder..... | 51 |
| BTM-Shells Post-Processing | 53 |
| 15. Nonlinear Cyclic Static Analysis Reinforced Concrete Wall Components | 55 |
| Case Study A: Diagonal Tension Failure of a Squat Barbel Wall | 55 |
| Case Study B: Diagonal Crushing of a C-Shape Wall Under Multiaxial Loading | 59 |
| Case Study C: Plastic Hinge Out-of-Plane Buckling of a Planar Wall..... | 63 |
| Case Study D: Bar Buckling and Shear Failure of a Full-Scale RC Special Moment Frame 4-ft Deep Beam Designed per ACI 318-08..... | 66 |
| Case Studies Presented in Deng et al. (2020) | 68 |
| 16. Nonlinear Dynamic Analysis of a 20-Story Core Wall Building (Case Study E)..... | 71 |
| 17. References..... | 77 |
| 18. Appendix A: Online Tutorials | 81 |

1. Abstract

This report presents a new computational framework ([downloads](#)) that enables the advanced and practical analysis of reinforced concrete structural wall (RCSW) components and building systems. Compared with analysis methods used in current performance-based seismic design (PBSD) and retrofit practice in U.S., this framework results in two major advancements: the accurate computation of various severe damage and failure modes of RCSWs and building systems that consider the nonlinear behavior of all structural components. The methodology uses the new BTM-shell element, based on the beam-truss-model (BTM), and the new finite-element program FE-MultiPhys that enables nonlinear (material and geometry) static and dynamic analysis as well as parallel processing (multi-threaded) for the efficient analysis of large (entire buildings) fully-nonlinear models. The program is compatible with the graphical pre- and post-processor LS-PrePost. The BTM has been extensively validated based on experimental testing results of reinforced (RC) walls, columns, beams, and slabs under cyclic static and dynamic load, and computes accurately various critical damage and failure modes of RC walls. The computational efficiency of the BTM for large structural systems was demonstrated in the 2010 Chile M8.8 earthquake collapse simulation of the Alto Rio building (281K nonlinear elements).

The BTM-shell is enhanced here using a recently published material model for cyclic behavior of reinforcing steel that enables efficient computation of bar buckling and rupture, as well as by considering the nonlinear out-of-plane shear behavior. The computational framework is validated using five case studies. Case Studies A to C analyze barbel, C-shape, and rectangular walls, respectively, that experienced the following failure modes during testing: (A) diagonal shear (tension); (B) diagonal crushing; and (C) out-of-plane plastic hinge buckling. Case Study D models the mixed bar buckling shear failure of the largest special moment frame RC beam that has been tested in U.S. Finally, Case Study E presents the nonlinear response history analysis for a Los Angeles-MCE-level ground motion of a 20-story RC-core wall building that models the nonlinear material behavior of 8480 elements of all components (walls, slabs, beams, and columns). The report serves as a User's Manual, providing detailed information, examples, and [online tutorials](#) on all input definitions (elements, materials, solvers, etc.) as well as on pre- and post-processing.

2. Introduction

Reinforced concrete structural walls, termed as walls from this point on, is the most common structural system for medium- and high-rise buildings in many regions of high seismic hazard (e.g. the West Coast of the U.S., Chile, and New Zealand). For new designs, code provisions include specific design and detailing requirements of walls aimed at ductile behavior. In U.S. practice, seismic analysis, and design of new RCSW buildings follow the prescriptive requirements of ASCE 7-16 for buildings with height within the limits described in Table 12.2-1 and paragraph 12.2.5.4. Buildings that exceed these limits follow the *Alternative Structural System* section (12.2.1.1), which leads to the use of PBSD guidelines for tall buildings. The seismic assessment and retrofit of existing RCSW buildings in U.S. follow the specific requirements of local jurisdictions (e.g., Non-ductile Concrete Ordinance of City of Los Angeles), which in general follow the requirements of ASCE 41.

In the U.S., seismic design practice following ASCE 7-16 uses linear response spectrum analysis and a response modification factor $R = 6$ for RCSW buildings up to 240 ft tall (*Seismic Design Category D and E*). Such methods of analysis and calculation of design forces result in significant underestimation of displacement and force demands [Panagiotou and Restrepo (2011), Panagiotou et al. (2011), Panagiotou (2017)] because of underestimation of higher mode effects, inadequate effective stiffness considerations, and inelastic displacement amplification.

Recently, ACI 318-19 introduced a design shear forces amplification factor based on Paulay and Priestley (1992) without any further capacity design considerations for the foundations as well as for the flexural design along the height of the building. For buildings that exceed this height limit, RCSW systems are permitted as an *Alternative Structural System* (Section 12.2.1.1) after submittal and approval by the local jurisdiction and independent structural design review of design criteria and nonlinear dynamic analysis data demonstrating less than 10% probability of collapse (for Risk Category II), conditioned on the occurrence of the risk-targeted maximum considered earthquake (MCE_R). The design criteria and nonlinear dynamic analysis of such buildings typically follow the PBSD guidelines of the Los Angeles Tall Buildings Structural Design Council (LATBSDC 2020) or of the PEER's Tall Buildings Initiative (TBI 2017). In PBSD practice, however, the collapse probability is not explicitly calculated. As discussed, next, the nonlinear analysis typically used in practice cannot support a realistic computation of severe damage and thus collapse.

As shown Figure 1, nonlinear dynamic analysis of RCSW in the U.S. uses fiber-section wall/beam elements to model vertical elements, while lump-plasticity (rotational or shear hinges) beam elements are used to model coupling and framing beams. For new designs, the shear behavior is modeled as equivalently linear, while in seismic assessments or retrofits the nonlinear behavior in shear of existing components is modeled with empirically calibrated nonlinear shear hinges. This type of modeling does not capture the major effects of flexure-shear interaction on the nonlinear response of RC components or severe damage development, deformation capacity, and failure. Per Lu and Panagiotou (2014), Figure 2 shows three examples of the inadequate assessment of the cyclic behavior of flanged RC walls modeled using Euler-Bernoulli fiber-section beam elements (plane-sections-remain-plane). In all three cases, the use of a fiber-section beam model resulted in overestimation of the stiffness and strength, as well as the hysteretic energy dissipation and deformation capacity.

Another major limitation of current analysis practice is the empirical calibration of plastic hinge lengths for RC walls and the use of a single fiber hinge per story; see Figure 1. Such modeling assumes that vertical tension and compression wall strains are constant (gauge length equal to story height), thus failing to compute peak local strains associated with severe damage (bar buckling and rupture, local crushing, and diagonal tension) in RC walls and initiation of strength and stiffness degradation described in subsequent sections.

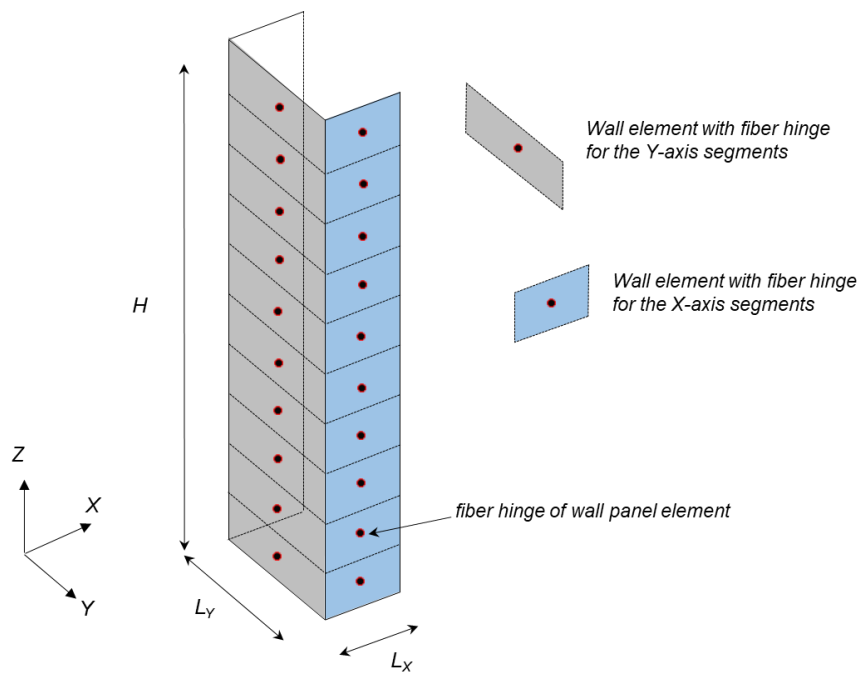


Figure 1. Modeling of 10-story C-shape wall, following current practice, using one wall panel element and fiber hinge per story and per wall segment.

To calibrate adequately the analysis procedures and design acceptance criteria in PBSD of RCSWs, the lack of experimental testing data for the following parameters is critical: (1) flanged walls and coupled core walls with the level of vertical loads; (2) shear stresses; and (3) appropriate boundary conditions for tall RC wall buildings. Noteworthy, the shear–stress acceptance criteria for wall plastic hinge regions used in today’s PBSD practice of tall RC core-wall buildings are largely based on uniaxial tests of barbel walls (Oesterle et al. 1976 and 1979, Kayebasawa 1998), which are fundamentally different (geometry, stress states, boundary conditions, etc.) compared to core-walls of tall buildings.

For example, a common critical condition in the PBSD of tall core-wall buildings is the occurrence of large shear stresses, near the factored limit of $\phi = 0.75 \times 10\sqrt{f'_{c,exp}}$ in the plastic hinge regions with concurrent significant inelastic strain demands. This level of average shear stress is at least 35% larger than the peak average shear stress, any C- or T-shape wall under bi-axial or multiaxial load has developed in testing. To the best of the author’s knowledge, the C-shape wall that has developed the peak average shear stress is the specimen TUB presented in Beyer et al. (2008). Furthermore, in current nonlinear analysis practice, the coupling of most slab regions [depending on the span length (LATBSDC 2020)] with walls and columns is ignored, together with the effects of vertical inertia and vertical component of the excitation.

To overcome all these limitations and improve the current state-of-practice of nonlinear analysis of RCSW buildings, developed herein is a new computational framework for the advanced and practical nonlinear analysis of RCSW components and buildings. The framework advances the state of nonlinear seismic analysis by capturing accurately all common severe damage and failure modes of RC walls, thus enabling the efficient fully nonlinear analysis of entire RC wall building systems. The methodology, based on the user-friendly newly developed BTM-shell element, uses an enhanced version of the beam-truss-method (BTM) coupled with a recently published material model for reinforcing steel that efficiently and accurately models bar buckling and rupture and the parallel processing capabilities of the program FE-MultiPhys (Koutromanos and Farhadi, 2018). The BTM-shell is further enhanced by including the out-of-plane nonlinear shear behavior of walls and slabs. The report serves as a User Manual providing detailed information, examples, and [online tutorials](#) on all input definitions (elements, materials, solvers, etc.), pre- and post-processing. The framework presented herein is validated based on five case studies, three of which are experimentally tested wall components experiencing different failure modes, the largest SMF RC beam ever tested in US, and the nonlinear dynamic analysis of a 20-story RC core-wall building.

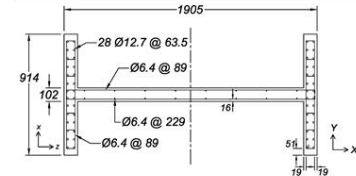
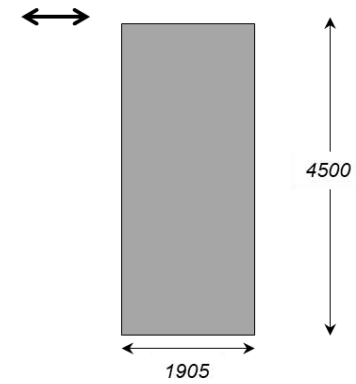
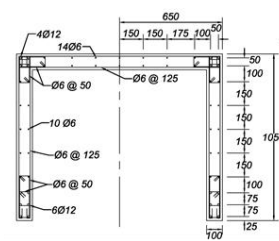
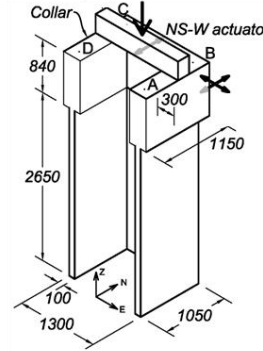
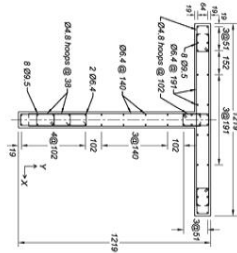
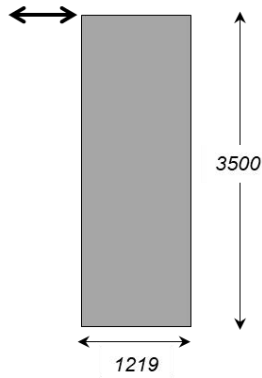
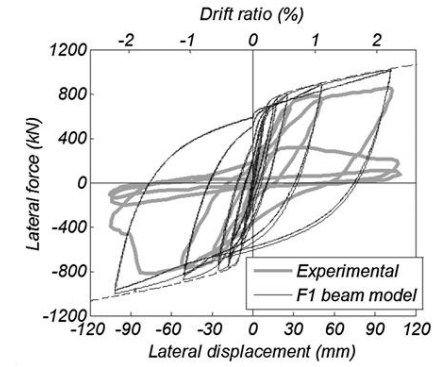
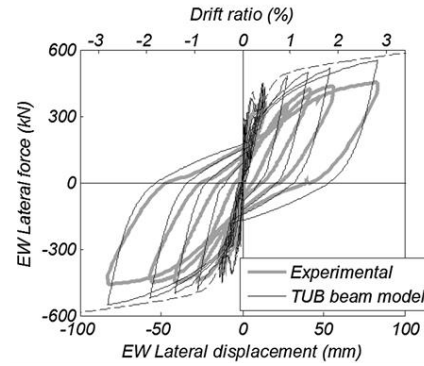
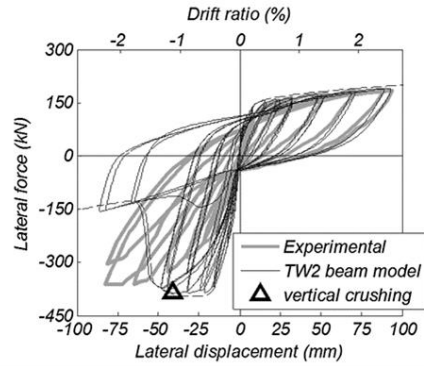
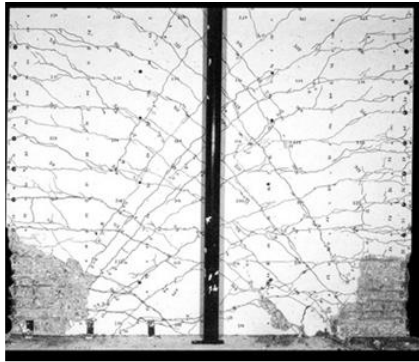


Figure 2. Three case studies of non-planar (flanged) RC walls per Lu and Panagiotou (2014), where the agreement between a fiber-section beam model versus the experimentally measured force-displacement behavior is poor.

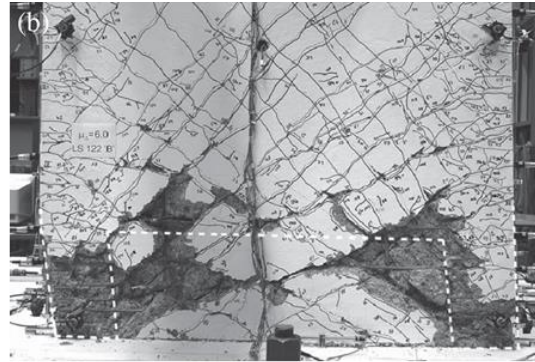
3. Behavior and Failure Modes of Reinforced Concrete Walls

Ductile RC structural walls experience a variety of failure modes depending on their characteristics and their design. This report only considers walls that develop their nominal flexural strength, M_n , before they fail in any of the modes described below. The case of walls that fail before developing M_n is outside the scope of this report. The nominal moment, M_n , follows the definition of Priestley et al. (2007), as the moment where steel reaches 1% tension strain or when the outer concrete fiber reaches 0.3% compression strain, whichever of the two occurs first. Figure 3 depicts some of the failure modes of RC walls observed in experimental testing or in earthquakes. The most common severe damage and failure modes are:

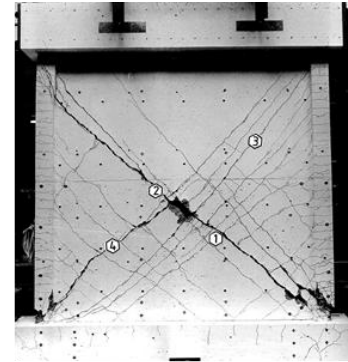
- (1) Bar buckling and rupture
- (2) Crushing of confined boundary elements
- (3) Unconfined web crushing
- (4) Diagonal tension
- (5) Global out-of-plane plastic hinge buckling
- (6) Vertical failure of boundary elements/web interface
- (7) Sliding



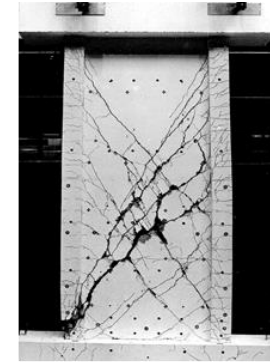
*Crushing of boundary element, hoops rupture
Dazio et. al. 2009*



Diagonal crushing, Beyer et al. 2008



Diagonal tension, Mestyanek 1986

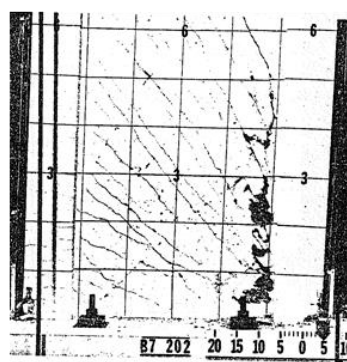


Dashti, 2017

Global out-of-plane plastic hinge buckling



*Elwood et al. 2011
Christchurch earthquake*



*Web crushing, barbel wall
Oesterle et al. 1979*



*Maffei and Yuen 2007
Kobe earthquake,
Diagonal Tension*



*Dazio et al. (2009b), L'Aquila earthquake
Web diagonal tension, flange buckling and crushing*



Figure 3. Severe damage and failure modes of RC structural walls experimentally tested and in earthquakes.

4. Beam-Truss-Model for Reinforced Concrete Walls, Slabs, Beams, and Columns

The beam-truss model (BTM) is a modeling methodology described in Lu, Panagiotou and Koutromanos (2014, 2016) and Lu and Panagiotou (2016) for RC components (walls, beams, and slabs). It has been developed over the past decade and implemented in the finite-element program OpenSees [Concretewbeta material and elements Truss2 and N4truss, Lu and Panagiotou (2013a, 2013b, 2016)]. As shown in Figure 4, the BTM approach discretizes each planar segment of a RC wall in a grid of vertical and horizontal nonlinear fiber-section beam elements, adding diagonal truss elements that model the diagonal compression field including biaxial effects. The efficacy of the BTM approach has been validated with experimental test results of components and structural systems. It computes with an excellent degree of accuracy the nonlinear cyclic response of RC walls, including critical damage and failure modes affected by flexure-shear interaction such as diagonal failures.

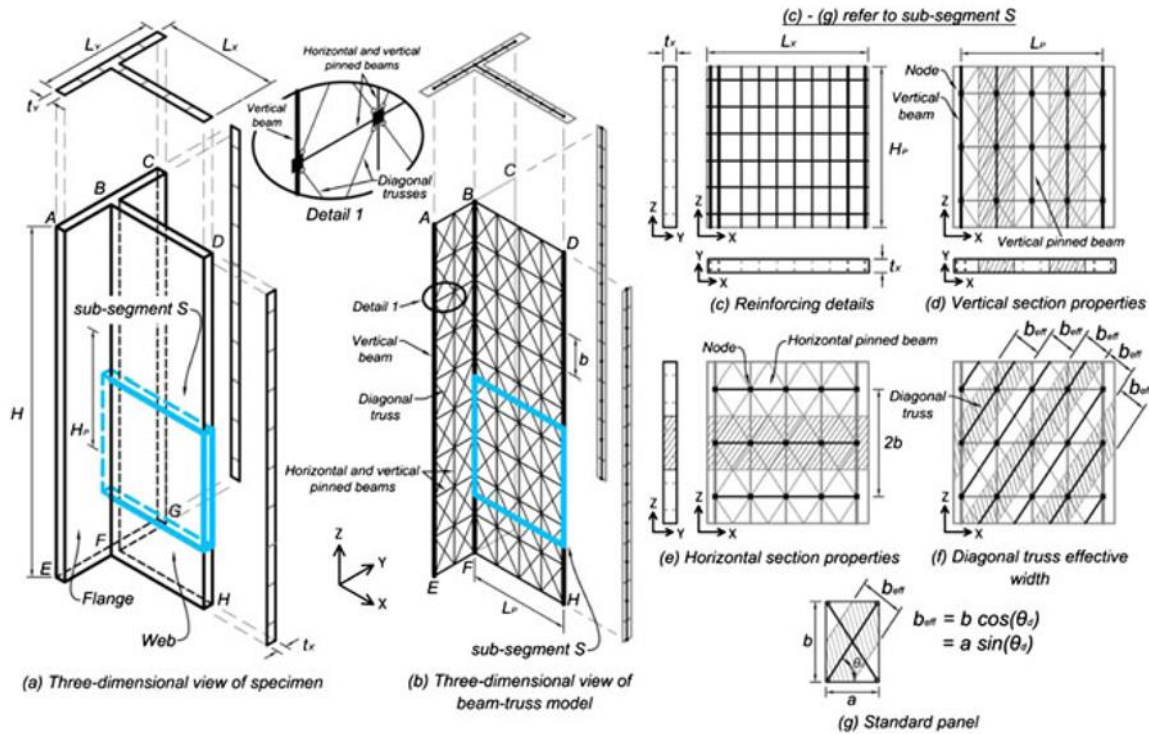


Figure 4. Schematic description of the BTM approach for a T-shape wall.

The precursor of the BTM is the nonlinear cyclic truss model for RC walls presented in Panagiotou et al. (2012). The truss model, which computes accurately the nonlinear cyclic response of rectangular uncoupled and coupled walls, was the first model of its kind that accounted for mesh-size effects and bi-axial behavior of concrete (weakening and softening of concrete diagonals due to transverse tension). Based on the truss model, Lu and Panagiotou (2014) introduced the first version of the BTM, which was validated by computing the cyclic test response and failure of three flanged walls two of which experienced diagonal crushing with a very good degree of accuracy. This first version of the BTM was significantly modified and enhanced by Lu, Koutromanos, and Panagiotou (2014, 2016) and by Lu and Panagiotou (2016) to capture the diagonal tension failure of planar, flanged, and coupled walls as follows: (a) the elimination of in-plane nonlinear flexural rigidity in the all beams; and (b) the explicit calculation of the angle of the diagonal truss elements based on ratio expected shear force demand to capacity.

The BTM-shell presented here is based on the BTM of Lu et al. (2014, 2016) validated by comparing the computed and experimentally measured responses of nine specimens subjected to uniaxial or multiaxial cyclic loading including cases of dynamic loading. The response, damage, and failure modes were determined by flexure-shear interaction and included many cases of diagonal failures after developing the flexural strength of the specimens. Selected cases from this study are shown in Figure 5. These studies also validated the BTM for coupled walls (Figure 6) and slabs (Figure 8).

Recently, Alvarez et al. (2019) developed an enhanced nonlinear cyclic truss model to capture the experimental test response of the landmark RC coupled wall specimens of Santhakumar (1974) and Paulay and Santhakumar (1976). The enhancements of the truss model included the modeling of dowel action of wall piers and coupling beams, as well as of the effect of strain penetration of horizontal and diagonal reinforcement of coupling beams. The model captured accurately the nonlinear cyclic response and failure of the two specimens, including the sliding shear failure of the coupling beams of the first specimen shown in Figure 6. Alvarez et al. (2020) enhanced the BTM by incorporating the effects of strain penetration of the reinforcement of coupling beams and modeled the tests of Santhakumar (1974, 1976). Recently, the BTM was extended and validated by Alvarez et al. (2020), based on four RC wall tests, to compute accurately the global out-of-plane plastic hinge buckling of four RC walls, see Figure 8.

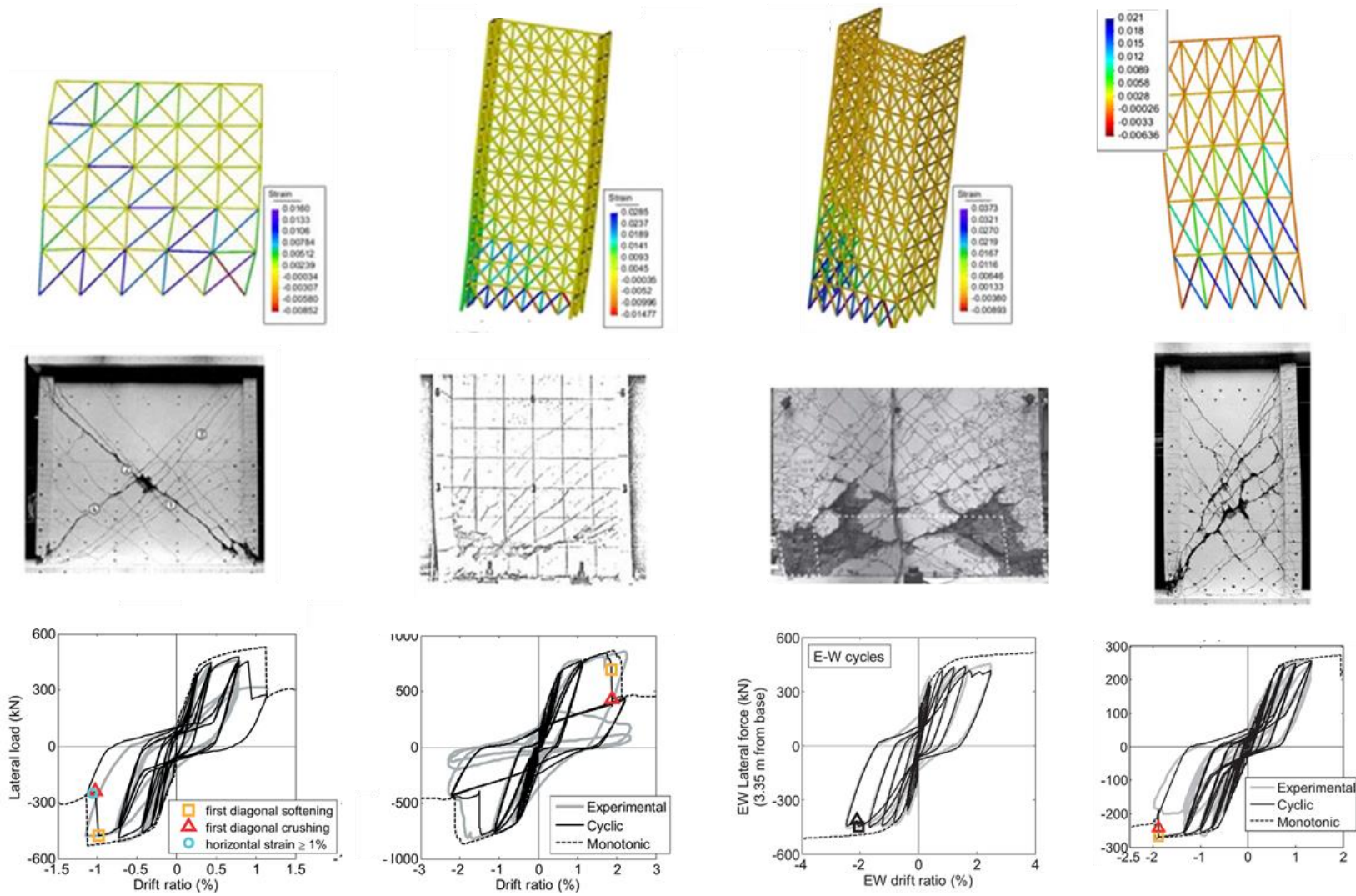


Figure 5. Validation of the BTM for individual walls and various failure modes determined by flexure shear interaction as presented in Lu, Panagiotou, and Koutromanos (2014, 2016). [Link to report](#)

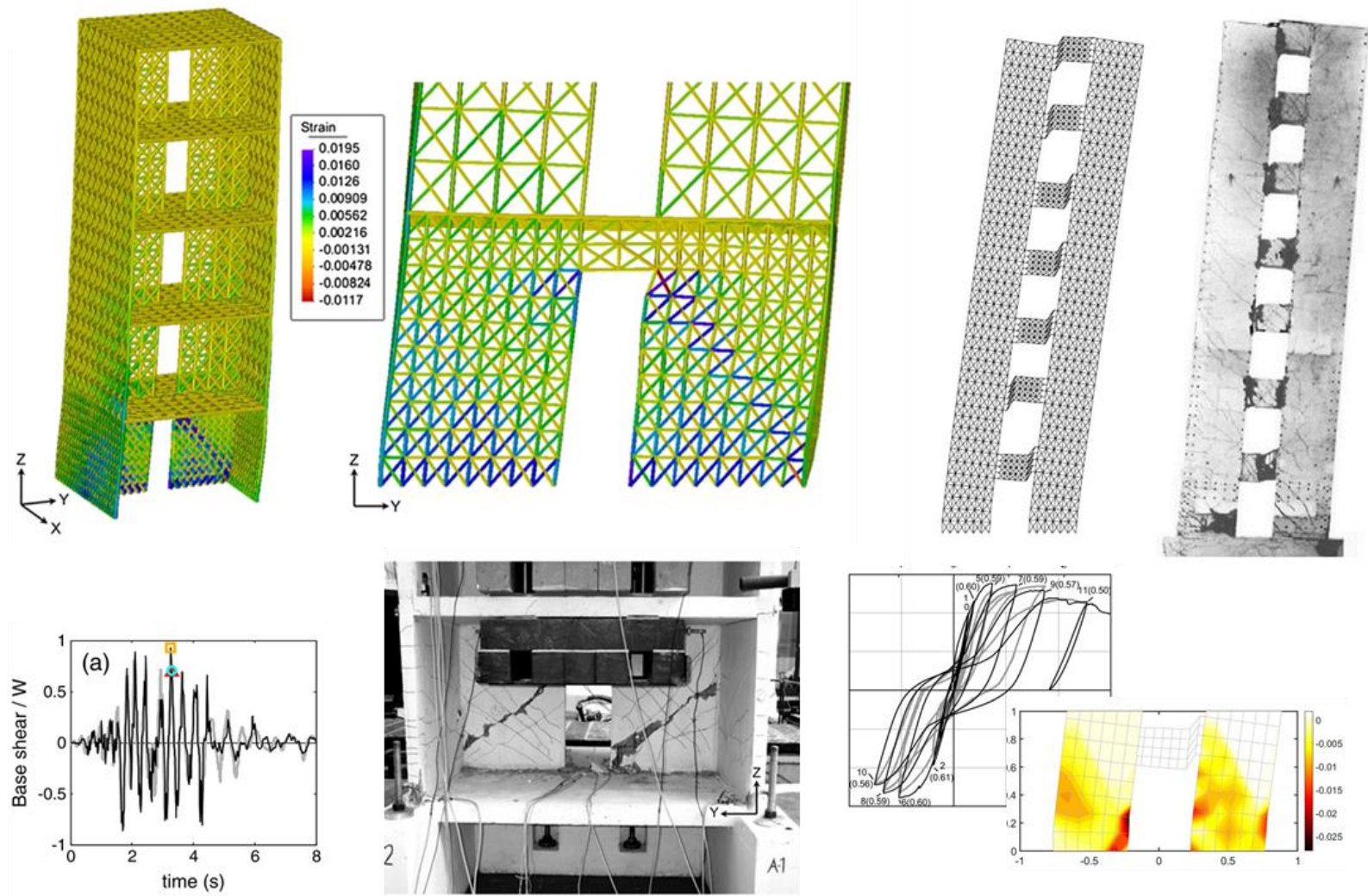


Figure 6. Validation of the BTM for coupled RC structural walls and various failure modes determined by flexure shear interaction as presented in Lu, Panagiotou, and Koutromanos (2014, 2016) and in Alvarez, Restrepo, and Panagiotou (2019).

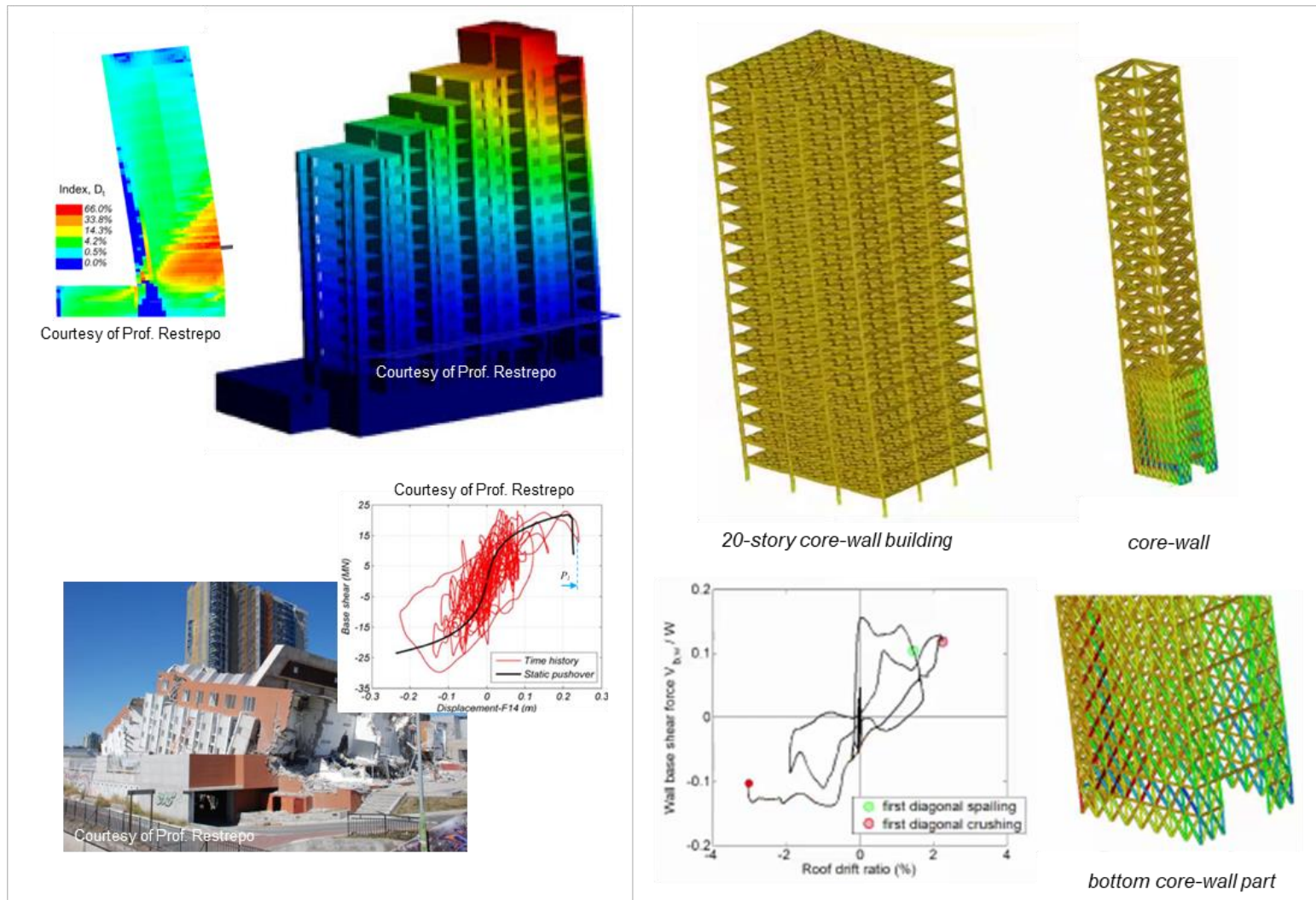


Figure 7. Collapse simulation of the Alto Rio building (Zhang et al. 2017) and seismic analysis of a 20-story RC core-wall building (Lu and Panagiotou 2015) using the BTM for the walls and the slabs.

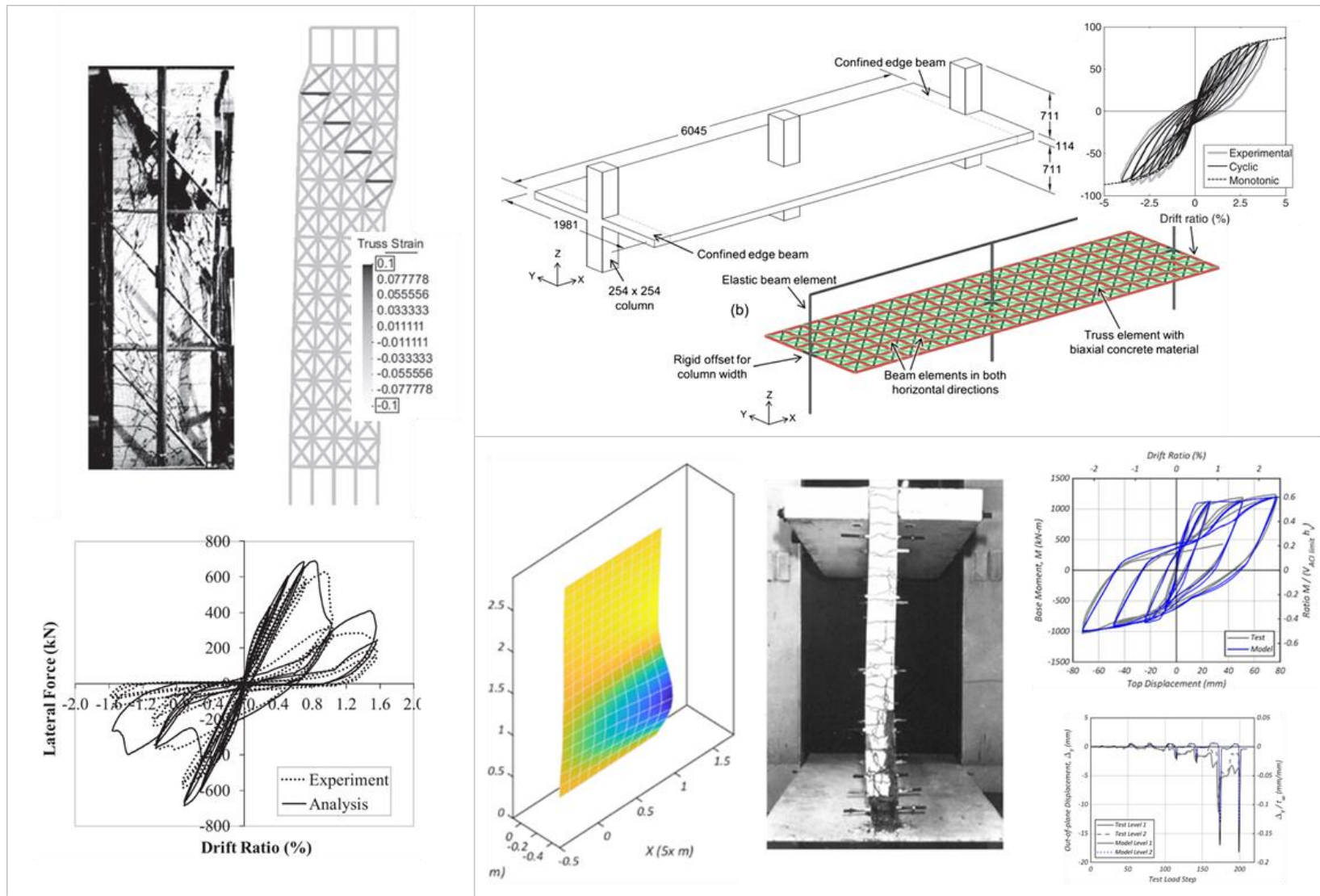


Figure 8. Truss model for shear critical columns (Moharrami et al. 2014); BTM for RC slabs (Lu, Panagiotou, and Koutromanos 2014, 2016); BTM for global out-of-plane plastic hinge buckling of C walls (Alvarez et al. 2020).

The BTM has also been used for the simulation by Zhang et al. (2017) of the Alto Rio building that collapsed during the 2010 Chile M8.8. earthquake. Shown in Figure 7 are simulations of 20-story tall RC core-wall buildings including nonlinear modeling of all the slabs per Lu and Panagiotou (2015). The BTM model of the Alto Rio building is the largest finite-element model (280K elements, 60K nodes) of a building subjected to earthquake ground shaking that we are aware of.

Finally, Moharrami et al. (2014) developed a two-dimensional cyclic truss model for shear-critical RC columns that was validated with the experimental test response of two column and one frame specimens. In addition, Moharrami et al. (2015) computed the diagonal and sliding shear failure of experimentally tested reinforced masonry walls as well as the shake-table test response of a two-story reinforced masonry specimen that experienced diagonal shear failure.

Links to Videos from BTM Simulations of RC Walls and Buildings in OpenSees

A list of links to videos from computational simulations using the BTM in OpenSees of RC wall components and buildings follows:

1. [Diagonal Tension Failure of a Barbel Squat Wall](#)
2. [Diagonal Compression Failure of a C-shape Wall under Multiaxial Loading](#)
3. [Diagonal Tension Failure of a 5-story Coupled Walls Slabs System under Triaxial Shaking](#)
4. [Seismic Analysis of a 20-story RC Core-wall Building](#)
5. [Seismic Analysis of a 20-story Rocking Core-wall Building](#)
6. [Seismic Analysis of a 20-story Base Isolated Rocking Core-wall Building](#)
7. [Out-of-Plane Plastic Hinge Buckling of four RC walls](#)

5. Finite Element Program FE-MultiPhys and Installation

FE-MultiPhys is a new finite-element program developed by Koutromanos and Farhadi (2018) that simulates nonlinear static and dynamic problems involving coupling of physical processes. The program enables parallel processing (multi-threaded) for analysis of large fully nonlinear structural building models. A concise theory and input manual of the program is found in Koutromanos and Farhadi (2018) which does not include any information on the BTM-shell, the *concretewbeta* material, or most of the information presented in this report.

Before FE-MultiPhys can be used, the latest Microsoft supported Visual C++ for Visual Studio 2015, 2017, and 2019 as well as Fortran Compiler (Update 5) redistributables need to be installed. These redistributables can be downloaded here:

[Visual C++ for Visual Studio](#)

[Fortran Compiler Redistributables](#)

6. Overview of the Computational Framework

The computational framework consists of the parts A, B, and C described below and shown in Figure 9. Figure 10 shows the four files that should be included in the analysis folder: (1) the .exe file of FE-MultiPhys; (2) the .k file, which is the pre-processing file developed in LSPP; (3) the input .txt file of FE-MultiPhys; and (4) the readingp.txt file, which includes only the name of the .txt input file. The three parts are:

- A. Pre-processing in LS-PrePost (.k file)
- B. FE-MultiPhys Input (.txt file)
- C. Post-processing in LS-PrePost (d3plot file)

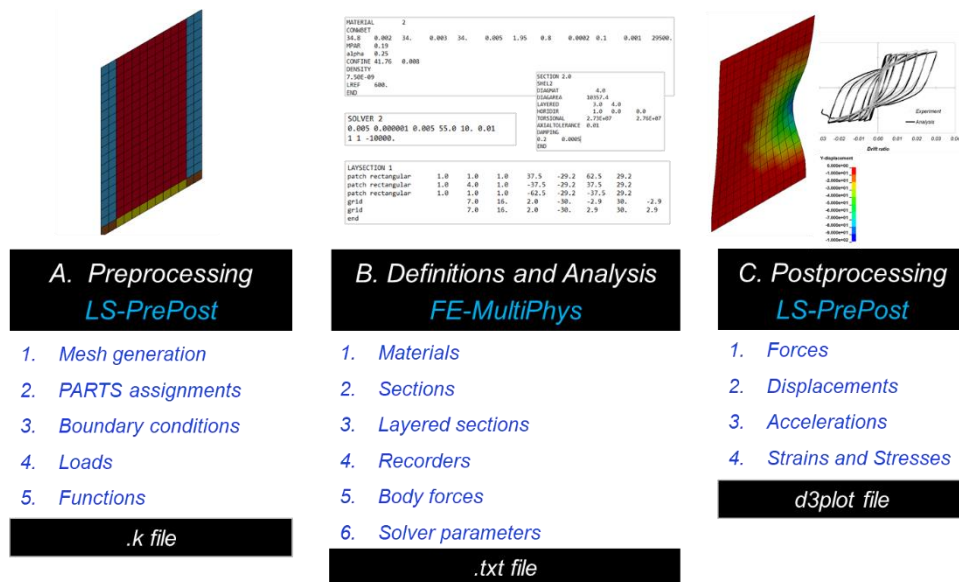


Figure 9. Overview of the computational framework.

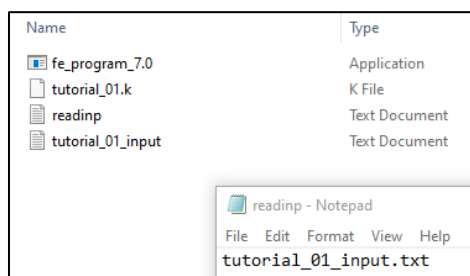


Figure 10. Four files included in the analysis folder of tutorial 01.

Pre-Processing in LS-PrePost (.k file)

Pre-processing is conducted in the program LS-PrePost of Ansys / LST ([download](#)); Version 4.7.10 of LS-PrePost was used here. The pre-processing consists of the following steps: (1) Mesh generation; (2) Assignment of mesh PARTS (Sections); (3) Assignment of boundary conditions; and (4) Assignment of loads and load functions. Step-by-step examples of pre-processing in LS-Prepost of FE-MultiPhys input specifically developed as part of this report are included in the [online tutorials](#) described in Section 18. The outcome of pre-processing in LSPP is a .k file ([.k file](#)).

FE-MultiPhys Input File (.txt file)

The FE-MultiPhys input file is a [txt file](#) that includes all the definitions of materials, element sections, fiber-sections (layered sections), analysis options, solver parameters, and recorders as described in Sections 7 to 14. The [online tutorials](#) present examples on development of FE-MultiPhys input files covering all necessary definitions. Figure 11 shows the overall layout and structure of the .txt input file, including ten blocks of commands and input parameters.

The first block is a single line of ten parameters. All these parameters except *ndim* (number of dimensions) and *ndof* (number of degrees-of-freedom per node) are set equal to zero. For three-dimensional analysis $ndim = 3$ and $ndof = 6$.

The second block includes up to five lines of commands and parameters described in different parts of this report. Blocks 03, 04, and 05 define the materials, element sections, and layered sections, respectively. Block number 06 calls the .k file. Blocks 07 and 08 define the section cuts and the body forces, respectively. The command **ENDDA** is a single command block before the last block that defines the **SOLVER** parameters.

It is noted that FE-MultiPhys enables the definition of all nodes and elements as well as loads and functions within the .txt file by adding the corresponding blocks of commands as described in Koutromanos and Farhadi (2018) without the need of pre-processing in LS-PrePost.

| COMMANDS AND INPUT PARAMETERS | | | | | | | | | | | COMMENTARY | |
|-------------------------------|-----------------|-------------|-------------|------------|------------|------------|------------|---------------|-------------|-------------|------------|----------------------------------|
| | 0 | 3 | 6 | 0 | 0 | 0 | 0 | 0 | 0 | 0 | ! | Block 01 - First line of input |
| ! | <i>nnod</i> | <i>ndim</i> | <i>ndof</i> | <i>ndT</i> | <i>ndM</i> | <i>ndC</i> | <i>nel</i> | <i>nnodpe</i> | <i>nmat</i> | <i>nsec</i> | ! | |
| | | | | | | | | | | | | |
| | NCPUS | nthreads | | | | | | | | | ! | Block 02 |
| | ACCUR | | | | | | | | | | ! | |
| | ITERLOG | | | | | | | | | | ! | |
| | ROTSSCALE | 0 | | | | | | | | | ! | |
| | STATICTODYNAMIC | | | | | | | | | | ! | |
| | | | | | | | | | | | | |
| | MATERIAL | 1 | | | | | | | | | ! | Block 03: Materials |
| | : | | | | | | | | | | ! | |
| | END | | | | | | | | | | ! | |
| | : | | | | | | | | | | ! | |
| | MATERIAL | N | | | | | | | | | ! | |
| | : | | | | | | | | | | ! | |
| | END | | | | | | | | | | ! | |
| | | | | | | | | | | | | |
| | SECTION | 1 | | | | | | | | | ! | Block 04: Sections |
| | : | | | | | | | | | | ! | |
| | END | | | | | | | | | | ! | |
| | : | | | | | | | | | | ! | |
| | SECTION | N | | | | | | | | | ! | |
| | : | | | | | | | | | | ! | |
| | END | | | | | | | | | | ! | |
| | | | | | | | | | | | | |
| | LAYSECTION | 1 | | | | | | | | | ! | Block 05: Layered sections |
| | : | | | | | | | | | | ! | |
| | END | | | | | | | | | | ! | |
| | : | | | | | | | | | | ! | |
| | LAYSECTION | N | | | | | | | | | ! | |
| | : | | | | | | | | | | ! | |
| | END | | | | | | | | | | ! | |
| | | | | | | | | | | | | |
| | LSPREPOST | | | | | | | | | | ! | Block 06: Connection with k file |
| | name.k | | | | | | | | | | ! | |
| | | | | | | | | | | | | |
| | CUTPLANE | | | | | | | | | | ! | Block 07: Section cuts |
| | : | | | | | | | | | | ! | |
| | END | | | | | | | | | | ! | |
| | CUTPLANE | | | | | | | | | | ! | |
| | : | | | | | | | | | | ! | |
| | END | | | | | | | | | | ! | |
| | | | | | | | | | | | | |
| | BODYF | 1 | | | | | | | | | ! | Block 08: Body forces |
| | : | | | | | | | | | | ! | |
| | END | | | | | | | | | | ! | |
| | BODYF | N | | | | | | | | | ! | |
| | : | | | | | | | | | | ! | |
| | END | | | | | | | | | | ! | |
| | | | | | | | | | | | | |
| | ENDDA | | | | | | | | | | ! | Block before last: End statement |
| | | | | | | | | | | | | |
| | SOLVER | | | | | | | | | | ! | Last Block: Solver parameters |
| | : | | | | | | | | | | ! | |

Figure 11. Layout of the txt input of FE-MultiPhys and description of main input blocks.

Post-Processing in LS-PrePost (d3plot file)

All the analysis post-processing—except the section plane cuts—is conducted in LSPP after loading the **d3plot file** generated in the analysis folder. Figure 12 shows the files generated in the analysis folder after the analysis is completed including the d3plot file.

| Name | Type |
|-----------------------|---------------|
| fe_program_7.0 | Application |
| tutorial_01.k | K File |
| readinp | Text Document |
| tutorial_01_input | Text Document |
| d3plot | File |
| information | Text Document |
| tutorial_01_inputrest | File |
| bndout | File |
| d3plot01 | File |
| iterlog | Text Document |
| iterlog2 | Text Document |
| messagelog | Text Document |
| spcforc | File |

Figure 12. Analysis folder files of tutorial 01 example (completed analysis).

7. Elements and Layered Sections Definition

BTM-Shell Element (**SHEL2**) and Layered Sections

The BTM-shell element is called by using the **SHEL2** command in FE-Multiphys. The relation between a four-node shell element, defined in pre-processing, and the BTM-shell macroelement, developed internally in FE-MultiPhys, is shown in Figure 13. The BTM-shell consists of six elements: four fiber-section nonlinear three-dimensional beam elements (**BEAM2**), two verticals and two horizontals, and two diagonal truss elements that account for the strain field normal to their direction. The BTM-shell is a user-friendly implementation of the BTM developed and presented in Lu. et al. (2014, 2016) with enhancements described below.

Figure 14 shows how the properties of the six internal elements of a BTM-shell are determined using as an example the RC panel shown in Figure 14(a). A single BTM-shell element is used to model the panel region of length ℓ (X- axis), height h (Z-axis), and thickness t (Y-axis). The BTM-shell modeling this region is shown in Figure 14(b). Each fiber-section of the four beams represents half of the panel's section in the corresponding direction (vertical or horizontal).

To achieve a pure truss in-plane-behavior, the patch used for the concrete fibers have multiple divisions along the thickness t of the shell element (y-local-axis), while a single division is used in the other direction (z-local-axis) of the section (1×4 patch shown in Figure 14). The steel fibers are modeled in their exact location along the thickness t (y-local-axis of the section) where they are placed with a small eccentricity ($e = 2$ mm default value) in other direction of the section (z-local-axis). This eccentricity is used to ensure a small non-zero in plane flexural rigidity, which is needed for numerical stability under nonlinear geometry analysis (*P-delta* or *Corotational*).

The area of the diagonal truss elements $A_d = w_d t$ is calculated according to Lu et al. (2016), where w_d is the width of the diagonal concrete strut, which in turn depends on the dimensions of the element and the angle θ_d of the diagonals. The calculation of the θ_d is discussed in next section; it is an essential part of developing an accurate BTM of any RC component and determines the aspect ratio of the shell elements used in the mesh generation.

Figure 15 shows a definition example of a **SHEL2** section in FE-Multiphys including twelve lines of commands and parameters. The number following the command **DIAGMAT** describes the material id number used in the diagonal truss elements. The number following the command **DIAGAREA** is the area of each of the two diagonals. The two numbers following the command

LAYERED describe the ID of the layered sections used in the horizontal and vertical beams, respectively. The three numbers following the command **HORIDIR** describe the orientation vector (in global coordinates) of the direction of the horizontal beams. The number following the command **TORSIONAL** is the torsional rigidity GJ used for each of the horizontal and vertical beams. Based on Lu et al. (2016), a value of $GL = 0.02GJ_g$ is recommended, where GJ_g is the gross section torsional rigidity of the beam section. The command **ROTMASS** activates the modeling of the rotatory mass. The command **PDELTA** activates the P-delta nonlinear geometry analysis option which overwrites the corotational formulation in case the latter has been activated in the beginning of the input file (block 02). Finally, the two numbers below the command **DAMPING** are the mass and stiffness coefficients, respectively, of the initial stiffness and mass proportional Rayleigh damping.

Figure 16 shows a definition example of a fiber section (**LAYSECTION**) including seven lines of commands and parameters. The second line defines the rectangular patch layout of the concrete fibers including the concrete material ID and the divisions of the patch along the local y and z axes as well as the local coordinates $[(y_1 \ z_1) \text{ and } (y_3 \ z_3)]$ of the two anti-diagonal corners of the rectangular patch. Lines 3 and 4 describe the two grids of steel fibers used where A_{sf} is the area of each steel fiber. Each grid of steel fibers is defined based on the coordinates of the two end points: e.g. (y_{s1}, z_{s1}) and (y_{s2}, z_{s2}) for the first grid. The number of steel fibers used in each grid is also required. The recording command **RECORD** is discussed later in this report.

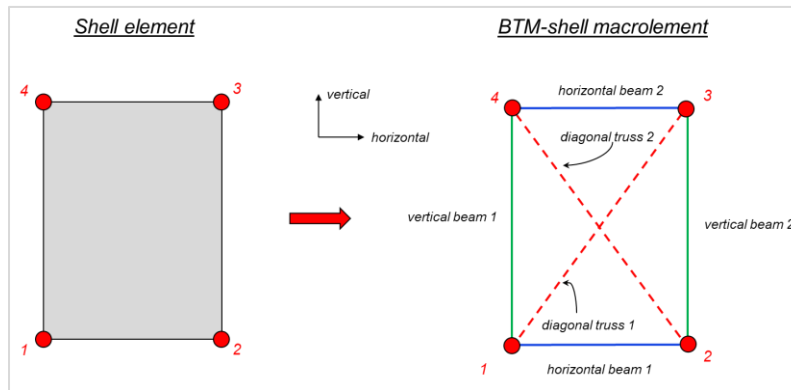


Figure 13. Relation between a four-node shell-element as defined in pre-processing and the BTM-shell macroelement used in FE-MultiPhys.

Angle θ_d of Diagonals and Aspect Ratio of BTM-Shell Elements

The angle of θ_d is a critical parameter of the BTM methodology and determines the nonlinear response including the shear strength, the extent of flexure-shear interaction, and inelastic response. The θ_d determines the aspect ratio of the BTM-shell elements and thus the layout of the mesh. For solid walls (without openings), θ_d is calculated according to Lu et al. (2016) using Eq. (1a) where V_{\max} is the peak shear force demand, and V_s is the shear capacity considering the contribution of the shear reinforcement only for 45° plastic truss theory (e.g., V_s of ACI 318). In Eq. (1b), V_s is replaced with $f_{yt}\rho_t t d$, where f_{yt} is the yield strength of shear (transverse) reinforcement, ρ_t the shear reinforcement ratio, t the thickness of the section, and d the shear depth of the section (distance from extreme compression fiber to the outer reinforcement in tension). This relation describes that the peak shear force demand is resisted entirely from the shear reinforcement (concrete shear resistance $V_c = 0$) forming an up to 65° angle of the diagonal compression concrete struts. Equations (1c) and (1d) are equivalent expressions in terms of the average shear stress τ_{\max} and the shear stress ratio $r_{\max} = \tau_{\max} / \sqrt{f_c}$ where f_c is the concrete compressive strength (expected) in psi. Figure 17 plots the calculated θ_d versus ρ_t for four levels of T_{\max} and for $f_{yt} = 70$ ksi, $f_c = 7$ ksi.

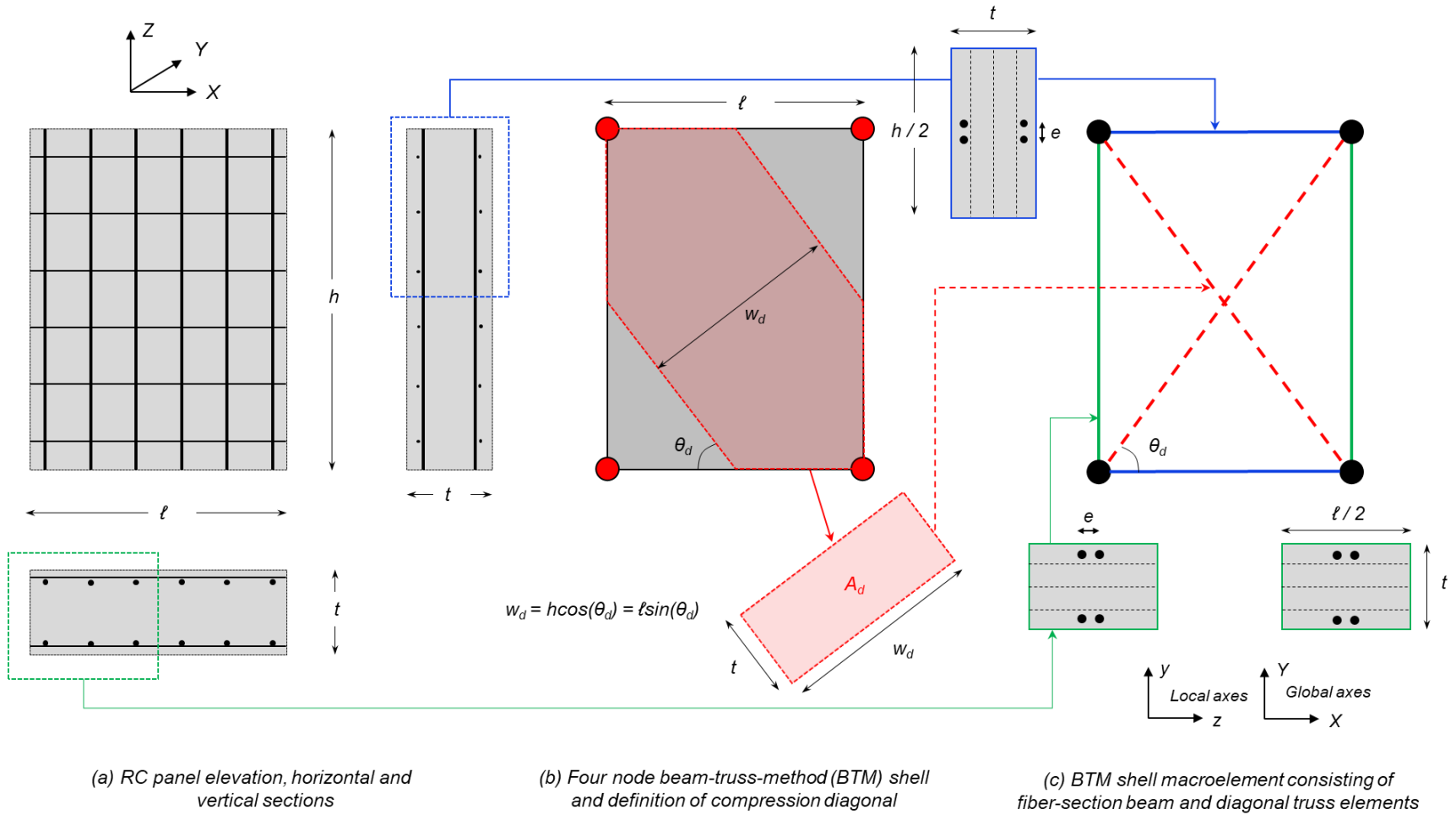


Figure 14. Description of the BTM-Shell macroelement and determination of properties of the six elements that compose it.

| CALL OF FUNCTIONS in the txt input file | VALUES OF FUCNTION PARAMETERS | | | COMMENTARY | |
|---|----------------------------------|---|---|------------|--|
| SECTION | # | | | ! | Section number corresponding to the PART number defined in LS prepost |
| SHEL2 | | | | ! | SHEL2 is the SECTION description of a BTM shell |
| DIAGMAT | # | | | ! | Material ID number used for the diagonal truss elements |
| DIAGAREA | # | | | ! | Area of each of the two diagonals |
| LAYERED | # | # | | ! | Layred sections ID of horizontal and vertical beams |
| HORIDIR | # | # | # | ! | Direction vector for horizontal beams |
| TORSIONAL | # | | | ! | Torsional rigidity GJ of each of the four beams of the BTM-shell |
| ROTMASS | | | | ! | Consideration of rotational mass |
| PDELTA | | | | ! | Activation of PDELTA for the elements using this SECTION |
| DAMPING | | | | | |
| # | # | | | ! | Mass and stiffness Rayleigh damping coefficients |
| END | | | | | |
| | | | | | |
| SECTION | 2 | | | ! | Section number is set equal to 2 |
| SHEL2 | | | | ! | SHEL2 is the SECTION description of a BTM shell |
| DIAGMAT | 3 | | | ! | Diagonals use material ID number 3 |
| DIAGAREA | 1400000 | | | ! | The area of each diagonal is 1400000 |
| LAYERED | 3 | 4 | | ! | The horizontal and vertical beams use the LAYRED sections number 3 and 4, respectively |
| HORIDIR | 1 | 0 | 0 | ! | The horizontal beams are parallel to the X global axis (as defined in LS prepost) |
| TORSIONAL | 4.50E+13 | | | ! | The torsional rigidity of each of the four beams is GJ=4.5E+13 |
| ROTMASS | | | | ! | Consideration of rotational mass |
| PDELTA | | | | ! | Activation of PDELTA for the elements using SECTION 2 |
| DAMPING | | | | | |
| 0.025 | 0.0003 | | | ! | Mass and stiffness proportional Rayleigh damping with coefficients 0.025 (mass) and 0.0003 (stiffness) |
| END | | | | | |
| | | | | | |

Figure 15. Definition of a BTM-Shell SECTION in a txt input file.

| | CALL OF FUNCTIONS in the bt input file | VALUES OF FUNCTION PARAMETERS | | | | | | | | Commentary | | |
|--------|--|-------------------------------|--------------|------------------------|------------------|------|------|------|-----|------------|--|--|
| Line 1 | LAYSECTION | # | | | | | | | | ! | ID number of LAYSECTION | |
| Line 2 | patch | rectangular | material ID | y axis divisions | z axis divisions | y1 | z1 | y3 | z3 | ! | concrete patch | |
| Line 3 | grid | steel material ID | Asf | number of steel fibers | ys1 | zs1 | ys2 | zs2 | | ! | first grid of steel fibers | |
| Line 4 | grid | steel material ID | Asf | number of steel fibers | ys3 | zs3 | ys4 | zs4 | | ! | second grid of steel fibers | |
| Line 5 | RECORD | y coordinate | z coordinate | material ID | | | | | | ! | first recorded fiber | |
| Line 6 | RECORD | y coordinate | z coordinate | material ID | | | | | | ! | second recorded fiber | |
| Line 7 | end | | | | | | | | | | | |
| Line 1 | LAYSECTION | 4 | | | | | | | | ! | LAYSECTION of ID 4 | |
| Line 2 | patch | rectangular | 1 | 4 | 1 | -610 | -375 | 610 | 375 | ! | 4 x 1 concrete patch with material ID 1 | |
| Line 3 | grid | 2 | 2288 | 2 | -549 | -1.0 | 549 | -1.0 | | ! | 1 st grid of 2 steel fibers of material 2 | |
| Line 4 | grid | 2 | 2288 | 2 | -549 | 1.0 | 549 | 1.0 | | ! | 2 nd grid of 2 steel fibers of material 2 | |
| Line 5 | RECORD | 20 | 30 | 1 | | | | | | ! | recorded fiber closest to (20, 30) of material 1 | |
| Line 6 | RECORD | -10 | -40 | 2 | | | | | | ! | recorded fiber closest to (-10, 40) of material 1 | |
| Line 7 | end | | | | | | | | | | | |

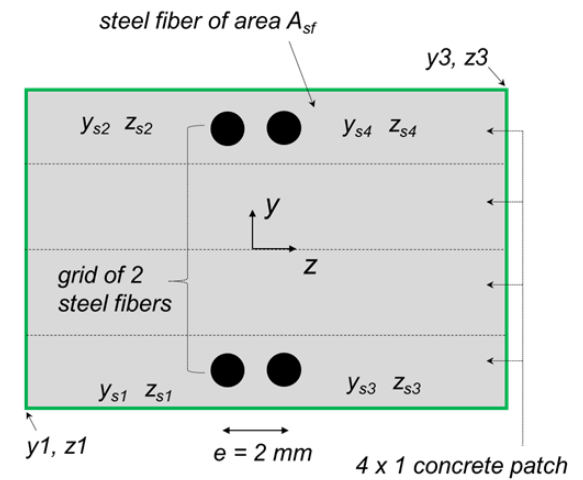


Figure 16. Definition of a layered section (fiber-section used in BTM-shell or nonlinear beam).

$$45^\circ \leq \theta_d = \tan^{-1} \left(\frac{V_{\max}}{V_s} \right) \leq 65^\circ \quad (1a)$$

$$45^\circ \leq \theta_d = \tan^{-1} \left(\frac{V_{\max}}{f_{yt} \rho_t t d} \right) \leq 65^\circ \quad (1b)$$

$$45^\circ \leq \theta_d = \tan^{-1} \left(\frac{\tau_{\max}}{f_{yt} \rho_t} \right) \leq 65^\circ \quad (1c)$$

$$45^\circ \leq \theta_d = \tan^{-1} \left(\frac{r_{\max} \sqrt{f'_c}}{f_{yt} \rho_t} \right) \leq 65^\circ \quad (1d)$$

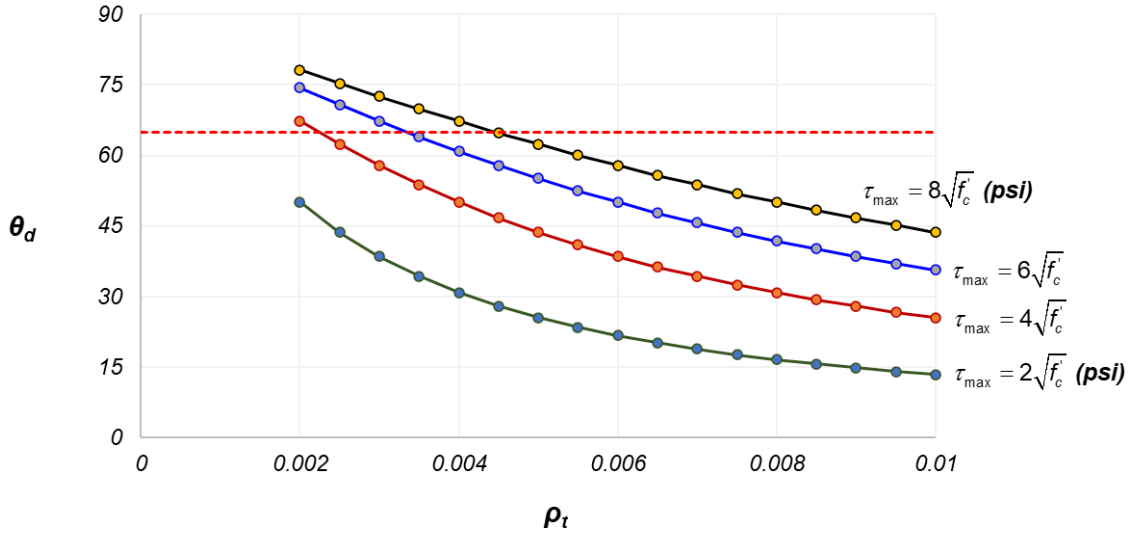


Figure 17. Calculation of θ_d for $f_{yt} = 70$ ksi (482 MPa) and $f'_c = 7$ ksi (48.2 MPa) for four levels peak shear stress.

Nonlinear Out-of-Plane Shear Modeling in BTM-Shells

The nonlinear out-of-plane shear behavior in a BTM-shell is modeled only in the vertical beams of the BTM-shell by adding a line with the **SHEARDEG** command followed by the value of five constant parameters in the following command line format:

SHEARDEG α_1 α_2 θ_1 θ_2 F_{res}

This option allows for moment strength degradation due to nonlinear out-of-plane shear behavior. At each instant of the analysis, the shear forces in each vertical beam is compared to a shear strength, V_r , obtained from the expression $V_r = V_{r0} \cdot F(\theta)$, where V_{r0} is a reference shear strength value, and F is a dimensionless reduction factor that depends on the element drift ratio, θ (defined as the relative transverse displacement of the two nodes of a beam, divided by the beam length). The value of V_{r0} is obtained as follows:

$$\begin{aligned} V_{r0} &= \alpha_1 + \alpha_2(-N) & \text{if } N < 0 \\ V_{r0} &= \alpha_1 & \text{if } N > 0 \end{aligned}$$

where N is the element axial force (positive for tension) and α_1 , α_2 user-defined constant parameters. The dimensionless factor F is a function of θ , as shown in Figure 18, involving three user-defined positive constant parameters, θ_1 , θ_2 , and F_{res} ($F_{res} < 1$). These control parameters allow to model the coupling between axial force and shear strength (V_c part).

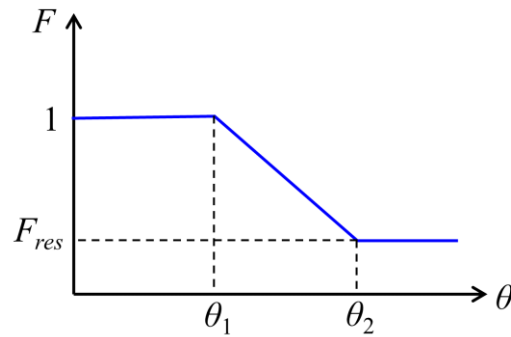


Figure 18. Control of relation between the dimensionless factor F and element drift ratio θ via the user-defined positive constant parameters, θ_1 , θ_2 , and F_{res}

Nonlinear Fiber-Section Three-Dimensional Beam Element (BEAM2)

Nonlinear fiber-section three-dimensional beam elements, termed as beams from this point on, are used to model columns, coupling beams (in a simplified manner instead of using BTM-shells), moment frame beams. Furthermore, beams are used to model the corners of flanged walls such as the corners of the C-shape wall of Case Study B and the corners of the 20-story core wall building of Case Study E. Beams model the corners of flanged walls to avoid the overlap of areas resulting from the connection of two orthogonal BTM-shells.

This type of element is called with command **BEAM2** in FE-Multiphys and uses an enhanced strain beam formulation (Koutromanos and Bowers 2016) that resolves several issues of commonly used nonlinear displacement-based beam elements. While all the studies and applications presented in Koutromanos and Bowers (2016) are two-dimensional, the formulation was extended to three-dimensional beams and implemented in FE-MultiPhys.

Figure 19 shows the definition block of a **BEAM2** used to model the columns in the 20-story case study described below. Each **BEAM2 SECTION** uses a **LAYSECTION** (*fiber-section*) which is defined separately in the layered sections block of the input file. Eleven lines of commands and definition parameters are included in the definition block. The commands **LAYERED**, **TORSIONAL**, **ROTMASS**, **PDELTA**, and **DAMPING** were described as part of the **SHEL2** definition above and have the same meaning for **BEAM2**. The **ORIENTATION** vector for a **BEAM2** is always parallel to the local y-axis of the **LAYERED** (SECTION) and thus normal to the longitudinal axis of the beam. The **AXIALTOLERANCE** (0.01 value recommended) enforces an iterative procedure for improving accuracy. Elimination of the **AXIALTOLERANCE** results in a non-iterative procedure that is faster but less accurate. In the latter case, a finer mesh of beams is required to achieve the same level of accuracy. In the modeling of columns in buildings with story height approximately equal to 3 m, use of four beam elements per story is recommended.

The nonlinear behavior in shear in both orthogonal directions of a **BEAM2** element is modeled with the **SHEARDEG** command, as described above for a **SHEL2** element. The control constant parameters are defined only once and are identical for both directions (there is no capability to model different shear strength in the two directions).

| CALL OF FUNCTIONS in the txt input file | | VALUES OF FUNCTION PARAMETERS | | | | | COMMENTARY |
|---|----------------|-------------------------------|-----|--------|--------|------|--|
| | SECTION | # | | | | | ! Section number corresponding to the PART number defined in LS prepost |
| | BEAM2 | | | | | | ! BEAM2 is the SECTION description of a nonlinear fiber section beam element |
| | LAYERED | # | | | | | ! Layered section number used |
| | ORIENTATION | # | # | # | | | ! Orientation vector (1.0 is always the axis parallel to the width of the section which is the local y axis) |
| | AXIALTOLERANCE | # | | | | | ! Tolerance ratio value. Removing this line uses a non-iterative procedure |
| | TORSIONAL | # | | | | | ! Torsional rigidity GJ |
| | ROTMASS | | | | | | ! Activates the consideration of rotational mass. Removing this line uses zero rotational mass |
| | PDELTA | | | | | | ! Activates PDELTA formulation. For COROTATIONAL or LINEAR GEOMETRY formulation this line should be removed |
| | DAMPING | | | | | | |
| | # | # | | | | | ! Mass and stiffness Rayleigh damping coefficients |
| | SHEARDEG | # | # | # | # | # | ! Modeling of nonlinear shear behavior |
| ! | | a1 | a2 | theta1 | theta2 | Fres | comment line |
| | END | | | | | | |
| | | | | | | | |
| | SECTION | 5.0 | | | | | ! Section number corresponding to the PART number defined in LS prepost |
| | BEAM2 | | | | | | ! BEAM2 is the SECTION description of a nonlinear fiber section beam element |
| | LAYERED | 7.0 | | | | | ! Layered section number used |
| | ORIENTATION | 1.0 | 0.0 | 0.0 | | | ! The local y axis of the section is parallel to the global X axis |
| | AXIALTOLERANCE | 0.01 | | | | | ! Tolerance ratio equal to 0.01 |
| | TORSIONAL | 7.00E+13 | | | | | ! Torsional rigidity GJ |
| | ROTMASS | | | | | | ! Activates the consideration of rotational mass |
| | PDELTA | | | | | | ! Activates PDELTA formulation. |
| | DAMPING | | | | | | |
| | 0.025 | 0.0003 | | | | | ! Mass and stiffness Rayleigh damping coefficients |
| | SHEARDEG | 100 | 0.1 | 0.005 | 0.03 | 0.3 | |
| ! | | a1 | a2 | theta1 | theta2 | Fres | comment line |
| | END | | | | | | |
| | | | | | | | |

Figure 19. Definition of nonlinear fiber-section beam element (**BEAM2**).

8. Concrete, Reinforcing Steel, and Post-Tension Steel Materials

Uniaxial Unconfined Concrete Material **CONWBET**

The concrete material used here is the *concretewbeta* material presented in Lu et al. (2014, 2016), which models the uniaxial cyclic behavior of concrete including softening in tension and compression. The material has been implemented in FE-MultiPhys to automatically adjust the compression softening branch based on the size of the BTM-shell (vertical, horizontal, and diagonal) and the reference length parameter L_{REF} . The cyclic response of the material including definition points are shown in Figure 20. The cyclic stress–strain behavior is fully defined based on the eleven parameters (1-11) described Table 1. The command **CONWBET** calls the material. When the initial modulus E_c is not explicitly defined (zero value as input), it is calculated as $E_c = 5700\sqrt{f_c}$ (MPa). When the tension stiffening parameter **MPAR** is defined, the softening behavior follows the RC behavior, accounting for tension stiffening as described in Lu et al. (2014, 2016), and the tension softening parameters f_{int} , ϵ_{int} , f_{tres} , and ϵ_{tres} shown in Figure 20 (top) are not used. When the command line **MPAR** is omitted, the tension softening branch is controlled with the following four parameter f_{int} , ϵ_{int} , f_{tres} , and ϵ_{tres} . More information about these parameters can be found in the [online tutorials](#) and in Lu et al. (2014, 2016). Recommended value for the parameters: **alpha**, **LAMDA**, and **LREF** are included below.

Table 1. Parameters of the **CONWBET** material.

| | | |
|---|-------|---|
| $(\epsilon_{co} \ f_c)$ | (1-2) | Compressive strength point |
| $(\epsilon_{cint} \ f_{int})$ | (3-4) | Intermediate point of the softening branch in compression |
| $(\epsilon_{cres} \ f_{cres})$ | (5-6) | Residual strength point in compression |
| $f_{ct} = 0.33\sqrt{f_c}$ (MPa) | (7) | Tensile strength of concrete |
| $MPAR = (75 \text{ mm}) \frac{\rho_s}{d_b}$, d_b in mm | (8) | Tension stiffening parameter |
| | | ρ_s : steel ratio in the axial direction of the material d_b : rebar diameter in the axial direction of the material |
| α | (9) | Control parameter for the reloading target point in compression $\alpha = 0.5 - 1.0$ (recommended for verticals and horizontals) $\alpha = 0.1 - 0.5$ (recommended for diagonals) |
| $LAMDA$ | (10) | Control parameter of unloading stiffness in compression $LAMDA = 0.25 - 0.5$ (recommended) |
| $LREF$ | (11) | Reference length for adjustment of compression softening $LREF = 600$ mm for vertical and horizontal beams $LREF = 850$ mm for diagonals |
| $E_c = 5700\sqrt{f_c}$ (MPa) | | |

| | | | | | | | | | | | | |
|----------|-----------------|------------|-------------------|------------|-------------------|----------|------------|-------------------|------------|-------------------|-------|--|
| CONWBET | | | | | | | | | | | | |
| f_c | ϵ_{co} | f_{cint} | ϵ_{cint} | f_{cres} | ϵ_{cres} | f_{ct} | f_{tint} | ϵ_{tint} | f_{tres} | ϵ_{tres} | E_c | |
| MPAR | # | | | | | | | | | | | |
| alpha | # | | | | | | | | | | | |
| LAMDA | # | | | | | | | | | | | |
| DENSITY | | | | | | | | | | | | |
| # | | | | | | | | | | | | |
| LREF | # | | | | | | | | | | | |
| END | | | | | | | | | | | | |
| | | | | | | | | | | | | |
| CONWBET | | | | | | | | | | | | |
| 40.0 | 0.002 | 20.0 | 0.0040 | 5.0 | 0.005 | 2.1 | 0.8 | 0.0002 | 0.1 | 0.001 | 0.0 | |
| MPAR | 0.1 | | | | | | | | | | | |
| alpha | 0.5 | | | | | | | | | | | |
| LAMDA | 1.0 | | | | | | | | | | | |
| DENSITY | | | | | | | | | | | | |
| 2.25E-09 | | | | | | | | | | | | |
| LREF | 600 | | | | | | | | | | | |
| END | | | | | | | | | | | | |

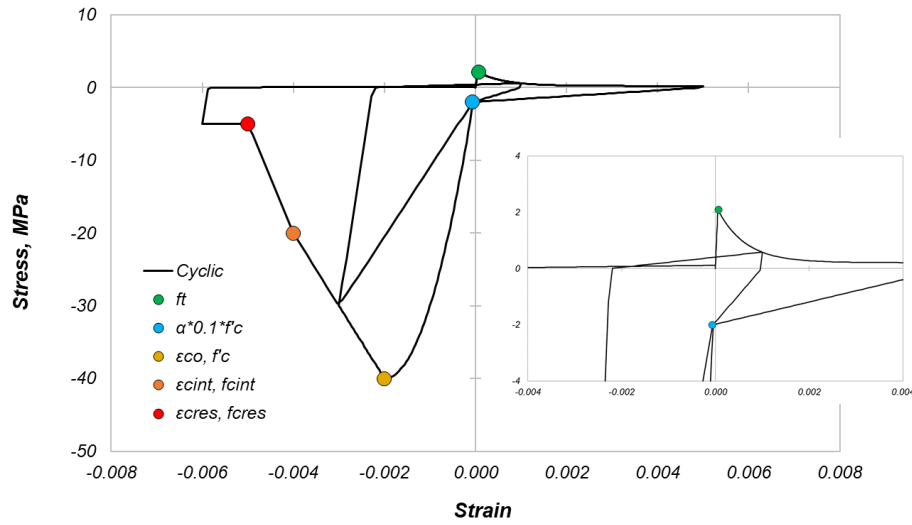


Figure 20. (Bottom) Cyclic stress-strain behavior of unconfined concrete. (Top) Material parameters definition.

Uniaxial Confined Concrete Material CONWBET

Confined concrete material is defined with the addition of the command line **CONFINE** followed with the constant parameters f_{cc} and ϵ_{cc} , which define the stress–strain point at which the confined strength is reached; see Figure 21. The constant parameters f_{tint} , ϵ_{tint} , f_{tres} , and ϵ_{tres} control the degrading branch in compression. We recommend $L_{REF} = 450$ mm [the gauge length in the specimens tested by Mander et al. (1988b)] based on Deng et al. (2020), who studied RC walls that experienced crushing of boundary elements.

| | | | | | | | | | | | |
|----------|-----------------|-------------------------|-------------------|-------------------------|-------------------|----------|------------|-------------------|------------|-------------------|-------|
| CONWBET | | | | | | | | | | | |
| f'_c | ϵ_{co} | f_{cint} | ϵ_{cint} | f_{cres} | ϵ_{cres} | f_{ct} | f_{tint} | ϵ_{tint} | f_{tres} | ϵ_{tres} | E_c |
| MPAR | # | | | | | | | | | | |
| alpha | # | | | | | | | | | | |
| LAMDA | # | | | | | | | | | | |
| BETA | β_{int} | $\epsilon_{t\beta int}$ | β_{res} | $\epsilon_{t\beta res}$ | | | | | | | |
| CONFINE | f_{cc} | ϵ_{cc} | | | | | | | | | |
| DENSITY | | | | | | | | | | | |
| value | | | | | | | | | | | |
| LREF | # | | | | | | | | | | |
| END | | | | | | | | | | | |
| CONWBET | | | | | | | | | | | |
| 40.0 | 0.002 | 50.0 | 0.0150 | 5.0 | 0.018 | 2.1 | 0.8 | 0.0002 | 0.1 | 0.001 | 0.0 |
| MPAR | 0.1 | | | | | | | | | | |
| alpha | 0.5 | | | | | | | | | | |
| LAMDA | 1.0 | | | | | | | | | | |
| BETA | 0.4 | 0.01 | 0.1 | 0.04 | | | | | | | |
| CONFINE | 60 | 0.008 | | | | | | | | | |
| DENSITY | | | | | | | | | | | |
| 2.25E-09 | | | | | | | | | | | |
| LREF | 450 | | | | | | | | | | |
| END | | | | | | | | | | | |

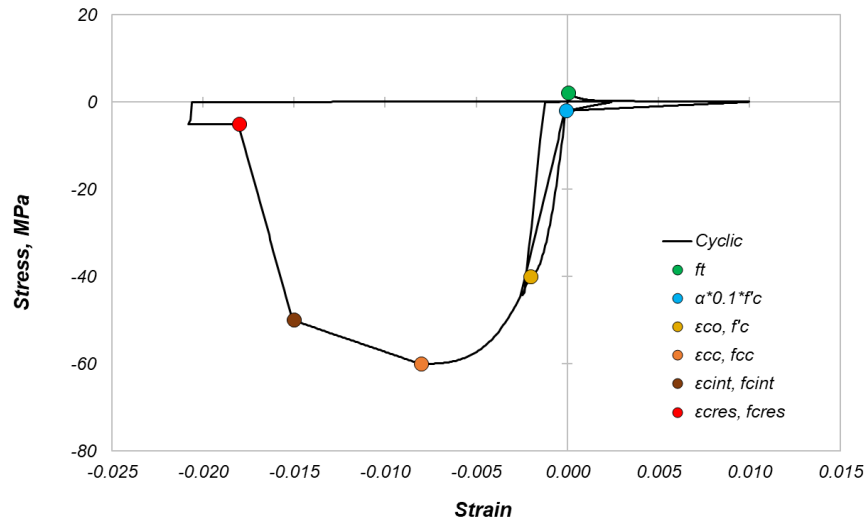


Figure 21. (Top) Definition of confined concrete material; (bottom) cyclic stress-strain behavior.

Biaxial Concrete Material **CONWBET** for Diagonals

The truss elements of the BTM-shells use the **CONWBET** material with the addition of the command line **BETA** followed by four constant parameters with the following default values: $\beta_{int} = 0.4$, $\epsilon_{t\beta int} = 0.01$, $\beta_{res} = 0.1$, and $\epsilon_{t\beta res} = 0.04$. The recommended values are based on Lu et al. (2014, 2016) (see Figure 23): $L_{REF} = 850$ mm. The **BETA** command line enables the material to account for biaxial effects on concrete's diagonal compression field behavior; see Figure 23. At each analysis step, the normal strain ϵ_n of each diagonal truss is computed. Based on the input trilinear β - ϵ_n relation, the behavior is modified (compressive stress is multiplied with β).

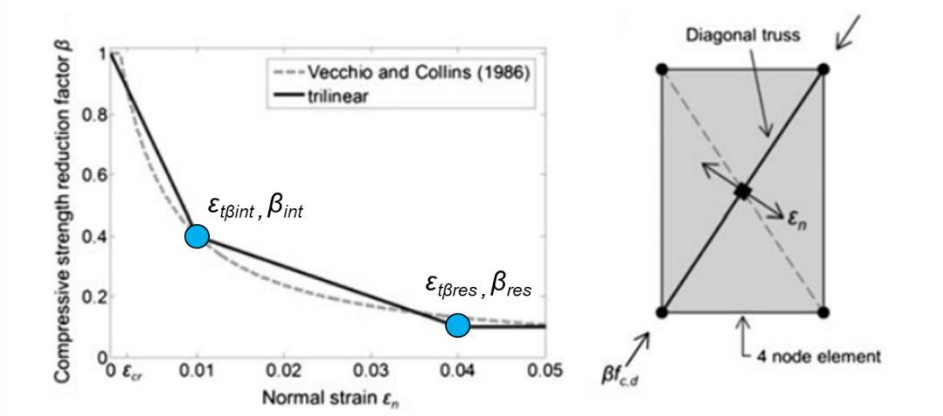


Figure 22. β - ϵ_n relation for biaxial effects of diagonal compression field of the BTM-shell.

| | | | | | | | | | | | |
|----------|-----------------|---------------------------|-------------------|---------------------------|-------------------|----------|------------|-------------------|------------|-------------------|-------|
| CONWBET | | | | | | | | | | | |
| f_c | ϵ_{co} | f_{cint} | ϵ_{cint} | f_{cres} | ϵ_{cres} | f_{ct} | f_{tint} | ϵ_{tint} | f_{tres} | ϵ_{tres} | E_c |
| MPAR | # | | | | | | | | | | |
| alpha | # | | | | | | | | | | |
| LAMDA | # | | | | | | | | | | |
| BETA | β_{int} | $\epsilon_{t\beta_{int}}$ | β_{res} | $\epsilon_{t\beta_{res}}$ | | | | | | | |
| DENSITY | | | | | | | | | | | |
| # | | | | | | | | | | | |
| LREF | # | | | | | | | | | | |
| END | | | | | | | | | | | |
| | | | | | | | | | | | |
| CONWBET | | | | | | | | | | | |
| 40.0 | 0.002 | 20.0 | 0.0040 | 5.0 | 0.005 | 2.1 | 0.8 | 0.0002 | 0.1 | 0.001 | 0.0 |
| MPAR | 0.1 | | | | | | | | | | |
| alpha | 0.5 | | | | | | | | | | |
| LAMDA | 1.0 | | | | | | | | | | |
| BETA | 0.4 | 0.01 | 0.1 | 0.04 | | | | | | | |
| DENSITY | | | | | | | | | | | |
| 2.25E-09 | | | | | | | | | | | |
| LREF | 850 | | | | | | | | | | |
| END | | | | | | | | | | | |

Figure 23. (Top) β - ϵ_n relation for biaxial effects of diagonal compression field of the BTM-shell; and (bottom) concrete material definition including biaxial effects.

Important note regarding concrete materials density used in the BTM-shells: The concrete material density used for the verticals and the horizontals should be half of the actual concrete density. This is because in a BTM-shell, the areas of concrete of the vertical and horizontal beams overlap. For the diagonals, a separate material with a small (1/1000 of actual) nonzero value of density is recommended to avoid numerical problems.

Reinforcing Steel Material **STEELDR**

The reinforcing steel material **STEELDR** follows the formulation described in Kim and Koutromanos (2016); it is based on the Dodd and Restrepo (1995) material model. The material models accurately the cyclic behavior of reinforcing steel including Bauschinger effect, yield plateau and strain hardening, as well as the effect of local bar buckling and fracture. Its formulation eliminated the iterative procedure of the Dodd-Restrepo model.

The linear elastic properties are described by the parameters (1-4) shown in Figure 24. Parameters (2-4) are not used in this report. The nonlinear monotonic envelope is fully described using the six parameters (5–10) that include the following four points: (a) yield; (b) initiation of strain hardening; (c) intermediate point of hardening regime; and (d) ultimate stress point. Any part of the material definition that is not used (*notinuse*) requires a fake input value to be complete.

The local buckling behavior is controlled with the L / D parameter (14), see Figure 25, which is the effective length of lateral supports to the supported bar diameter. The ratio L / D can be assumed equal to s / d_b , where s is the spacing of transverse anti-buckling reinforcement (closed hoops or ties with 135° or 180° hooks), and d_b the bar diameter of interest. When the rebars of interest are laterally supported by ties with 90° hooks, the value of L / D can increase to account for the reduced effectiveness of such ties, as shown in the experimental testing work of Panagiotou et al. (2013) and Visnjic et al. (2016).

Parameters S_{par} , t_{par} , and D_{cr} , (11-13) control the rupture due to low-cycle fatigue; see Figure 26. The use of $D_{cr} = 0$ disables the low-cycle fatigue option. For $S_{par} = -1$, the material uses the default formulation presented in Kim and Koutromanos (2016); a value of $t_{par} = 1$ is recommended. The value of D_{cr} is calibrated based on experimental test results of rupture occurring at the measured strain value of reinforcing steel under monotonic tension loading. In the example of Figure 26 for $D_{cr} = 0.25$, results in monotonic rupture at 13% strain. For the specific cyclic history, the rupture occurs in the cycle after developing 6% tension strain. A different calibration of D_{cr} (smaller values) can be used to approximate the coupling between bar buckling and rupture.

Finally, the Bauschinger effect is controlled with the **OMEGA** parameter with a value equal to 1 to be the default. Figure 27 shows the effect of **OMEGA** parameter for values equal to 0.9, 1.0 (default), and 1.1.

| | | | | | | | |
|-----------------|-----------|------------------|-----------|--------------|----------|----------|----------|
| STEELDR | | | | | | | |
| E | ν | G | K_{vol} | notinuse | notinuse | notinuse | notinuse |
| ϵ_{sh} | f_y | ϵ_{sh1} | f_{sh1} | ϵ_u | f_u | notinuse | notinuse |
| S_{par} | t_{par} | D_{cr} | L/D | notinuse | notinuse | notinuse | notinuse |
| OMEGA | # | | | | | | |
| DENSITY | | | | | | | |
| # | | | | | | | |
| END | | | | | | | |
| | | | | | | | |
| STEELDR | | | | | | | |
| 200000.0 | 0.3 | 130000.0 | 0.0 | 0.0 | 0.0 | 0.0 | 0.0 |
| 0.01 | 483.7 | 0.03 | 586.3 | 0.12 | 689.0 | 0.0 | 0.0 |
| -1.0 | 1.0 | 0.0 | 0.0 | 0.0 | 0.0 | 0.0 | 0.0 |
| OMEGA | 1.0 | | | | | | |
| DENSITY | | | | | | | |
| 7.85E-09 | | | | | | | |
| END | | | | | | | |

| | | |
|------------------|---|------|
| E | Elastic modulus | (1) |
| ν | Poisson ratio | (2) |
| G | Shear modulus | (3) |
| K | Bulk modulus | (4) |
| | | |
| ϵ_{sh} | Strain at initiation of hardening | (5) |
| f_y | Yield stress | (6) |
| ϵ_{sh1} | Strain of hardening regime intermediate point | (7) |
| f_{sh1} | Stress of hardening regime intermediate point | (8) |
| ϵ_u | Strain at ultimate stress | (9) |
| f_u | Ultimate stress | (10) |
| | | |
| S_{par} | Rupture parameter due to low cycle fatigue | (11) |
| t_{par} | Rupture parameter due to low cycle fatigue | (12) |
| D_{cr} | Rupture parameter due to low cycle fatigue | (13) |
| L/D | Local buckling parameter | (14) |
| | | |
| OMEGA | Bauschinger parameter | (15) |

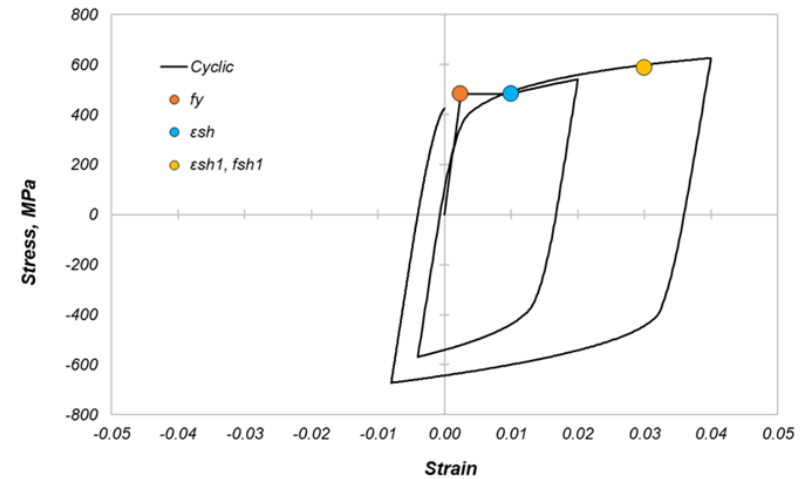
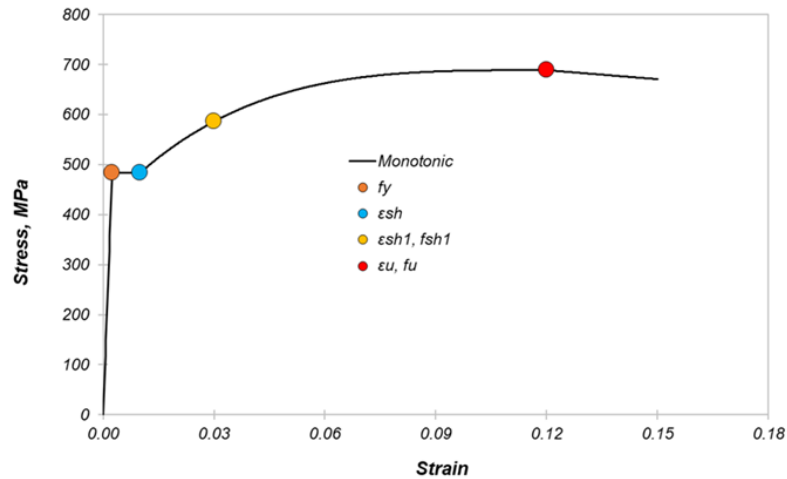


Figure 24. **STEELDR** material definition and example of monotonic and cyclic response without buckling and rupture activated.

| | | | | | | | |
|-----------------|-----------|------------------|-----------|--------------|----------|----------|----------|
| STEELDR | | | | | | | |
| E | ν | G | K_{vol} | notinuse | notinuse | notinuse | notinuse |
| ϵ_{sh} | f_y | ϵ_{sh1} | f_{sh1} | ϵ_u | f_u | notinuse | notinuse |
| S_{par} | t_{par} | D_{cr} | L / D | notinuse | notinuse | notinuse | notinuse |
| OMEGA | # | | | | | | |
| DENSITY | | | | | | | |
| # | | | | | | | |
| END | | | | | | | |
| STEELDR | | | | | | | |
| 200000.0 | 0.3 | 130000.0 | 0.0 | 0.0 | 0.0 | 0.0 | 0.0 |
| 0.01 | 483.7 | 0.03 | 586.3 | 0.12 | 689.0 | 0.0 | 0.0 |
| -1.0 | 1.0 | 0.0 | 8.0 | 0.0 | 0.0 | 0.0 | 0.0 |
| OMEGA | 1.0 | | | | | | |
| DENSITY | | | | | | | |
| 7.85E-09 | | | | | | | |
| END | | | | | | | |

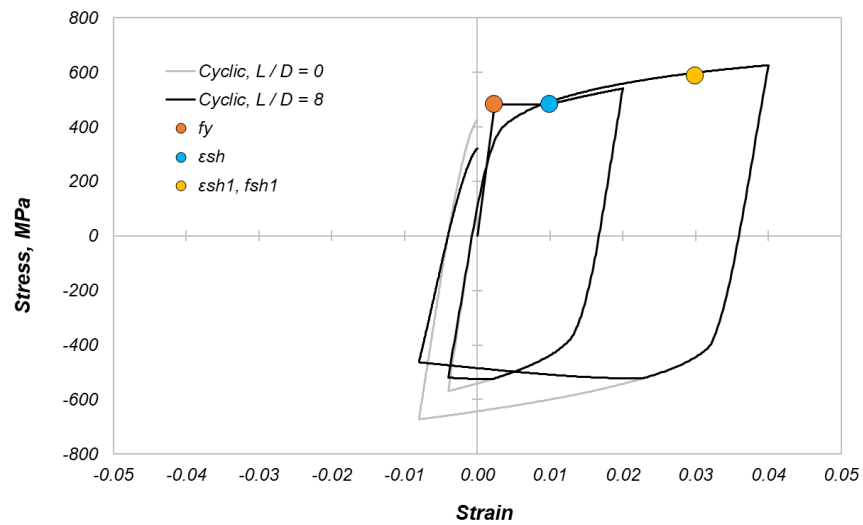


Figure 25. Effect of local buckling parameter $L / D = 8$ for a cyclic strain history.

| | | | | | | | |
|-----------------|-----------|------------------|-----------|--------------|----------|----------|----------|
| STEELDR | | | | | | | |
| E | ν | G | K_{vol} | notinuse | notinuse | notinuse | notinuse |
| ϵ_{sh} | f_y | ϵ_{sh1} | f_{sh1} | ϵ_u | f_u | notinuse | notinuse |
| S_{par} | t_{par} | D_{cr} | L/D | notinuse | notinuse | notinuse | notinuse |
| OMEGA | # | | | | | | |
| DENSITY | | | | | | | |
| # | | | | | | | |
| END | | | | | | | |
| STEELDR | | | | | | | |
| 200000.0 | 0.3 | 130000.0 | 0.0 | 0.0 | 0.0 | 0.0 | 0.0 |
| 0.01 | 483.7 | 0.03 | 586.3 | 0.12 | 689.0 | 0.0 | 0.0 |
| -1.0 | 1.0 | 0.25 | 0.0 | 0.0 | 0.0 | 0.0 | 0.0 |
| OMEGA | 1.0 | | | | | | |
| DENSITY | | | | | | | |
| 7.85E-09 | | | | | | | |
| END | | | | | | | |

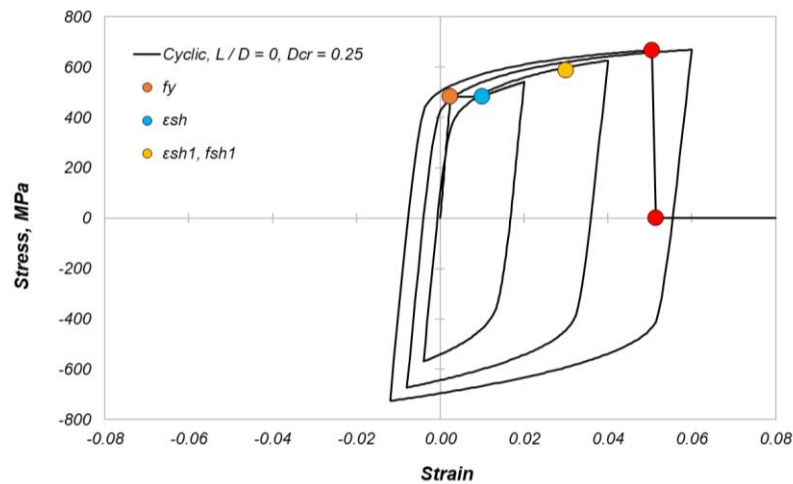
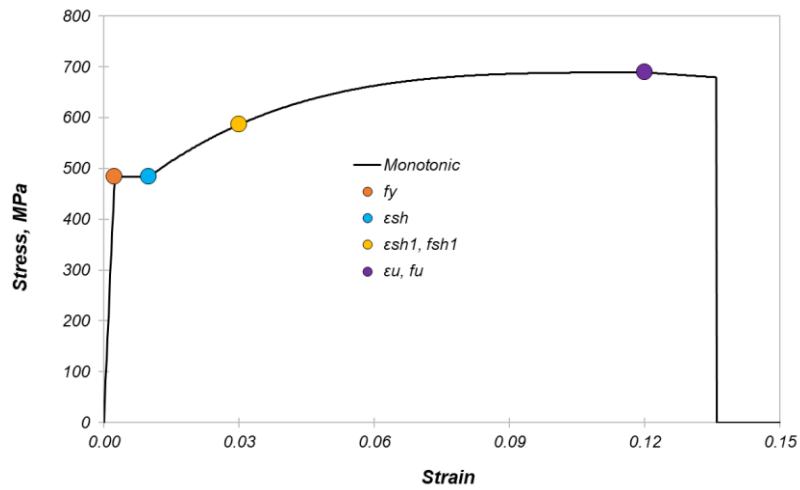


Figure 26. (Top): Input parameters for low-cycle fatigue rupture; effect of rupture parameter $D_{cr} = 0.25$ for: (middle) monotonic tension loading; and (bottom) cyclic strain history.

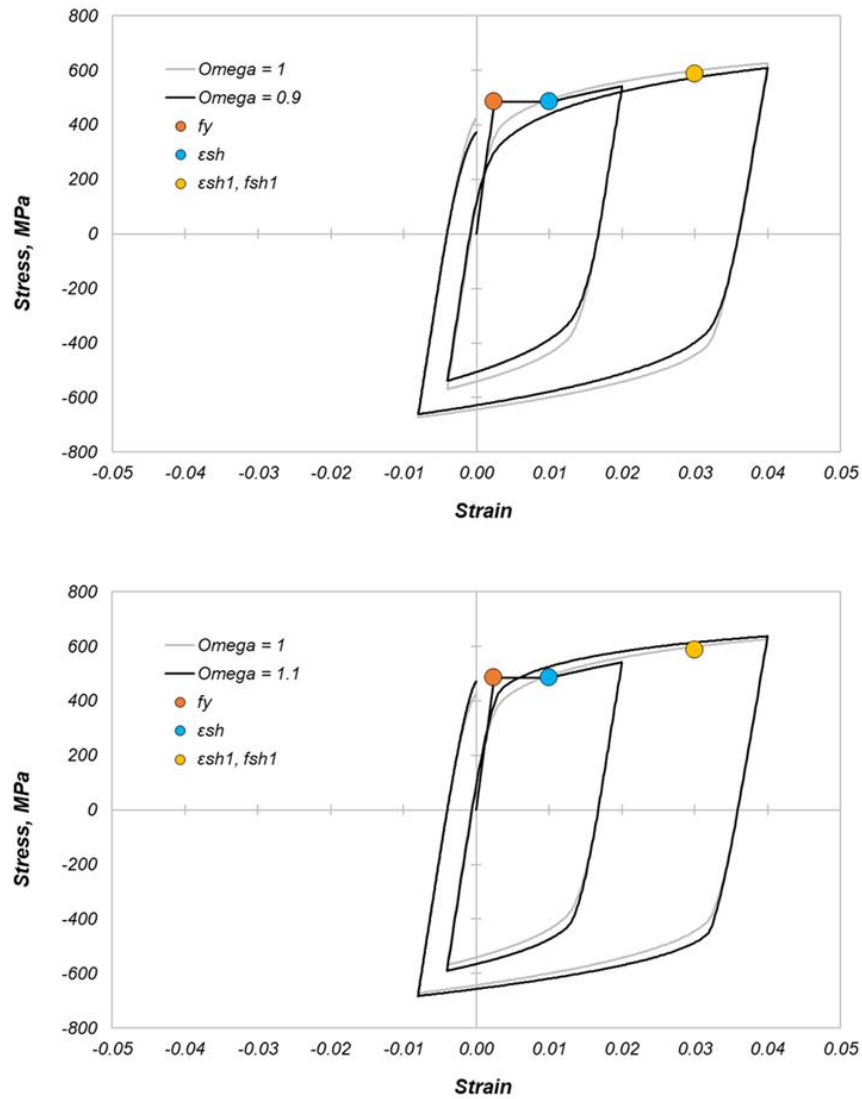


Figure 27. Effect of the **OMEGA** parameter.

Bilinear Steel Material (**STEEL01**)

A bilinear steel material is defined with the command **STEEL01** followed by a line below by six parameters: E , f_y , H , $itype$, $notinuse$, and ν . E is the elastic modulus, f_y the yield strength, and H the post-yield tangent modulus. There are two options for $itype$: 1 for isotropic hardening and 2 for kinematic hardening. The fifth parameter is not used; it has zero value but is required in the input. The sixth parameter is the Poisson's ratio. The **STEEL01** material is much simpler but less accurate than the **STEELDR** material.

| CALL OF FUNCTIONS in the txt input file | Constant parameters | | | | | | COMMENTARY |
|--|---------------------|--------|-----|-----|-----|---|--|
| MATERIAL | # | | | | | ! | |
| STEEL01 | | | | | | ! | |
| # | # | # | # | # | # | ! | E, fy, H, itype (1 for isotropic, 2 for kinematic), notinuse, notinuse |
| DENSITY | | | | | | ! | |
| # | | | | | | ! | |
| END | | | | | | ! | |
| | | | | | | | |
| MATERIAL | 4 | | | | | ! | |
| STEEL01 | | | | | | ! | |
| 200000.0 | 1860.0 | 2000.0 | 2.0 | 0.0 | 0.0 | ! | E, fy, H, itype (1 for isotropic, 2 for kinematic), notinuse, notinuse |
| DENSITY | | | | | | ! | |
| 7.00E-09 | | | | | | ! | |
| END | | | | | | ! | |

Figure 28. Definition of bilinear steel with kinematic hardening.

Modeling of Post-Tension via Initial Strain Material (**AUTOGENOUS**)

Post-tension is modeled using the **AUTOGENOUS** command in the STEEL01 material to apply an initial strain to the material. The strain is applied using a curve time function the ID, which is defined below the command **CURVEID**; see Figure 29.

| CALL OF FUNCTIONS in the txt input file | | | | | | | COMMENTARY |
|--|------|------|---|---|------|---|------------------------------|
| MATERIAL | # | | | | | ! | |
| STEEL01 | | | | | | ! | |
| # | # | # | # | # | # | ! | E, fy, H, itype, notinuse, v |
| AUTOGENOUS | | | | | | ! | |
| CURVEID | | | | | | ! | |
| # | | | | | | ! | |
| DENSITY | | | | | | ! | |
| # | | | | | | ! | |
| END | | | | | | ! | |
| | | | | | | | |
| MATERIAL | 10 | | | | | ! | |
| STEEL01 | | | | | | ! | |
| 200000 | 1860 | 2000 | 2 | 0 | 0.25 | ! | E, fy, H, itype, notinuse, v |
| AUTOGENOUS | | | | | | ! | |
| CURVEID | | | | | | ! | |
| 2 | | | | | | ! | |
| DENSITY | | | | | | ! | |
| 7.00E-09 | | | | | | ! | |
| END | | | | | | ! | |

Figure 29. Post-tension strand modeling using initial strain loading (**AUTOGENOUS**).

9. Mass and Body Forces

The mass is automatically modeled using the materials density (see command **DENSITY**). For the BTM-shells, the density defined for the concrete materials of the horizontal and vertical beams should be 50% of the actual values to compensate for the overlap of concrete areas in the BTM-shell. The diagonals use concrete materials with a small density value (1/1000 of the actual) to avoid numerical issues (due to zero mass). Superimposed mass (due to dead load mass) is modeled by adjusting the density of the concrete materials of the BTM-shells. The modeling of nodal masses will be described in a future version of this report.

The gravity forces due to materials density are modeled using the body force command **BODYF**, followed by the ID number of the body force; see Figure 30. The block of body forces definition includes eight lines of commands and parameters. Below the **BODYF** command, the **SECTION** number at which the body force is applied is described. Lines three and four define the **DOF** along which the body force is applied, as well as the **CURVE** number used to describe the time function of the body force. The command **MASS** stipulates that the body force is defined per unit mass. Finally, the line below the command **PARAMETERS** includes ten parameter constants. The first of the parameters is the acceleration of gravity; the others are equal to zero.

| CALL OF FUNCTIONS in the txt input file | VALUES OF FUNCTION PARAMETERS | | | | | | | | | | COMMENTARY |
|--|-------------------------------|-----|-----|-----|-----|-----|-----|-----|-----|-----|---|
| BODYF | # | | | | | | | | | | ! define a body force |
| SECTION | # | | | | | | | | | | ! the SECTION ID at which the body force is applied |
| DOF | # | | | | | | | | | | ! the dof along which the body force is applied |
| CURVE | # | | | | | | | | | | ! the CURVE id describing the time dependance on time of the body force |
| MASS | | | | | | | | | | | ! stipulate that the body force is defined per unit mass |
| PARAMETERS | | | | | | | | | | | ! |
| # | 0.0 | 0.0 | 0.0 | 0.0 | 0.0 | 0.0 | 0.0 | 0.0 | 0.0 | 0.0 | ! the generic description uses 10 parameters. Only the first parameter is nonzero here and equals the acceleration of gravity . The other nine parameters should be given equal to 0 |
| END | | | | | | | | | | | ! |
| BODYF | 3.0 | | | | | | | | | | ! body force number 3 |
| SECTION | 3.0 | | | | | | | | | | ! body force number 3 is applied to SECTION 3 |
| DOF | 3.0 | | | | | | | | | | ! the body force is applied along dof = 3 (Global Z axis) |
| CURVE | 2.0 | | | | | | | | | | ! the time dependance follows curve number 3 |
| MASS | | | | | | | | | | | ! stipulate that the body force is defined per unit mass |
| PARAMETERS | | | | | | | | | | | ! |
| -9810.0 | 0.0 | 0.0 | 0.0 | 0.0 | 0.0 | 0.0 | 0.0 | 0.0 | 0.0 | 0.0 | ! acceleration of gravity = -9810 mm / s ² . MINUS sign |
| END | | | | | | | | | | | ! |

Figure 30. Definition example of body forces (**BODYF**) in the txt input file.

10. Load Pattern (*LOADPATTERN*)

The command **LOADPATTERN** followed by a line of six parameters (integer values) defines a load pattern (specific distribution of forces), with displacement control. A definition example is shown in Figure 31. The pattern vector depends on the coordinate X, Y, or Z (*ICoord*) of the nodes, and this dependence is obtained based on a curve (*ICURVP*), defined in LSPP or in the txt input file. The pattern vector is applied along a specific degree of freedom (*IDOF*), and at each step we control the value of the displacement for the same degree of freedom, at a specific nodal point (*INODCONT*). A curve, with ID *ICURVCONT*, defined in LSPP (or in the txt input file) describes the relation between magnitude of controlled displacement and time.

The controlled degree of freedom of the control nodal point must be unrestrained (free) in the model definition. The load pattern is applied only for those nodes which have a nonzero force defined. In other words, the user must define nodal loads (or loads on a nodal set) in the direction of the pattern and assign a unit value to all these loads. This must be done for all nodes at which we want to apply the load pattern.

In the example of Figure 31, the displacement is controlled along the X-axis (*IDOF* = 1) while the load pattern (forces) vary along the Z-axis (*ICoord* = 3). The curve with ID equal to 5 (*ICURVUP* = 5) describes how the load pattern varies with the control coordinate (Z here). The displacement control node has ID equal to 7817 while the curve with ID equal to 6 (*ICURVCONT* = 6) describes the time variation of the amplitude of control displacement. The load pattern in this example starts to be applied at $t = 0$ ($t0 = 0$).

| CALL OF FUNCTIONS in the txt input file | | | | | | |
|---|---|--|---|---|---|--|
| | LOADPATTERN | | | | | |
| | IDOF | ICoord | ICURVP | INODCONT | ICURVCONT | t0 |
| ! | the degree-of-freedom along which the load pattern is applied | the coordinate number on which the pattern value depends (1 = X, 2 = Y, 3 = Z) | the ID of the curve which gives the pattern value as a function of the nodal coordinate value | the ID of the node whose displacement is controlled | the ID of the curve which gives the value of the controlled displacement, as a function of time | the time at which the load pattern is activated (a zero value includes the pattern from the beginning of the analysis) |
| | END | | | | | |
| | LOADPATTERN | | | | | |
| | 1 | 3 | 5 | 7817 | 6 | 0 |
| ! | the degree-of-freedom along which the load pattern is applied | the coordinate number on which the pattern value depends (1 = X, 2 = Y, 3 = Z) | the ID of the curve which gives the pattern value as a function of the nodal coordinate value | the ID of the node whose displacement is controlled | the ID of the curve which gives the value of the controlled displacement, as a function of time | the time at which the load pattern is activated (a zero value includes the pattern from the beginning of the analysis) |
| | END | | | | | |

Figure 31. Definition example of Load Pattern

11. Nonlinear Geometry Analysis Options

The program enables the corotational nonlinear geometry type of analysis with the command **LARGE DEFORMATIONS** in block 02 of the input file. The three-dimensional corotational formulation applies to all **BEAM2** and truss elements that comprise the BTM-shell macroelement as well as to all individual **BEAM2** and truss elements. The command **GNLOFF** can be used within a **SECTION**'s block to deactivate the large deformations formulation from the specific section.

The **PDELTA** command can be used as part of the BTM-shells and individual **BEAM2** definitions, enabling the P-delta formulation for nonlinear geometry analysis. The **PDELTA** command overwrites the **LARGE DEFORMATIONS** command at the **SECTION** level. Case Studies C and D used the **LARGE DEFORMATIONS** formulation while Case Study E (the 20-story building) used the P-delta formulation for all vertical elements and linear geometry for all other elements. For analysis of large structural systems where P-delta effects are significant, it is recommended the **PDELTA** formulation to be used instead of the **LARGE DEFORMATIONS** as it is computationally more efficient.

12. Solver Parameters for Modal and Nonlinear Analysis

Three types of analysis are reported here: (a) Modal; (b) Nonlinear Implicit Static; and (c) Nonlinear Implicit Dynamic. The definition of any of the three solvers starts with calling the command **SOLVER** at the last block of the input file. The specific parameters for each of the three solvers are described next.

Modal Analysis

The command **MODAL** followed by the number of modes to be computed is used to conduct a modal analysis; see Figure 32. The mode shapes are viewed in the LSPP after loading the *d3eigv* output file.

| CALL OF FUNCTIONS in the txt | | | COMMENTARY | |
|------------------------------|--------|------------|------------|------------------|
| | SOLVER | | ! | |
| | MODAL | # | ! | |
| ! | | numofmodes | ! | |
| | | | | |
| | SOLVER | | ! | |
| | MODAL | 20 | ! | Compute 20 modes |
| ! | | numofmodes | ! | |
| | | | | |

Figure 32. Definition example of **SOLVER** for **MODAL** analysis.

Nonlinear Static Analysis

Figure 33 shows a **SOLVER** definition for nonlinear implicit static analysis. Two command lines and nine parameters are used. The second line includes the parameters *IANTYPE* and *ITERTYPE* define the type of analysis and type of iteration scheme; the third parameter describes the tolerance. More information regarding all the available types of analysis and iteration types are found in Koutromanos and Farhadi (2018). All the analyses reported here used the full Newton-Raphson iteration, which is activated for *ITERTYPE* = 1. The first line below the command **SOLVER** includes the six parameters:

- (1) dt : default time step
- (2) dt_{\min} : the minimum time step
- (3) dt_{\max} : the maximum time step
- (4) t_{end} : the time at which the analysis ends
- (5) $maxiter$: the maximum number of iterations used in a substep
- (6) dt_{post} : the time step of recorded output

Table 2 summarizes the values solver parameters used in the five case studies of this report. The convergence criterion of the **SOLVER** compares—at each iteration sub-step—the sum of the unbalanced forces of all nodes with the tolerance value. If the unbalanced force is smaller than the tolerance, then convergence has been achieved. If not, the time step is reduced up to dt_{\min} , and the maximum number of iterations are used. A negative value of tolerance ensures the analysis continues at those steps where convergence is not achieved. In such cases, the user should check the magnitude of residuals (reported in the interlog2.txt output file). In those cases where the magnitude of residual at specific steps is not acceptable, it will be necessary to modify the **SOLVER** parameters and rerun the analysis.

| CALL OF FUNCTIONS in the txt input file | | | | | | | COMMENTARY |
|---|---------|----------|-----------|--------|---------|--------|--|
| | SOLVER | | | | | | ! |
| | # | # | # | # | # | # | ! |
| ! | dt | dtmin | dtmax | tstop | maxiter | dtpost | ! |
| | # | # | # | | | | ! |
| ! | IANTYPE | ITERTYPE | tolerance | | | | ! |
| | | | | | | | IANTYPE = 1 for implicit static solution and ITERTYPE = 1 for full Newton - Raphson iteration |
| | SOLVER | | | | | | ! |
| | 0.01 | 0.00001 | 0.01 | 366.22 | 30 | 0.1 | ! |
| ! | dt | dtmin | dtmax | tstop | maxiter | dtpost | ! |
| | 1 | 1 | -10000 | | | | ! |
| ! | IANTYPE | ITERTYPE | tolerance | | | | ! |
| | | | | | | | IANTYPE = 1 for implicit static solution and ITERTYPE = 1 for full Newton - Raphson iteration |

Figure 33. Definition example of **SOLVER** for nonlinear static analysis.

Table 2. Solver parameters used in the five case studies.

| Case Study | Number of nodes | Number of elements | NCPUs | dt (s) | 1 / dt _{min} (1 / s) | dt _{max} (s) | t _{end} (s) | maxiter | dt _{post} (s) | tolerance (N) | tolerance ratio | cumulative roof displacement (mm) |
|------------|-----------------|--------------------|-------|--------|-------------------------------|-----------------------|----------------------|---------|------------------------|---------------|-----------------|-----------------------------------|
| A | 361 | 324 | 4 | 0.001 | 1.0E+05 | 0.005 | 45 | 50 | 0.01 | -7000 | 1.5% | 576 |
| B | 186 | 251 | 6 | 0.010 | 1.0E+05 | 0.010 | 366 | 30 | 0.10 | -10000 | 2.2% | 2921 |
| C | 319 | 300 | 6 | 0.001 | 1.0E+06 | 0.001 | 55 | 30 | 0.01 | -5000 | 2.1% | 2135 |
| D | 587 | 964 | 6 | 0.001 | 1.0E+06 | 0.001 | 200 | 20 | 0.10 | -20000 | 2.6% | 3812 |
| E | 8794 | 8480 | 1 | 0.010 | 1.0E+04 | 0.010 | 40 | 40 | 0.10 | -1000000 | 1.7% | 11846 |

Nonlinear Dynamic Implicit Analysis and Transition from Static

This type of analysis starts with static analysis until an input transition time (*transition_t*) where it switches to dynamic analysis. The command **STATICTODYNAMIC** in block 02 of the input file activates the transition. The **SOLVER** is defined with four lines of parameters shown in Figure 34.

| CALL OF FUNCTIONS in the .txt input file | | | | | | | | COMMENTARY |
|--|---------------|--------------|-----------|-------|---------|-------|---|--|
| ! | SOLVER | | | | | | ! | |
| ! | # | # | # | # | # | # | ! | time steps and max iteration parameters for both STATIC and DYNAMIC parts |
| ! | dt | dtmin | dtmax | tstop | maxiter | dpost | ! | |
| ! | # | # | # | | | | ! | type of static analysis and iteration type, tolerance common to STATIC and DYNAMIC parts |
| ! | IANYPE static | ITERTYPE | tolerance | | | | ! | |
| ! | # | # | | | | | ! | type of DYNAMIC analysis and transition time |
| ! | IANYPE dyna | transition_t | | | | | ! | |
| ! | # | # | # | | | | ! | parameters of HHT method |
| ! | HHT α | HHT β | HHT γ | | | | ! | |
| | | | | | | | | |
| ! | SOLVER | | | | | | ! | |
| ! | 0.01 | 0.0001 | 0.01 | 40.0 | 40.0 | 0.1 | ! | time steps and max iteration parameters for both STATIC and DYNAMIC parts |
| ! | dt | dtmin | dtmax | tstop | maxiter | dpost | ! | |
| ! | 1.0 | 1.0 | -1.00E+06 | | | | ! | type of static analysis and iteration type, tolerance common to STATIC and DYNAMIC parts |
| ! | IANYPE static | ITERTYPE | tolerance | | | | ! | |
| ! | 6.0 | 0.16 | | | | | ! | type of DYNAMIC analysis and transition time |
| ! | IANYPE dyna | transition_t | | | | | ! | |
| ! | 0.4225 | 0.8 | -0.3 | | | | ! | parameters of HHT method |
| ! | HHT α | HHT β | HHT γ | | | | ! | |

Figure 34. Definition example of **SOLVER** for nonlinear implicit dynamic analysis and transition from static analysis.

The first line was described in the *Static Analysis* section. The second line defines the type of static analysis as well as the iteration type and tolerance, with the latter two parameters being the same for the static and dynamic parts. The third line defines the type of the dynamic analysis and the transition time, while the fourth line lists the parameters of the Hilber-Hughes-Taylor (HHT) method used here. The HHT is defined by using IANYPE = 6 in the third line of parameters

```

SOLVER
0.001 0.00001 0.001 44.5 50. 0.01      !dt, dtmin,dtmax,tend, maxiter, dtprint
1 1 -7000.

```

```

SOLVER
0.01 0.0001 0.01 40. 40. 0.1      !dt, dtmin,dtmax,tend (time at which analysis stops), maxiter, dtprint
1 1 -1.0E+06      ! parameters (itype, itertype, tol) for the first static steps
6 1.1      ! iantypef, timswitch
0.4225 0.8 -0.3

```

Figure 35. (top): implicit static analysis **SOLVER** example; and (bottom) implicit dynamic analysis with transition from static **SOLVER** example.

Selection of Solver Parameters and Validation

The adequacy of a SOLVER scheme for nonlinear analysis can be confirmed only by comparing the differences in computed responses for different solver parameters. For example, the tolerance magnitude can be validated by comparing the force-displacement for two levels of tolerance. Figure 36 compares the computed force-displacement responses for two levels of tolerance (ratio of values equals two) for Case Studies A to D of this report. The difference in the computed responses is negligible in Case Studies B to D while for Case Study A the difference is small.

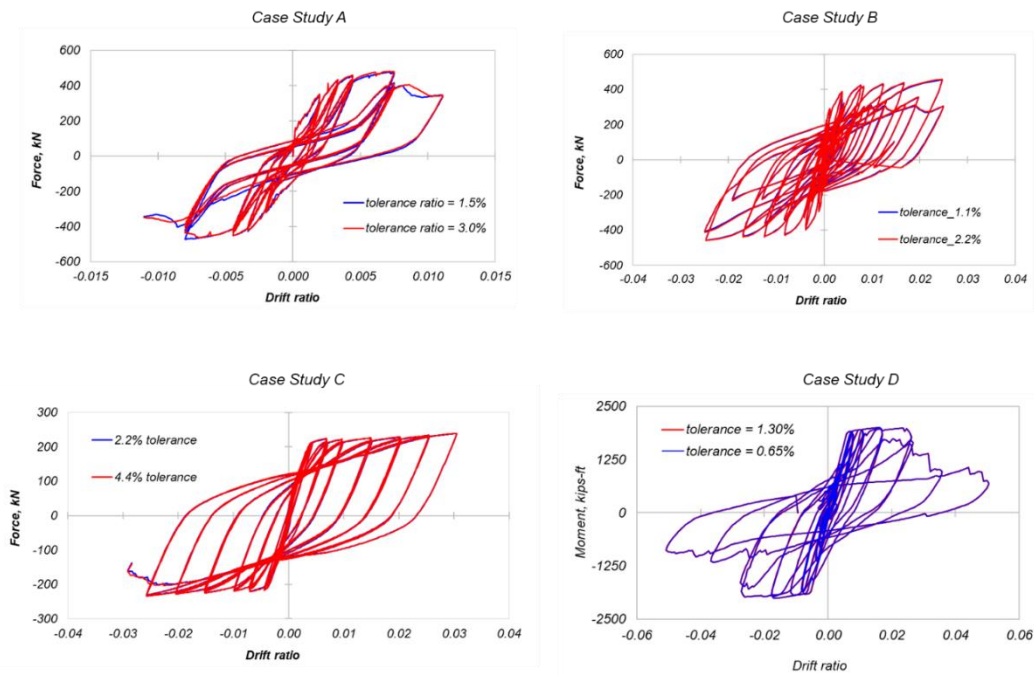
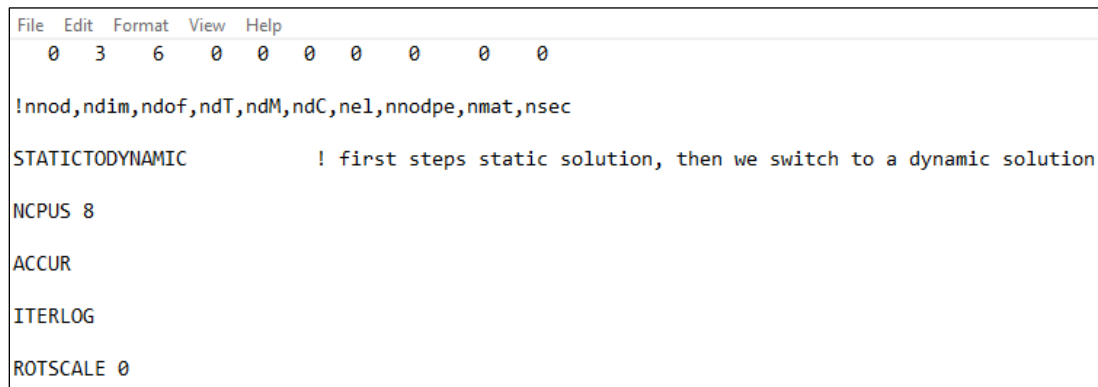


Figure 36. Validation of tolerance adequacy for Case Studies A to D. Comparison of computed force-displacement responses for two levels of tolerance.

13. Parallel Processing

The program has parallel processing (multi-thread) capabilities which are activated via the command **NCPUS** *nthreads* where *nthreads* is an integer number equal to the number of threads to be used. The command **ACCUR** should always be included as a separate line below **NCPUS** *nthreads* command in block 02 of the input file, see Figure 37.

Parallel processing analysis results differ depending on the number of threads used. The level of difference depends on the type of nonlinear problem, the size of the model, the number of threads used, and the characteristics of the computer used. It is recommended that the user compare the analyses using **NCPUS 1** with that of **NCPUS** larger than one to confirm that the level of difference is acceptable. The difference in the analyses for **NCPUS** larger than one was small (of the order of 1%) for Case Studies A to D presented below; therefore, this level of difference is not discussed. For Case Study E (8000+ nonlinear elements), however, the differences reached up to 5%. Parametric studies dependent on analysis results for large models versus number of threads used will be presented in future versions of this report.



```
File Edit Format View Help
0 3 6 0 0 0 0 0 0 0
!nnod,ndim,ndof,ndT,ndM,ndC,nel,nnodpe,nmat,nsec
STATICTODYNAMIC ! first steps static solution, then we switch to a dynamic solution
NCPUS 8
ACCUR
ITERLOG
ROTSKALE 0
```

Figure 37. Blocks 01 (first line of input) and 02 where the **NCPUS** and **ACCUR** commands are called.

14. Recorders and Post-Processing

The computed responses and available recording options include:

- (a) Nodal displacements
- (b) Nodal accelerations
- (c) Support reactions
- (d) Element forces
- (e) Strains and stresses of BTM-shell (**SHEL2**) and **BEAM2** elements
- (f) Section cut forces

All the computed responses listed above, except the section cut forces, are post-processed and plotted using LS-PrePost. Relevant information and examples on post-processing are found in the [online webinars](#) described in section 18. The histories of section cut forces are stored in separate txt files in the analysis folder.

Fiber Recorders - LAYSECTION

Up to five fiber recorders are called within a **LAYSECTION** block. The coordinates y_0 , z_0 , in the local coordinate system of the fiber section and the material number (**mat#**) are the three parameters that follow the recording command **RECORD**; see Figure 38. When a fiber with coordinates (y_0, z_0) does not exist, the nearest available fiber with the prescribed material available is recorded.

Section Cut Plane Recorder

Section cut plane recorders are defined in the *txt-input-file*, and the output appears in separate text files in the analysis folder. The results of section cut recorders cannot be accessed with LSPP. The command **CUTPLANE** is followed by three parameters, see Figure 39, which describe the direction normal to the plane of the section cut, the location of the **CUTPLANE**, and the point at which the resultant forces are reported define this recorder. When a **SECTION** is not included in the definition of a **CUTPLANE**, the section cut includes all **SECTIONS**. For section cuts through specific **SECTIONS** only, the **SECTION** numbers are included in separate lines of the definition, as shown in Figure 40. Results of section cut plane recorders are presented in Case Study E of the 20-story RC core-wall building.

| CALL OF FUNCTIONS in the txt input file | | | | | | | | | | COMMENTARY |
|---|------------|---------------------------------|---------------------------------|-----------------------------|-----|-----|-----|-----|----|--|
| | LAYSECTION | 23 | | | | | | | | |
| | patch | rectangular | 7 | 4 | 4 | -50 | -50 | 50 | 50 | ! fibers patch with material 7 |
| | grid | 2 | 113 | 2 | -40 | -40 | 40 | -40 | | ! grid of fibers with material 2 |
| | grid | 2 | 113 | 2 | -40 | 40 | 40 | 40 | | ! grid of fibers with material 2 |
| | RECORD | y0 | z0 | mat# | | | | | | ! record fiber with local coordinates (y0, z0) and material # |
| ! | | y coordinate of recording fiber | z coordinate of recording fiber | material of recording fiber | | | | | | |
| | RECORD | y0 | z0 | mat# | | | | | | ! record fiber with local coordinates (0, 0) and material # |
| ! | | y coordinate of recording fiber | z coordinate of recording fiber | material of recording fiber | | | | | | |
| | END | | | | | | | | | ! |
| | LAYSECTION | 23 | | | | | | | | |
| | patch | rectangular | 7 | 4 | 4 | -50 | -50 | 50 | 50 | ! fibers patch with material 7 |
| | grid | 2 | 113 | 2 | -40 | -40 | 40 | -40 | | ! grid of fibers with material 2 |
| | grid | 2 | 113 | 2 | -40 | 40 | 40 | 40 | | ! grid of fibers with material 2 |
| | RECORD | 0.0 | 0.0 | 7.0 | | | | | | ! record fiber with local coordinates (0, 0) and material 7 |
| ! | | y coordinate of recording fiber | z coordinate of recording fiber | material of recording fiber | | | | | | |
| | RECORD | 10.0 | -20.0 | 2.0 | | | | | | ! record fiber with local coordinates (10, -20) and material 2 |
| ! | | y coordinate of recording fiber | z coordinate of recording fiber | material of recording fiber | | | | | | |
| | END | | | | | | | | | ! |

Figure 38. Definition example of two recording fibers of a **LAYSECTION**.

| CALL OF FUNCTIONS in the txt input file | | | | | | COMMENTARY |
|---|----------|---------------------------------------|--|--|--|------------|
| | CUTPLANE | ider | X0 | Y0 | Z0 | ! |
| ! | | direction normal to the cutting plane | X coordinate of resultant forces calculation point | Y coordinate of resultant forces calculation point | Z coordinate of resultant forces calculation | ! |
| | END | | | | | ! |
| | CUTPLANE | 3 | 0 | 0 | 100 | ! |
| ! | | ider | X0 | Y0 | Z0 | ! |
| | END | | | | | ! |

Figure 39. Definition example of total X-Y section cut with location $Z = 100$ and coordinates of the resultant forces point $(X0, Y0) = (0, 0)$.

| CALL OF FUNCTIONS in the txt input file | | | | | | COMMENTARY |
|---|-----------------|---------------------------------------|--|--|--|------------|
| | CUTPLANE | <i>ider</i> | <i>X0</i> | <i>Y0</i> | <i>Z0</i> | ! |
| ! | | direction normal to the cutting plane | X coordinate of resultant forces calculation point | Y coordinate of resultant forces calculation point | Z coordinate of resultant forces calculation point | ! |
| | SECTION | # | | | | ! |
| | SECTION | # | | | | ! |
| | END | | | | | ! |
| | | | | | | |
| | CUTPLANE | 3 | 0 | 0 | 100 | ! |
| ! | | <i>ider</i> | <i>X0</i> | <i>Y0</i> | <i>Z0</i> | ! |
| | SECTION | 10 | | | | ! |
| | SECTION | 11 | | | | ! |
| | END | | | | | ! |

Figure 40. Definition example of section cut that includes specific **SECTION**.

BTM-Shells Post-Processing

The user has the capability to record histories for the two diagonal elements, and for up to five fibers from each of the sections used in the horizontal and vertical beams. For each fiber, the program outputs as history variables (hsv) three independent quantities (in a fixed order), namely, the values of stress, strain and h_i , where h_i is an “important history variable” of the uniaxial stress strain law. For the **CONWBETA** material model, h_i is equal to the β reduction factor; for the **STEELDR** material model, h_i is the value of parameter D (the accumulation of inelastic work ultimately leading to tensile rebar rupture); see Kim and Koutromanos (2016). The various output quantities are stored as history variables in the order shown in Figure 41.

Output stored in the “middle surface” of the shell elements

| | |
|-----------|--|
| hsv(1) | Strain of diagonal element 1 |
| hsv(2) | Stress of diagonal element 1 |
| hsv(3) | h_i of diagonal element 1 |
| hsv(4) | Strain of diagonal element 2 |
| hsv(5) | Stress of diagonal element 2 |
| hsv(6) | h_i of diagonal element 2 |
| hsv(7-10) | Not in use |
| hsv(11) | Strain of 1 st fiber for vertical element 1 |
| hsv(12) | Stress of 1 st fiber for vertical element 1 |
| hsv(13) | h_i of 1 st fiber for vertical element 1 |
| hsv(14) | Strain of 2 nd fiber for vertical element 1 |
| hsv(15) | Stress of 2 nd fiber for vertical element 1 |
| hsv(16) | h_i of 2 nd fiber for vertical element 1 |
| ... | ... |
| hsv(23) | Strain of 5 th fiber for vertical element 1 |
| hsv(24) | Stress of 5 th fiber for vertical element 1 |
| hsv(25) | h_i of 5 th fiber for vertical element 1 |
| hsv(26) | Strain of 1 st fiber for horizontal element 1 |
| hsv(27) | Stress of 1 st fiber for horizontal element 1 |
| hsv(28) | h_i of 1 st fiber for horizontal element 1 |
| hsv(29) | Strain of 2 nd fiber for horizontal element 1 |
| hsv(30) | Stress of 2 nd fiber for horizontal element 1 |
| hsv(31) | h_i of 2 nd fiber for horizontal element 1 |
| ... | ... |
| hsv(38) | Strain of 5 th fiber for horizontal element 1 |
| hsv(39) | Stress of 5 th fiber for horizontal element 1 |
| hsv(40) | h_i of 5 th fiber for horizontal element 1 |

Output stored in the “lower surface” of the shell elements

| | |
|-----------|--|
| hsv(1) | Strain of diagonal element 1 |
| hsv(2) | Stress of diagonal element 1 |
| hsv(3) | h_i of diagonal element 1 |
| hsv(4) | Strain of diagonal element 2 |
| hsv(5) | Stress of diagonal element 2 |
| hsv(6) | h_i of diagonal element 2 |
| hsv(7-10) | Not in use |
| hsv(11) | Strain of 1 st fiber for vertical element 2 |
| hsv(12) | Stress of 1 st fiber for vertical element 2 |
| hsv(13) | h_i of 1 st fiber for vertical element 2 |
| hsv(14) | Strain of 2 nd fiber for vertical element 2 |
| hsv(15) | Stress of 2 nd fiber for vertical element 2 |
| hsv(16) | h_i of 2 nd fiber for vertical element 2 |
| ... | ... |
| hsv(23) | Strain of 5 th fiber for vertical element 2 |
| hsv(24) | Stress of 5 th fiber for vertical element 2 |
| hsv(25) | h_i of 5 th fiber for vertical element 2 |
| hsv(26) | Strain of 1 st fiber for horizontal element 2 |
| hsv(27) | Stress of 1 st fiber for horizontal element 2 |
| hsv(28) | h_i of 1 st fiber for horizontal element 2 |
| hsv(29) | Strain of 2 nd fiber for horizontal element 2 |
| hsv(30) | Stress of 2 nd fiber for horizontal element 2 |
| hsv(31) | h_i of 2 nd fiber for horizontal element 2 |
| ... | ... |
| hsv(38) | Strain of 5 th fiber for horizontal element 2 |
| hsv(39) | Stress of 5 th fiber for horizontal element 2 |
| hsv(40) | h_i of 5 th fiber for horizontal element 2 |

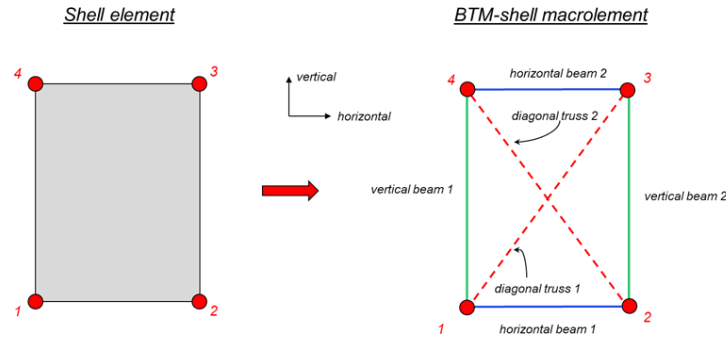


Figure 41. Order of stored history variables (hsv) of BTM-shell elements.

The histories are plotted in LSPP via the *History* window for *Shells* E-type. These variables can be plotted either via the *Element* or the *Int Pt* options in the *History* window. When the histories are plotted via the *Int Pt* option, the histories of both elements 1 and 2 are plotted independently of the *surface* selected. In addition to the strain and stress of the diagonals, and the recording fibers of the verticals and horizontal beams, the histories and contours of standard strains (X-, Y-, Z-, XY, XZ, YZ, Max Principal, Min Principal) of four node shell elements can be plotted in LSPP via the History-Element (for histories) and Fringe Component-Strain (for contours) option. Examples of max and min principal strain contour plots are presented in the sections of Case Studies A to E as well as in the [online tutorials](#).

15. Nonlinear Cyclic Static Analysis Reinforced Concrete Wall Components

This section of the report presents the nonlinear cyclic static analysis of four RC components that are then compared with experimental results of the same components. Case Studies A, B, and C are walls. Case Study D is a full-scale RC beam for special moment frames designed per ACI 318-08 and is the largest SMF RC beam ever tested in U.S. The three RC wall case studies experienced the following failure modes: (a) diagonal tension failure; (b) diagonal compression failure; and (c) global out-of-plane plastic hinge buckling. The beam of Case Study D experienced a coupled bar buckling – shear failure. Table 3 summarizes key characteristics and test responses of the four specimens, including the peak shear stress ratio, peak drift ratio, total longitudinal steel ratio, axial load ratio, shear span ratio, and the transverse steel ratio.

Table 3. Characteristics of the test specimens of Case Studies A to D.

| Case Study | Specimen name | Authors | Failure mode | Peak shear stress ratio | Peak drift ratio | Total long. steel ratio | Axial load ratio | Shear Span Ratio | Transverse steel ratio |
|------------|---------------|-------------------|------------------------------------|--|------------------|-------------------------|------------------|---------------------|------------------------|
| | | | | $\tau_{\max} / \sqrt{f'_c}$ (psi/psi) | Θ_{peak} | $\rho_{l,tot}$ | $N / f'_c A_g$ | $M / (V \cdot L_w)$ | ρ_t |
| A | Unit 1.0 | Mestyanek | Diagonal tension | 4.6 | 0.011 | 0.8% | 0.0% | 1.0 | 0.16% |
| B | TUB | Beyer et al. | Diagonal crushing | 5.7 | 0.025 | 1.0% | 4.4% | 2.3 | 0.45% |
| C | RWL | Dashti | Plastic hinge buckling | 2.6 | 0.030 | 2.3% | 6.0% | 3.8 | 0.84% |
| D | Beam A | Panagiotou et al. | Mixed bar buckling - shear failure | 1.77 | 0.026 | 1.3% | 0.0% | 3.75 | 0.28% |

Case Study A: Diagonal Tension Failure of a Squat Barbel Wall

The experimental test of this squat barbel wall, see Figure 42(a), is presented in Mestyanek (1986). The longitudinal and transverse steel ratio of this wall were 0.78%, and 0.16%, respectively; the axial load was zero. As shown in Figure 42(c), the wall experienced a diagonal tension failure resulting in stiffness and strength degradation during the cycle of peak drift ratio equal to 1.1%. The BTM-shell model used three section properties (*PARTS*) for the **SHEL2** elements to represent the following three distinct parts of the wall: (1) the unconfined part; (2) the confined end columns; and (3) an elastic row of shell elements at the top representing the cap

beam of the test setup. As shown in Figure 42(c), the computed force-displacement ($F-D$) response closely matched the experimental measurements and captured both the stiffness and strength degradation. Figure 42 (d) and (e) plot the contours of principal compression and tension strains at two instants of peak drift response. Excellent agreement was achieved with the observed failure mode capturing both diagonal failure planes including the concentration of inelastic deformations at the compression toes of the wall. Figure 43 shows the stress-strain response of selected concrete and steel fibers. At these locations, the tension strain of the reinforcing steel reached approximately 6% in the horizontal direction due to the diagonal failure plane opening. The peak compression strains were computed in the diagonal direction and were associated with the more than 5% principal tension strain, thus reducing the compression capacity of the concrete diagonals.

The analysis of this wall using the BTM-shell model is presented in detail in Deng et al. (2020). This wall was analyzed earlier and presented by Lu, Koutromanos, and Panagiotou (2014, 2016). Youtube videos from simulations of this wall can be found in the following links:

Links to Videos of Simulations:

[OpenSees simulation as presented in Lu et al.](#)

[BTM-Shell Simulation in FE-MultiPhys](#)

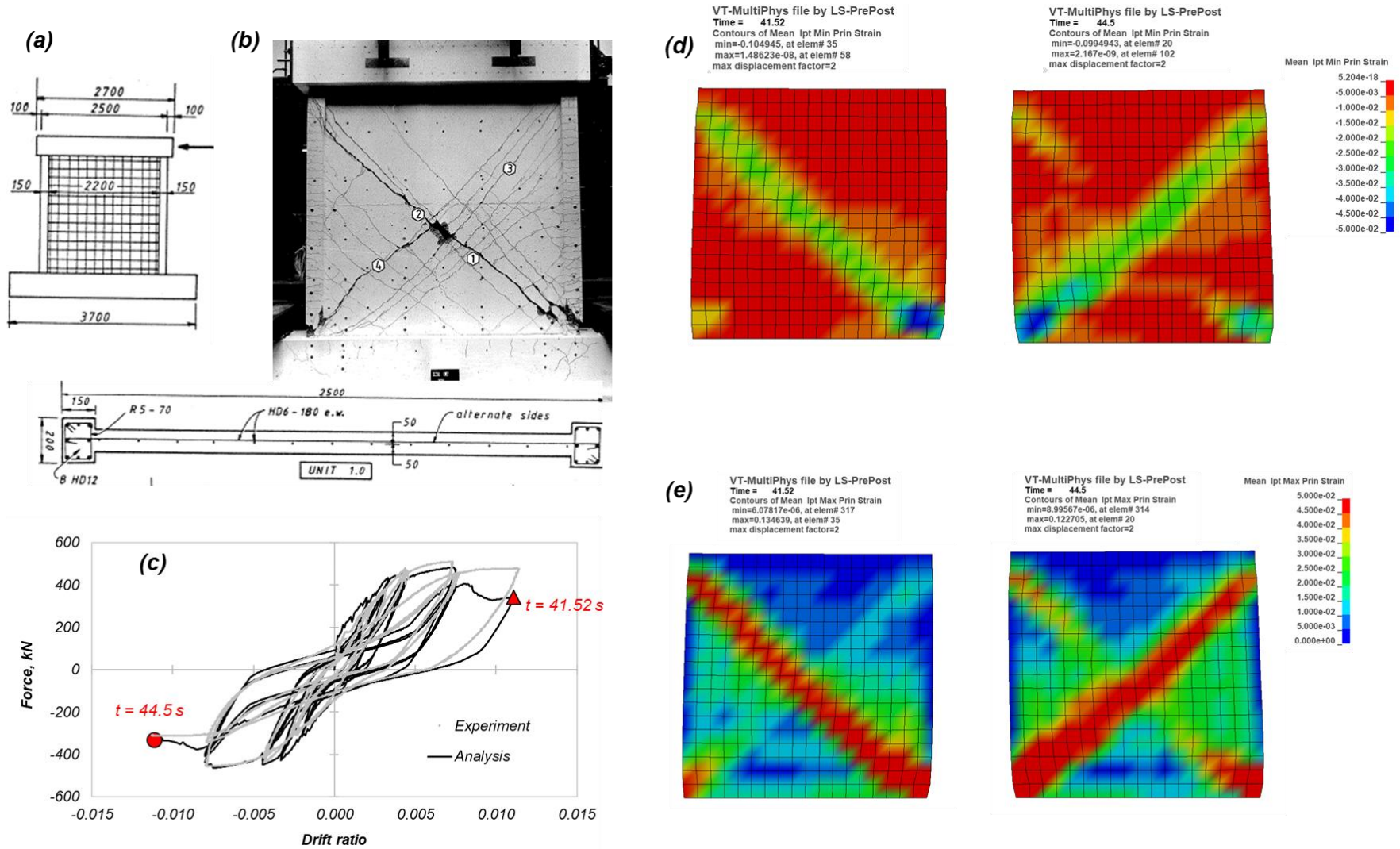


Figure 42. (a) Geometry and section characteristics; (b) experimentally measured and computed force-displacement response; (c) failure crack pattern at the end of the test; and (d) maximum principal strains at peak drift ratios.

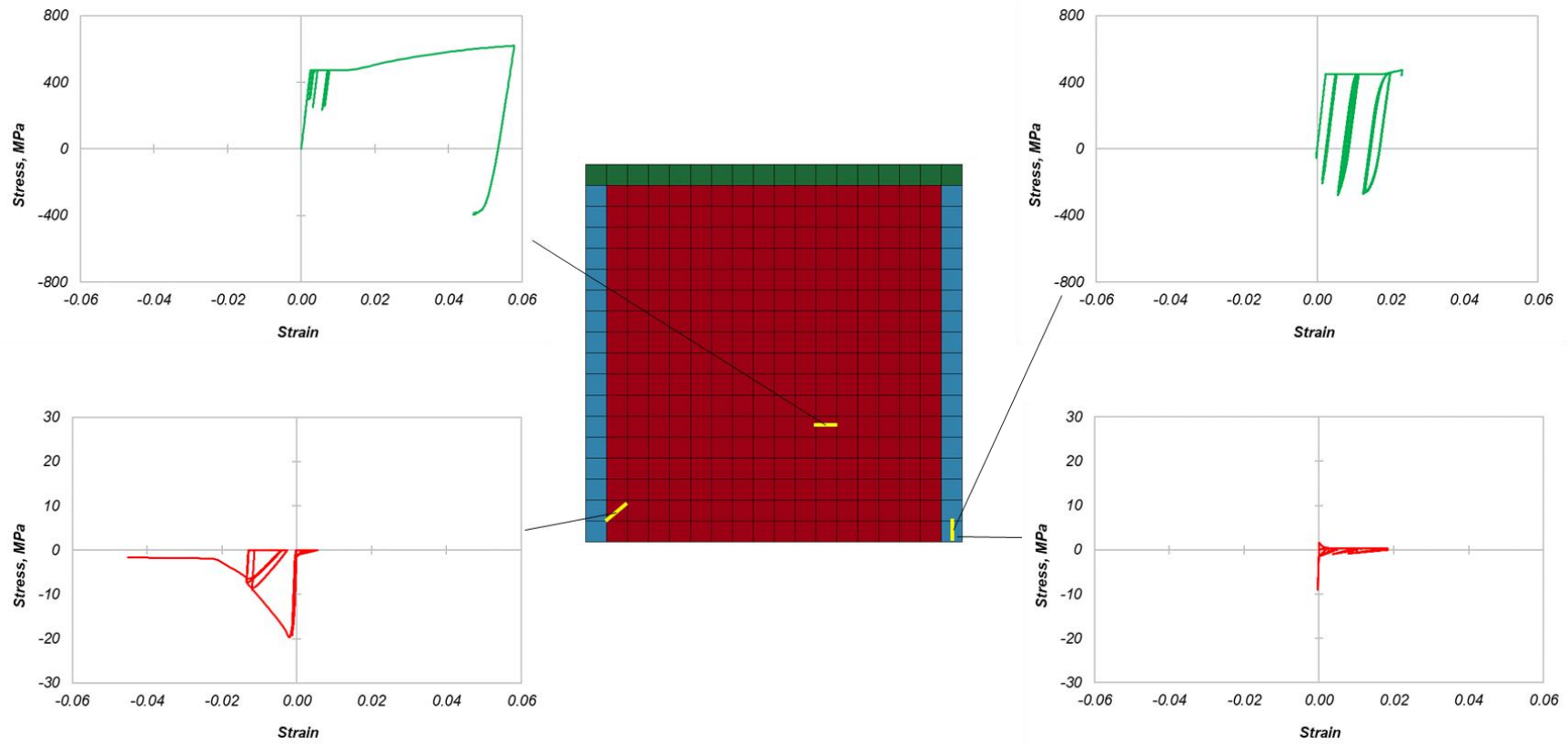


Figure 43. Concrete and steel fibers stress-strain response in the vertical, horizontal, and diagonal directions.

Case Study B: Diagonal Crushing of a C-Shape Wall Under Multiaxial Loading

The experimental test of this C-shape wall is presented in Beyer et al. (2008). The analysis of this wall using a BTM model was presented in Lu et al. (2014, 2016). A video from a relevant simulation is found [here](#). The wall has a longitudinal and transverse steel ratio of 1.0% and 0.45%, respectively; the axial load ratio is equal to 4%. The wall experienced diagonal compression failure in the web (parallel to East-West direction, X-axis of the model) after developing 2.5% drift ratio and $5.7\sqrt{f'_c}$ peak shear stress (psi) in the X-direction.

The BTM-shell model developed herein used distinct vertical **BEAM2** elements to model in detail the layout of the vertical steel (the laysection for the vertical beams of the **SHEL2** elements had dummy properties). Bar fracture as well as strain penetration were not modeled here. The latter resulted in overestimation of the peak tension strains of the flexural reinforcement.

The model computed with very good level of accuracy both the force-displacement responses in both directions as well as the failure mode; see Figure 44. Figure 45 plots the maximum and minimum principal strains at four instants of the response, indicating more than 5% tension strains and 2% compression strains. Figure 46 plots the stress-strain response of selected fibers and diagonals showing more than 8% strain in the vertical steel as well as degradation of a diagonal. The minimum principal strains shown here are significantly larger than peak compression strain of the diagonals because the angle of the direction of principal compression (computed based on the instantaneous strain field of the four-node shell element) is different than the angle, $\theta_d = 56^\circ$, of the diagonal truss elements of the web.

Links to Videos of Simulations:

[OpenSees simulation as presented in Lu et al.](#)

[BTM-Shell Simulation in FE-MultiPhys](#)

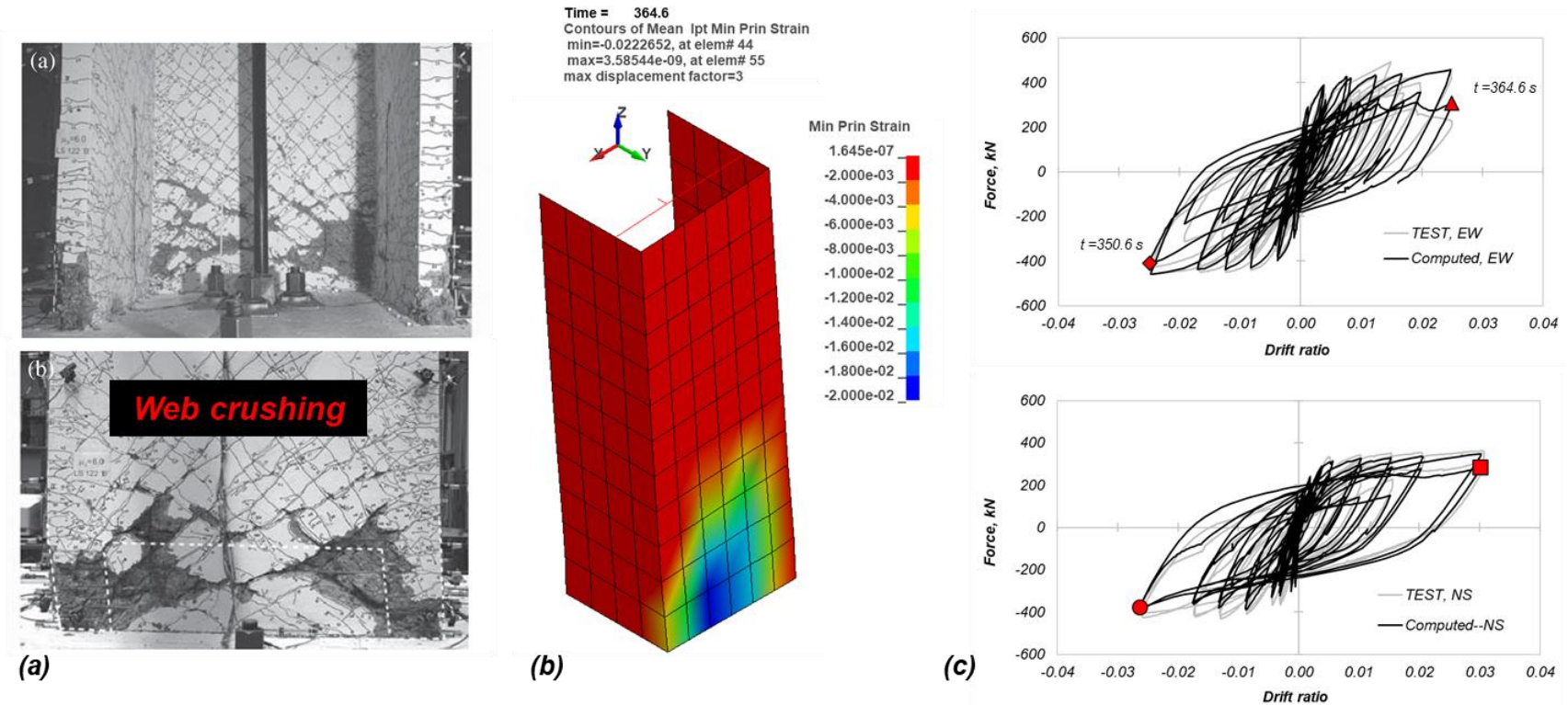


Figure 44. (a) Damage pattern at the of the test; (b) minimum principal strains and deformed shape at $t = 364.6$ sec at 2.5% drift ratio in the EW direction at the instant of diagonal crushing.

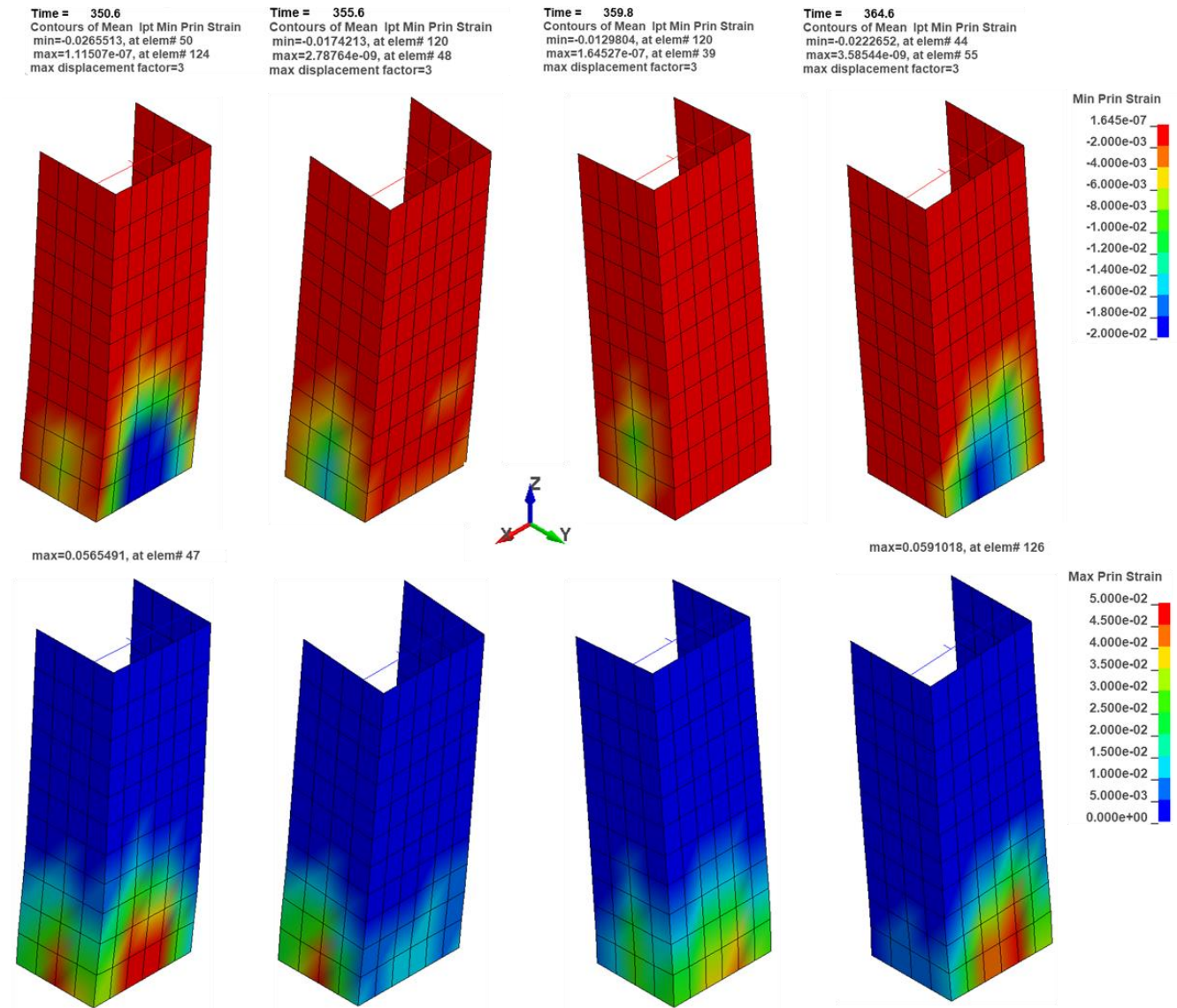


Figure 45. Contours of min(top) and max(bottom) principal strains at the four instants of peak drift ratio in the X- and Y-directions.

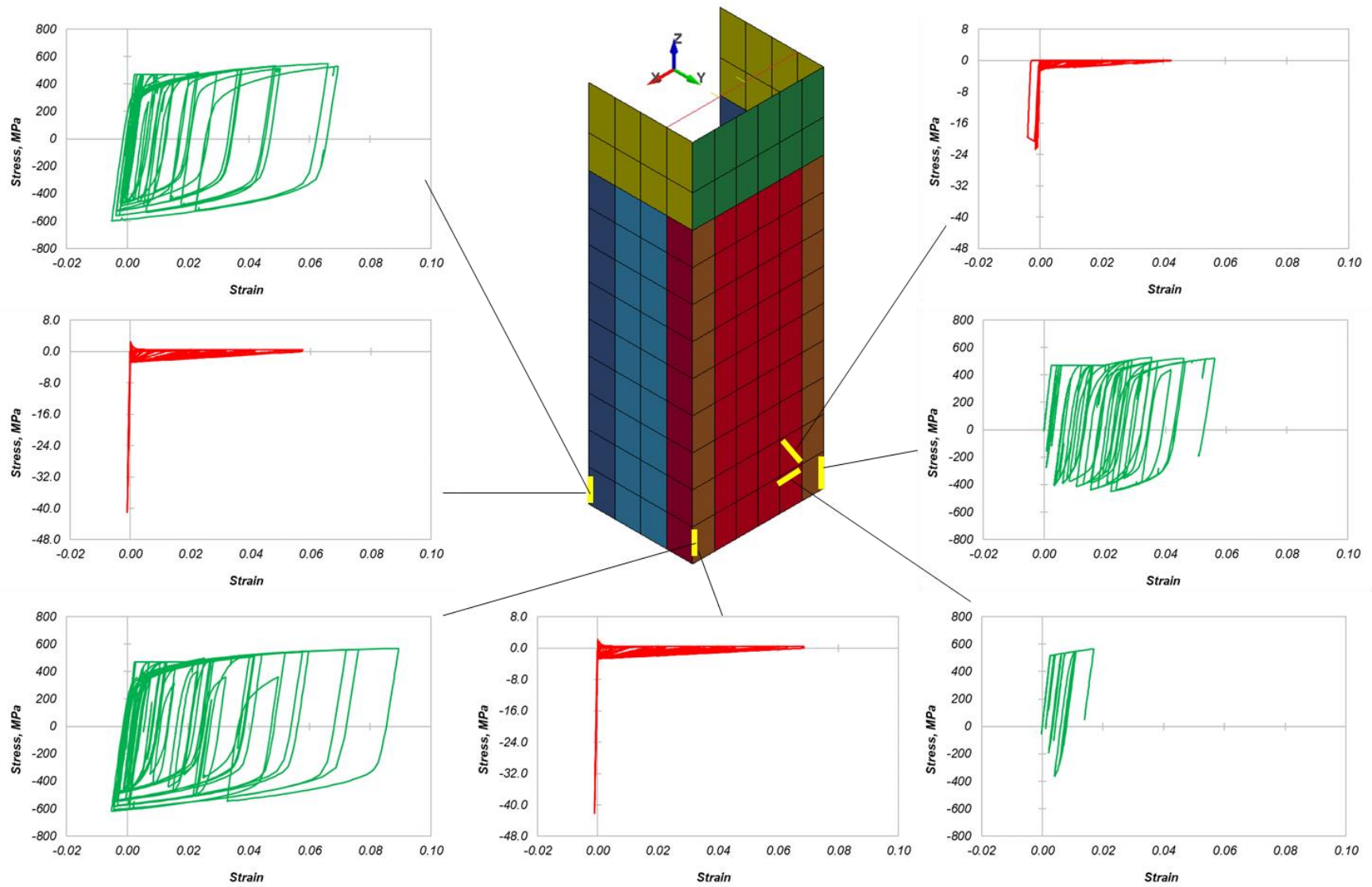


Figure 46. Concrete and steel fibers stress-strain response in the vertical, horizontal, and diagonal direction.

Case Study C: Plastic Hinge Out-of-Plane Buckling of a Planar Wall

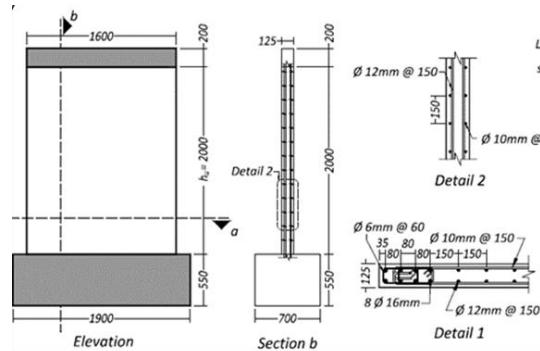
This case study tested a ductile rectangular wall; Figure 47(a) (Dashti 2017) . The test specimen included one-third of the physical effective height of the wall by controlling the moment at the top of the test specimen. The longitudinal and transverse steel ratio of the wall was 2.3% and 0.84%, respectively, while the axial load ratio was equal to 6%. The wall experienced global plastic hinge buckling during the cycle at 3% peak drift ratio. Alvarez et al. (2020) analyzed this wall using the BTM OpenSees; a video link from this simulation is provided below.

The BTM-shell analysis in FE-MultiPhys used the **LARGE DISPLACEMENTS** analysis option (nonlinear geometry, corotational formulation). Five sections (*PARTS*) were used to model the boundary elements and the unconfined part of the web, as well as the effect of strain penetration at the base. Alvarez et al. (2020) demonstrated that strain penetration at the base to be important for the accurate computation of the plastic hinge buckling. Figure 47(e) shows the excellent agreement between the computed and experimentally measured force-displacement response. Figure 47(d) shows the out of plane displacement contour at the instant of peak degradation.

Links to Videos of Simulations:

[OpenSees simulation as presented in Alvarez et al. \(xxx\)](#)

[BTM-Shell Simulation in FE-MultiPhys](#)



(a) Geometry and sections reinforcement

| | | | | | | | |
|---------------|----------|----------|----------|------|------|------|-------|
| Height | Length | 2 m | 1.6 m | | | | |
| Thickness | | 125 mm | | | | | |
| Shear span | | 6 m | | | | | |
| $P / f_c A_g$ | | 0.06 | | | | | |
| ρ_l | ρ_b | ρ_w | ρ_n | 2.3% | 4.2% | 1.1% | 0.84% |
| f_c | f_y | 34.8 MPa | 366 MPa | | | | |

(b) Key dimensions and properties



(c) Damage pattern at the end of the experiment

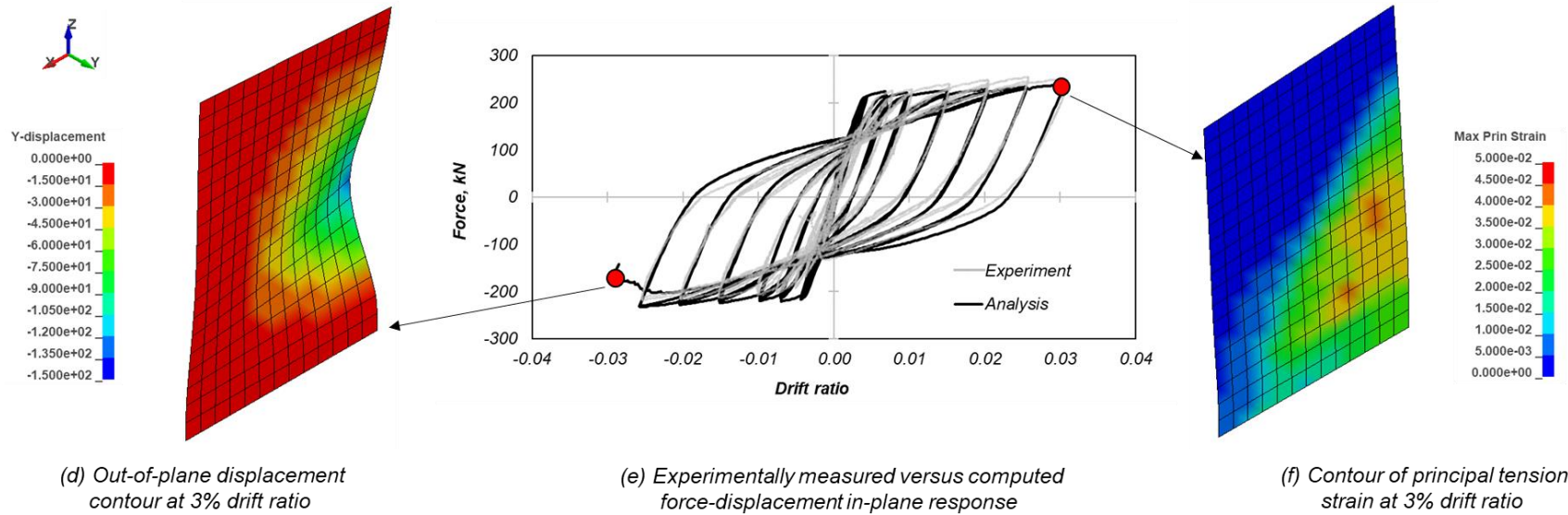


Figure 47. Specimen description and comparison of key experimentally measured and computed responses.

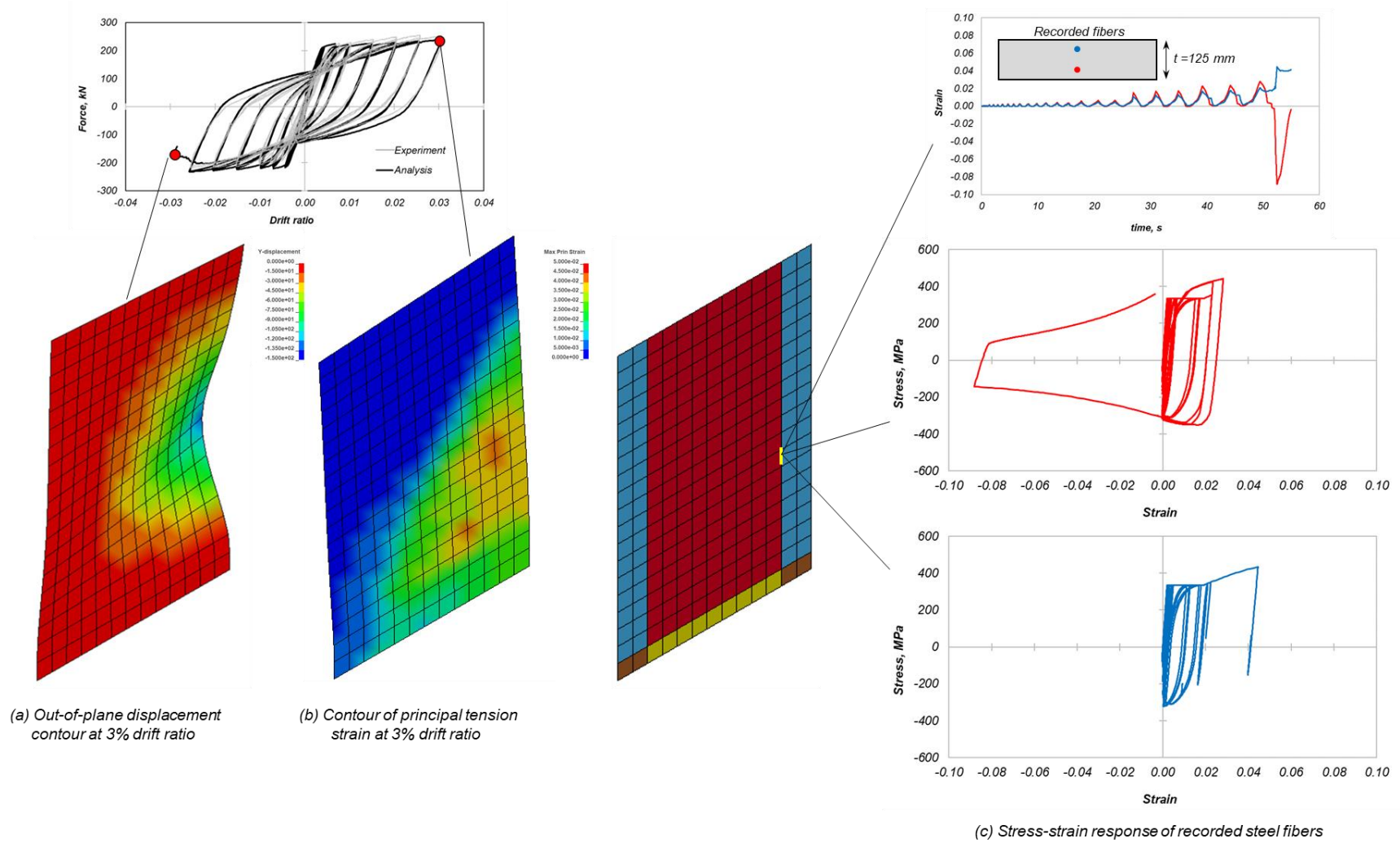


Figure 48. Computed stress-strain response of steel fibers in the region of peak out-of-plane buckling displacements.

Case Study D: Bar Buckling and Shear Failure of a Full-Scale RC Special Moment Frame 4-ft Deep Beam Designed per ACI 318-08

The experimental testing results of this beam is presented in Panagiotou et al. (2013) and in Visnjic et al. (2016). Two large RC special moment frame beams were tested to study the effectiveness of plastic hinge reinforcement detailing prescribed in ACI 318-08 as well as to test design and detailing improvements that were included in ACI 318-11. The test and analysis of Beam A, designed according to ACI 318-08, is presented herein. The 1220-mm-deep \times 762-mm-wide beam had five #11 bars at top and bottom corresponding to a total longitudinal steel ratio of 1.3%; see Figure 49. The shear and anti-buckling reinforcement consisted of three legs of #5 bars at 279-mm spacing corresponding to a transverse steel ratio of 0.28%.

As shown in Figure 50, the BTM-shell model of this beam computed with an excellent level of agreement the force-displacement behavior as well as the evolution of bar buckling and shear failure of the beam. The analysis used the **LARGE DISPLACEMENTS** formulation. The top and bottom #11 bars were modeled with distinct **BEAM2** (fiber section nonlinear beam elements) elements. The significant “fixed-end” strain penetration effects measured in the test were explicitly considered in the model using **BEAM2** elements that included the slip of the skin #4 reinforcement.

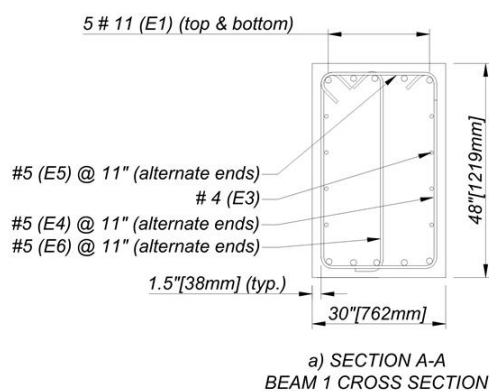


Figure 49. Section of the RC beam tested and global view of the test specimen and setup at 5.5% drift with plastic hinge failure in shear and bar buckling.

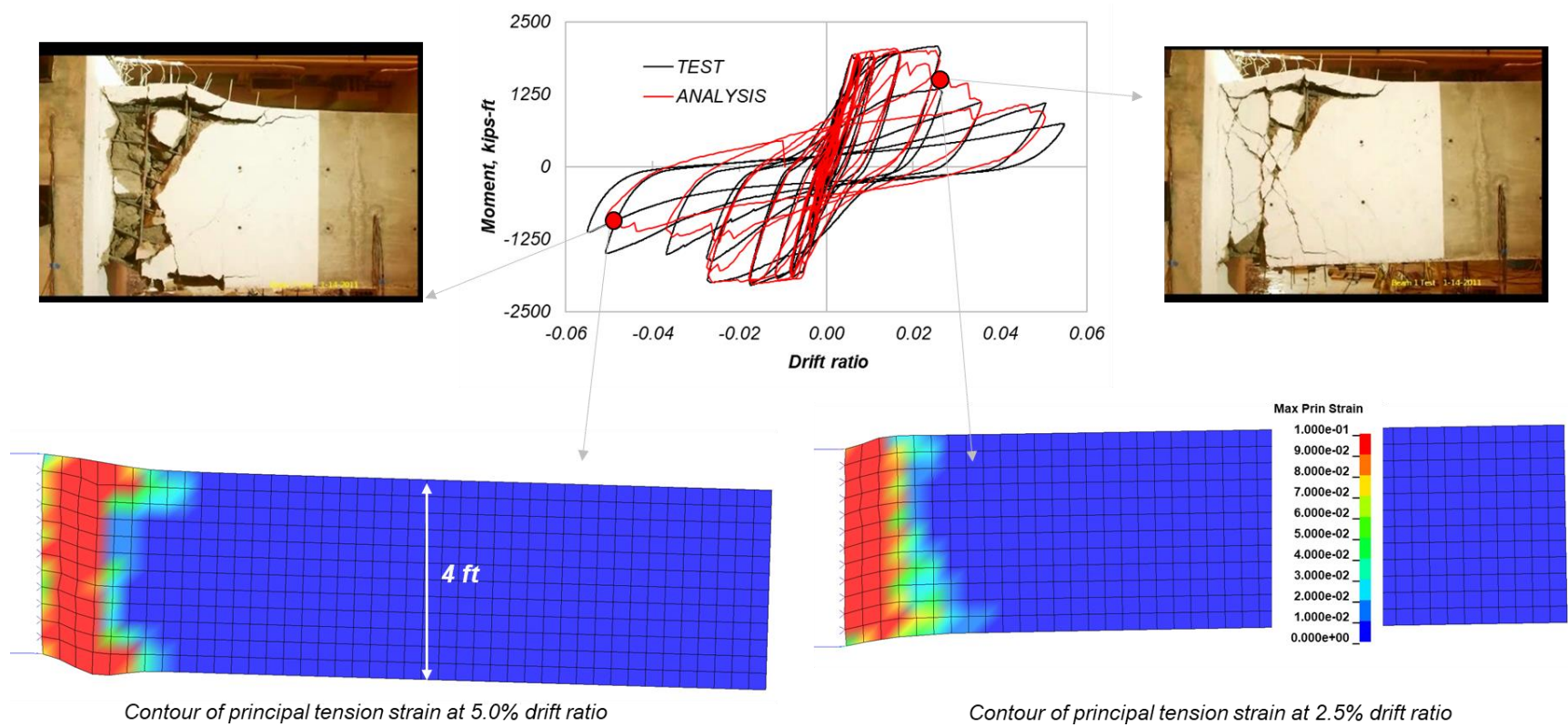


Figure 50. Computed versus experimentally measured force-displacement response of the large full-scale RC SMF beam A as well as comparison of displaced shapes and computed contours.

Case Studies Presented in Deng et al. (2020)

Deng et al. (2020) studied the critical damage and failure modes of vertical reinforcement bar buckling and rupture as well as that of vertical crushing of boundary elements of RC walls. In addition, this study determined the failure modes of diagonal tension and vertical boundary-web interface crushing along the height. Figure 51 compares the computed and test measured force-displacement responses of the six walls of this study; the corresponding comparison of the damage and failure modes is depicted in Figure 52. In all six cases, the BTM-shell models computed with particularly good level of agreement for both the force-displacement response and damage and failure modes. One of the walls studied by Deng was the wall tested by Mestyanek (1986) and presented as Case Study A herein. The test results of the other five walls can be found in Dazio et al. (2009a), Segura and Wallace (2018), Wallace et al. (2015), and Oesterle et al. (1979).

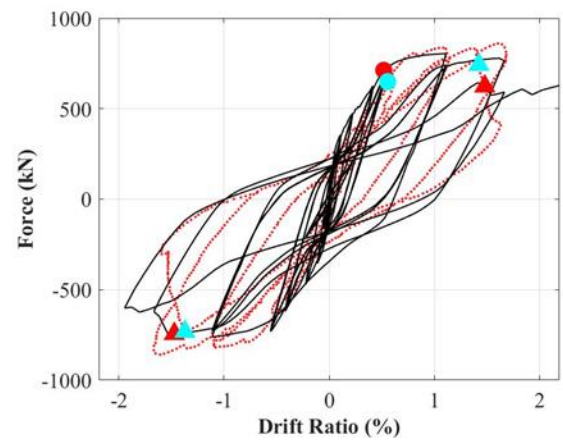
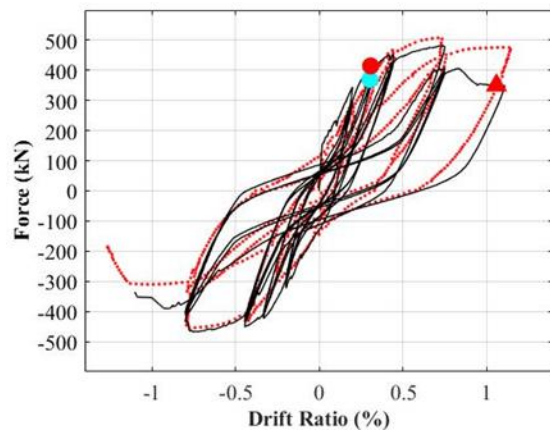
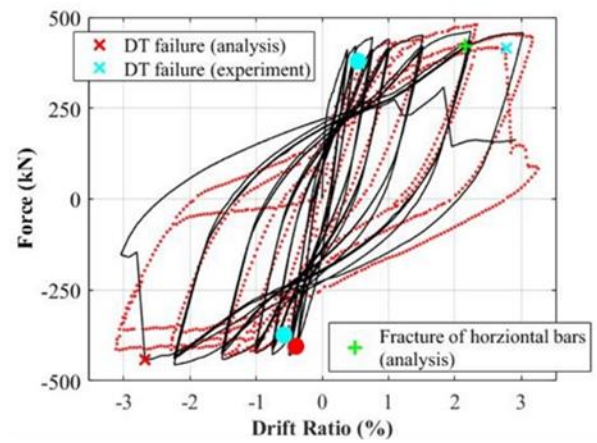
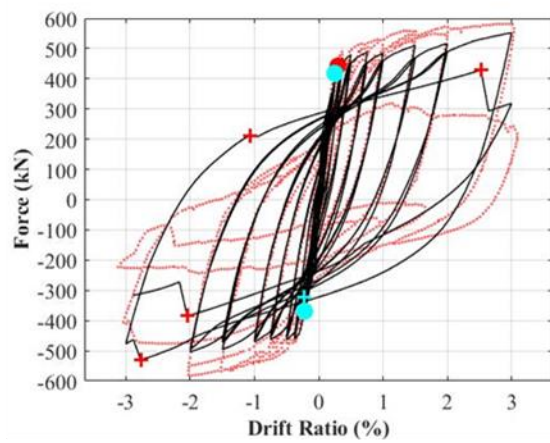
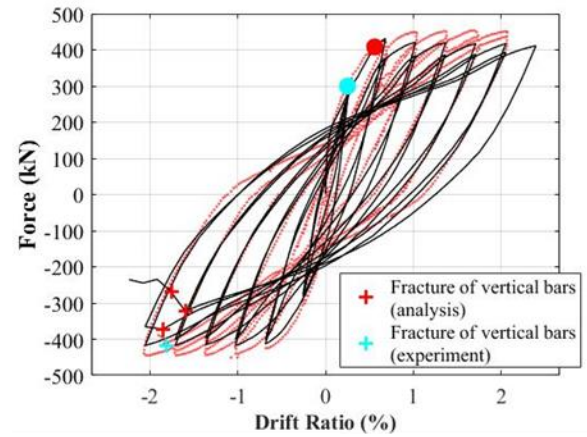
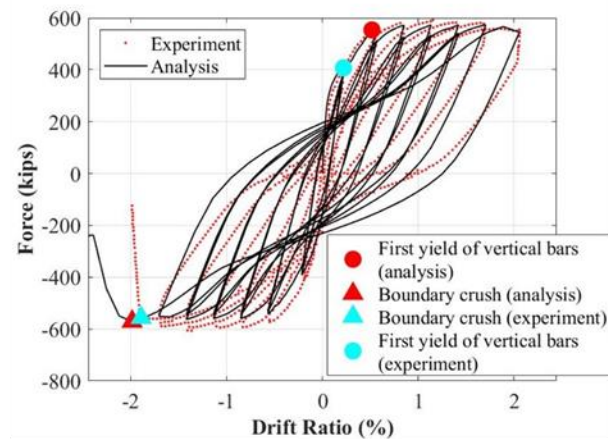


Figure 51. Comparison of computed (BTM-shell) and experimental measured force-displacement responses of six RC walls experiencing different failure modes as presented in Deng et al. (2020).

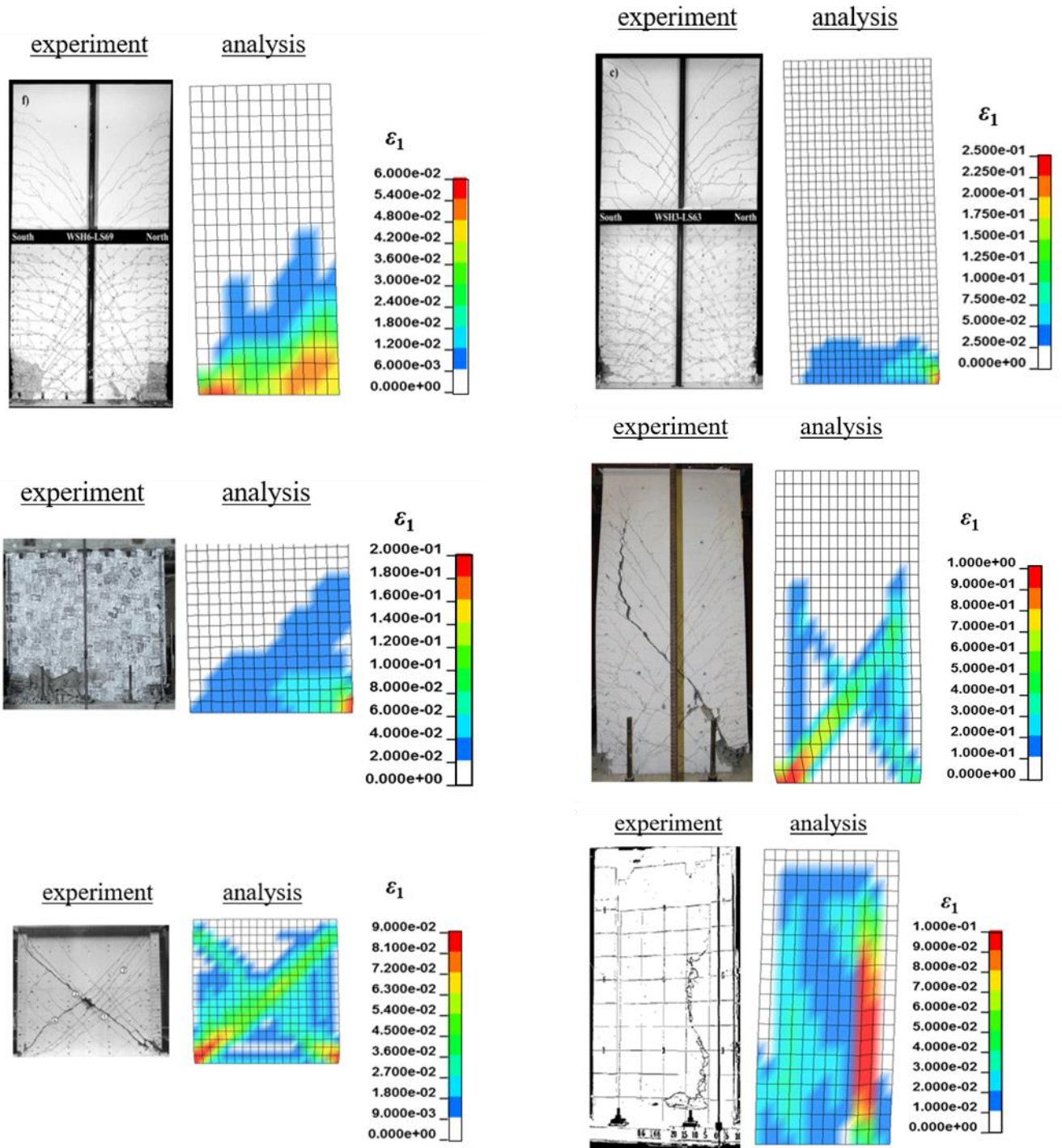


Figure 52. Comparison of computed (BTM-shell) maximum principal strain contours as well as deformed shapes with experimentally observed damage of six RC walls experiencing different failure modes as presented in Deng et al. (2020).

16. Nonlinear Dynamic Analysis of a 20-Story Core Wall Building (Case Study E)

The last case study presented here is the 20-story RC core-wall building shown in Figure 53. The floor plate is 30 m x 30 m and the total height $H = 70$ m (3.5 m story height). The structural system consists of a core-wall with coupling beams along the X -axis, 200-mm-thick post-tensioned slabs, and square columns along the perimeter. The total seismic weight is $W = 146$ MN. Key reinforcement and design characteristics of the building are summarized in Figure 53.

The overall model shown in Figure 53 consists of 8794 nodes and 8480 elements (8000 BTM-shells and 480 fiber-section beams). The material nonlinearity was modeled in all elements, including the floor slabs in which the post-tension was also modeled. P -delta effects were modeled in the vertical elements only (BTM-shells of the core wall and the nonlinear beam elements of the columns).

Figure 54 plots the deformed shapes and periods of modes one to four and mode six computed using the **MODAL** command and cracked concrete material properties. Figure 55 plots key response histories from a nonlinear dynamic analysis using a Los Angeles MCE-level ground motion. The responses presented include the base shear forces, base moment, roof drift ratio, and roof acceleration in the two principal directions. Figure 55 decomposes the base vertical force and base moment resisted in the overall system to the resistance components of the core wall and columns, indicating the significant effect of framing between the core wall the slab and the columns. Finally, Figure 57 plots the base shear force and base moment versus roof drift ratio hysteretic responses in the two directions

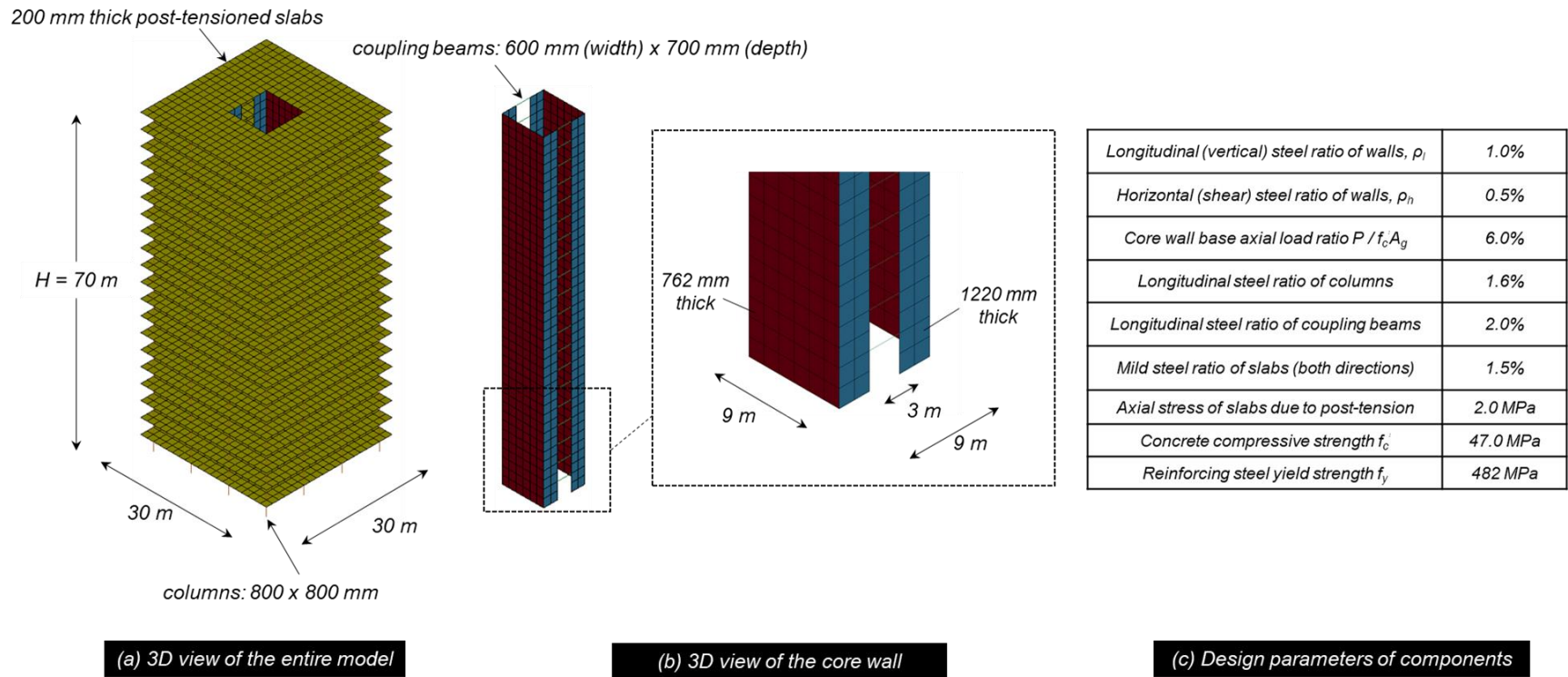


Figure 53. Description of the 20-story building model and key design parameters of structural components.

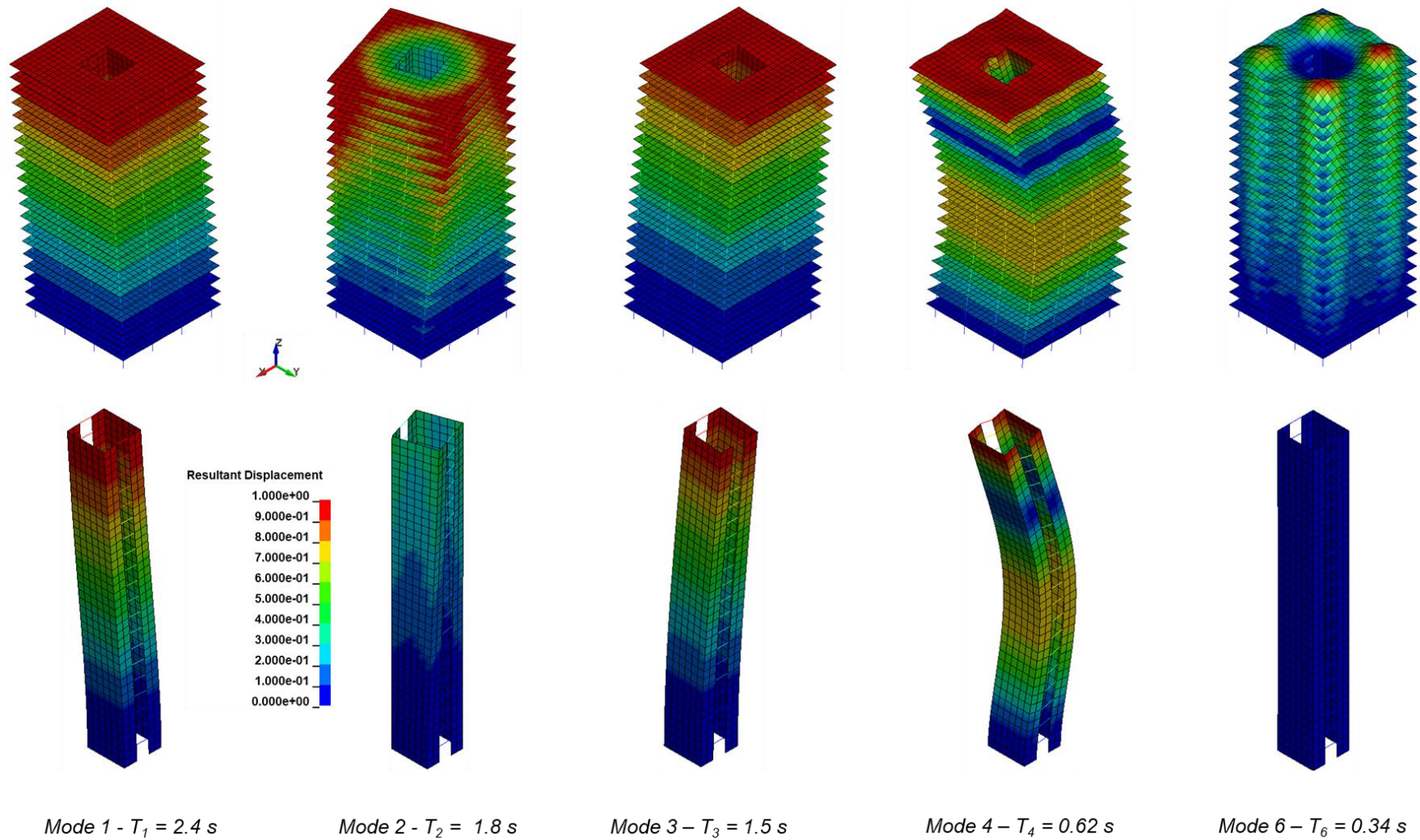


Figure 54. Displacement contours of mode shapes of the entire building (top) and the core-wall (bottom) for modes 1 to 4 and 6. This modal analysis used cracked concrete material properties ($0.35E_c$ for walls and columns, $0.25E_c$ for beams, and $0.15E_c$ for slabs). Displacement (mm) scale factor = 5000.

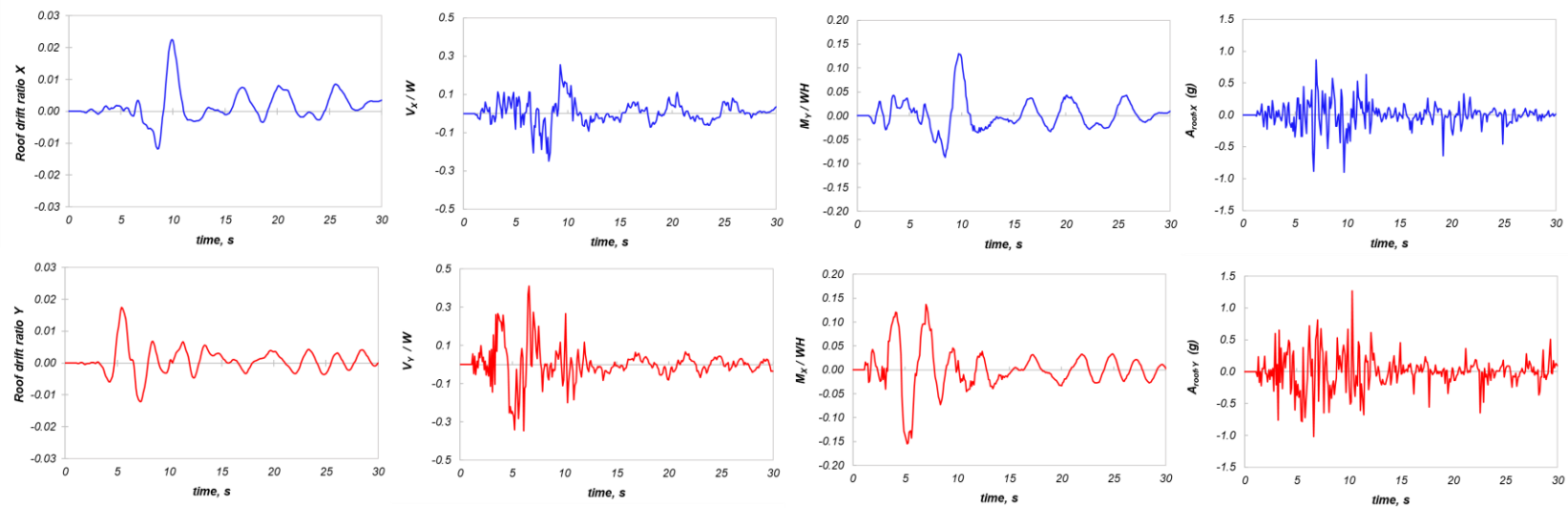


Figure 55. Response histories (X- and Y-directions) of roof drift ratio, base shear force ratio, base moment ratio, and roof acceleration.

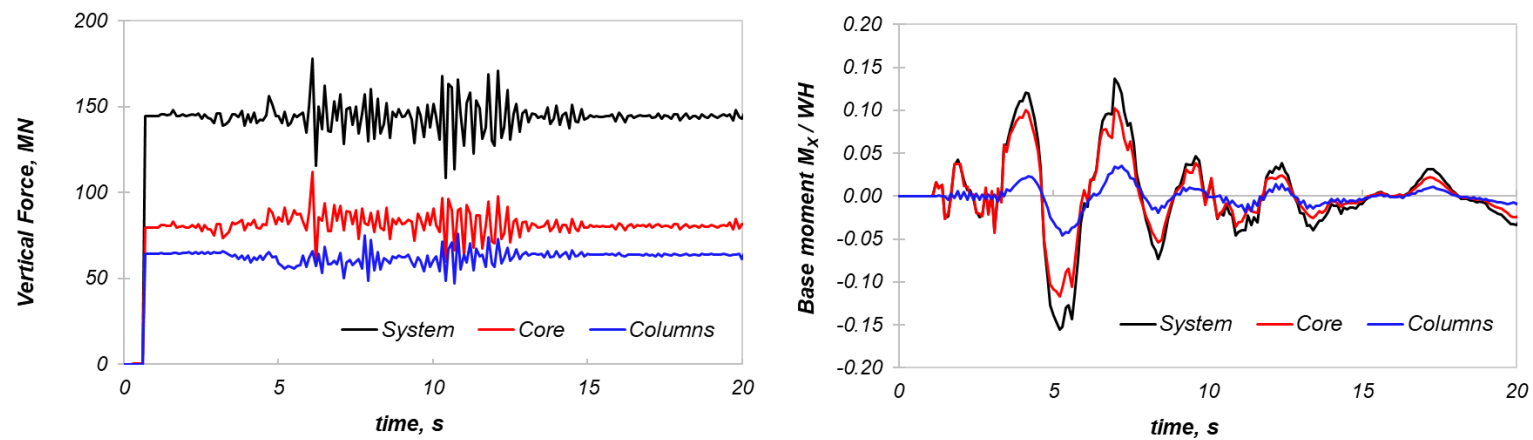


Figure 56. Response histories (X- and Y-directions) of section cuts groups at the base of the building indicating the significant coupling between the core-wall, slabs, and columns.

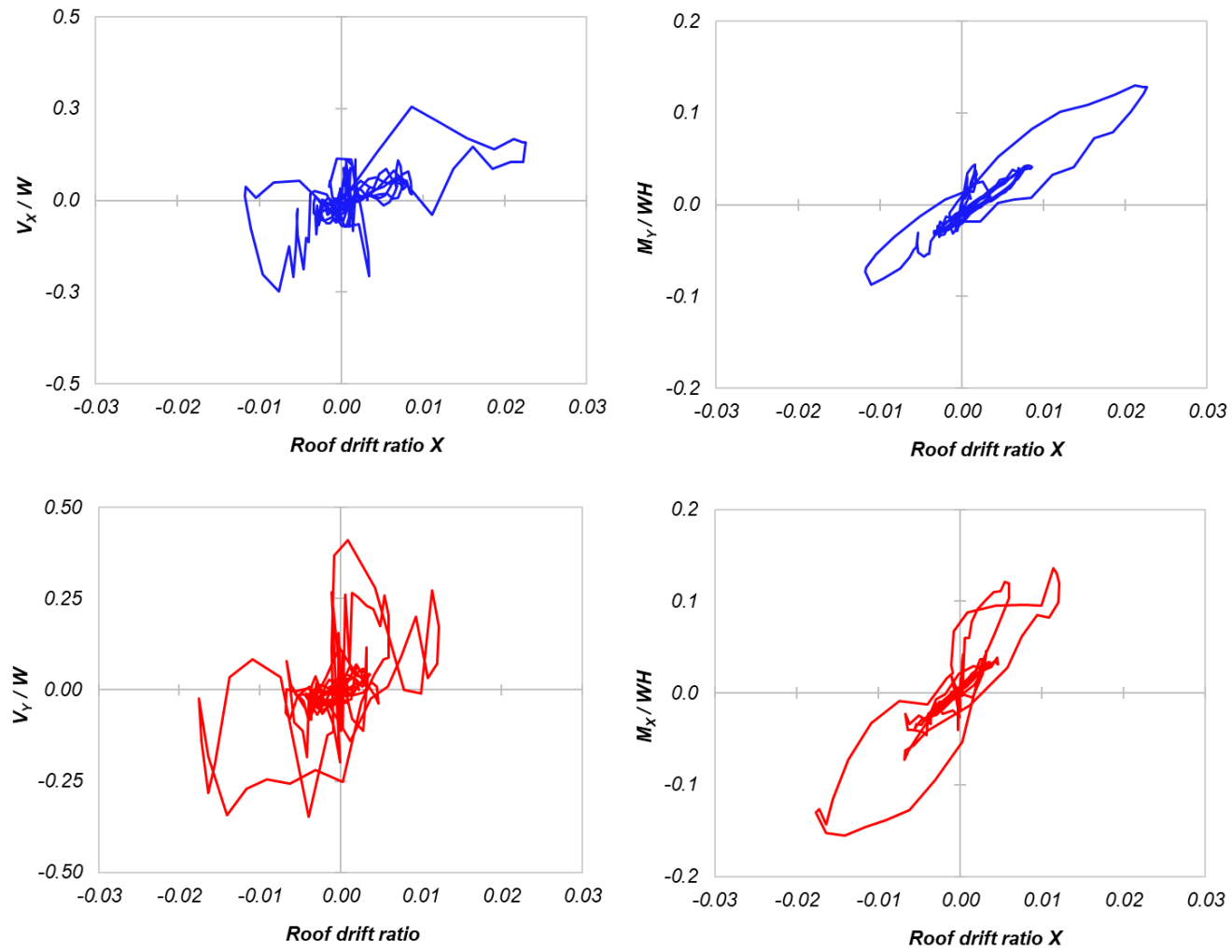


Figure 57. System hysteretic responses (base shear force and base moment) in the X- and Y-directions.

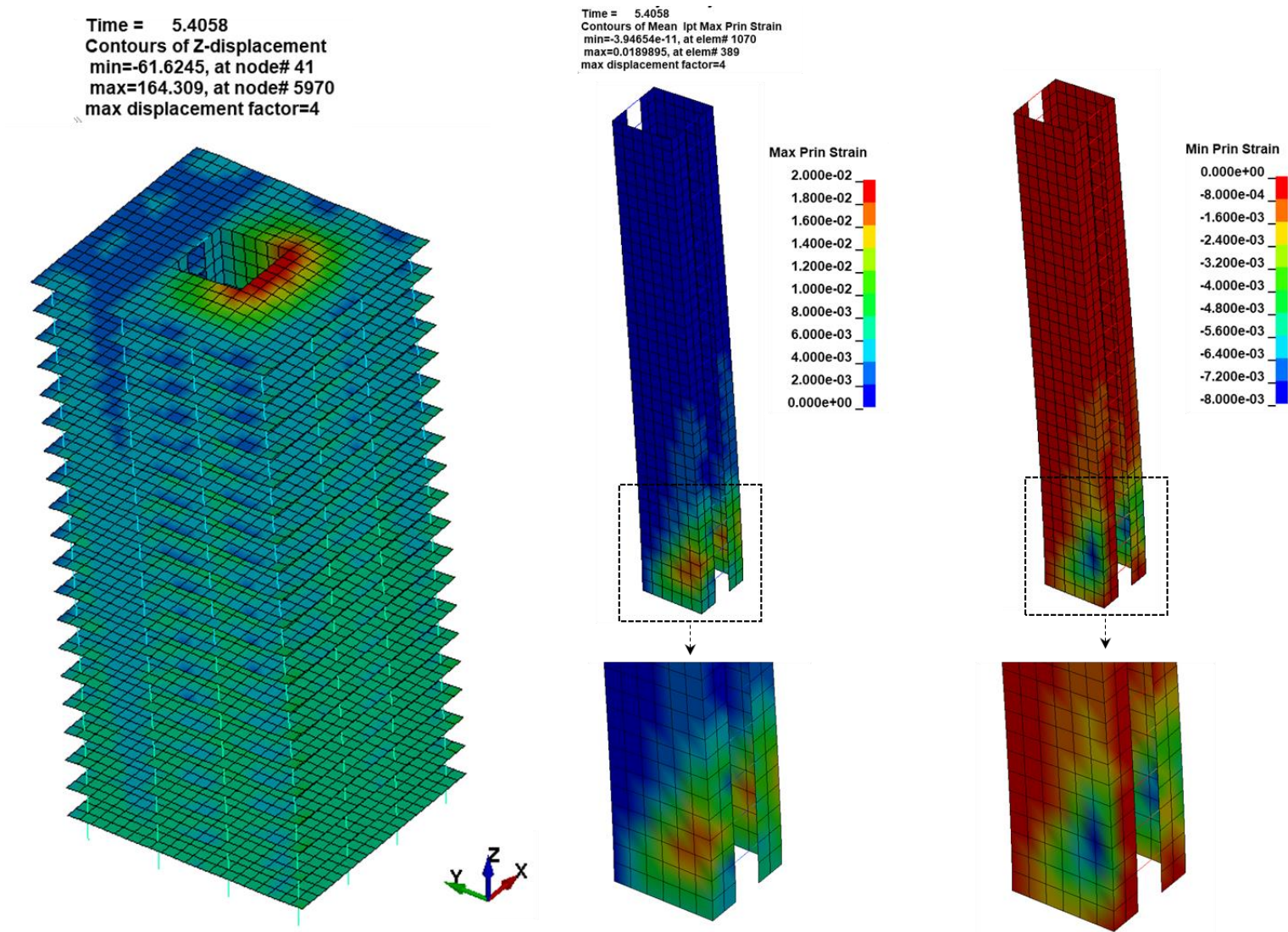


Figure 58. Contours of max and min principal strains of the core wall at $t = 5.4$ sec (1.8% roof drift ratio Y).

17. References

1. ACI-318. (2019). *Building Code Requirements for Structural Concrete* (ACI 318-14) and Commentary (ACI 318R-19). American Concrete Institute, Farmington Hills MI.
2. Alvarez R., Restrepo JI, Panagiotou M (2019). Nonlinear Cyclic Beam Truss Model for Analysis of Reinforced Concrete Coupled Structural Walls, *Bull. Earthq. Eng.*, 17(11), <https://doi.org/10.1007/s10518-019-00639-8>.
3. Alvarez R., Restrepo JI, Panagiotou M, Godinez S (2020a). Analysis of Reinforced Concrete Coupled Structural Walls Via the Beam-Truss Model, *Engineering Structures*. [Link](#)
4. Alvarez R., Restrepo JI, Panagiotou M. (2020b). Plastic Hinge Out-of-Plane Buckling in Structural Walls - Analysis Using the Beam-Truss Model, *ASCE, J. Struct. Eng.*, in press.
5. Ansys / LST. Download LSTC software products. <https://lstc.com/download> (accessed August 2020).
6. Ansys / LST. Download page of LS-PrePost <https://ftp.lstc.com/anonymous/outgoing/lsprepost/>. Accessed August 2020.
7. ASCE (2016). *Minimum Design Loads and Associated Criteria for Buildings and Other Structures* [ASCE/SEI 7-16]. American Society of Civil Engineers, Reston, Virginia.
8. ASCE (2017). *Seismic Evaluation and Retrofit of Existing Buildings* [ASCE/SEI 41-17]. American Society of Civil Engineers, Reston, Virginia.
9. Beyer K, Dazio A, Priestley MJN (2008). Quasi-Static Cyclic Tests of Two U-Shaped Reinforced Concrete Walls. *J. Earth. Eng.* 12(7): 1023–1053, doi: 10.1080/13632460802003272.
10. Dashti F. (2017). *Out-Of-Plane Instability of Rectangular Reinforced Concrete Walls Under In-Plane Loading*. Ph.D. Dissertation. Department of Civil and Natural Resources, University of Canterbury, Christchurch, NZ.
11. Dazio A, Beyer K, Bachmann H (2009a). Quasi-Static Cyclic Tests and Plastic Hinge Analysis of RC Structural Walls. *Eng. Struct.*, 31(7): 1556–1571.
12. Dazio A, Beyer K, Braune F, Fritsche S, Mittaz X (2009b). Das Mw=6.3 Erdbeben von L'Aquila am 6, *Report of SGEB-Erkundungsmission vom*, 150 pgs.
13. Deng X, Murcia-Delso J, Koutromanos I, Panagiotou M (2020). Strain-Based Seismic Performance Evaluation of RC Structural Walls, in review.
14. Dodd LL, Restrepo-Posada JI (1995). Model for Predicting Cyclic Behavior of Reinforcing Steel. *J. Struct. Eng.*, 121(3): 433–445, doi: 10.1061/(ASCE)0733-9445.
15. Elwood KJ, Pampanin S, Kam WY (2012). February 2011 Christchurch Earthquake and Implications for The Design of Concrete Structures, *Proceedings of the International*

Symposium on Engineering Lessons Learned from the 2011 Great East Japan Earthquake, Tokyo, Japan.

16. Kabeyasawa T, Hiraishi H (1998). Tests and Analyses of High-Strength Reinforced Concrete Shear Walls in Japan. American Concrete Institute, *ACI-Special Publication 176-13*, pp. 281–310.
17. Kim SH, Koutromanos I (2016). Constitutive Model for Reinforcing Steel under Cyclic Loading. ASCE, *J. Struct. Eng.*, 142(12), DOI: [10.1061/\(ASCE\)ST.1943-541X.0001593](https://doi.org/10.1061/(ASCE)ST.1943-541X.0001593).
18. Koutromanos I, Bowers J (2016). Enhanced Strain Beam Formulation Resolving Several Issues of Displacement-Based Elements for Nonlinear Analysis. ASCE, *J. Eng. Mech.*, 142(9).
19. Koutromanos I, Farhadi M (2018). *FE-MultiPhys*: A Finite Element Program for Nonlinear Analysis of Continua and Structures. Department of Civil and Environmental Engineering, Virginia Tech, Blacksburg, VA. [Link](#)
20. LATBSDC (2020). *An Alternative Procedure for Seismic Analysis and Design of Tall Buildings Located in the Los Angeles Region*. [Link](#)
21. Lu Y, Panagiotou M (2013a). *Truss2 Element in the finite element program OpenSees* https://opensees.berkeley.edu/wiki/index.php/Truss2_Element
22. Lu and Panagiotou (2013b). *Concretewbeta material model in the finite element program OpenSees*, https://opensees.berkeley.edu/wiki/index.php/ConcretewBeta_Material.
23. Lu Y, Panagiotou M (2015). Earthquake Damage Resistant Tall Buildings at Near Fault Regions Using Base Isolation and Rocking Core Walls. *Proceedings, Structures Congress*, Portland, OR.
24. Lu and Panagiotou (2016). *N4truss Element in the finite element program OpenSees*.
25. Lu Y, Panagiotou M. (2014). Three-Dimensional Nonlinear Cyclic Beam-Truss Model for Reinforced Concrete Non-Planar Walls. ASCE, *J. Struct. Eng.*, 140(3), [http://dx.doi.org/10.1061/\(ASCE\)ST.1943-541X.0000852](http://dx.doi.org/10.1061/(ASCE)ST.1943-541X.0000852).
26. Lu Y, Panagiotou M, Koutromanos I (2014). Three-Dimensional Beam-Truss Model for RC Walls and Slabs Subjected to Cyclic Static or Dynamic Loadin. PEER Report No. 2014/18, Pacific Earthquake Engineering Research Center, University of California, Berkeley, CA.
27. Lu. Y, Panagiotou M, and Koutromanos I. (2016). “Three-dimensional beam-truss model for RC walls and slabs, Part I: Model Description and Validation for Individual Walls. *Earthq.Eng. Struct. Dyn.*, 45(4): 1495–1513, <http://onlinelibrary.wiley.com/doi/10.1002/eqe.2719/full>.
28. Lu Y, Panagiotou M (2016). Three-Dimensional Beam-Truss Model for RC Walls and Slabs, Part II: Model Description and Validation for Coupled Walls and Slabs. *Earthq.Eng. Struct. Dyn.*, 45(11): 1707–1724, <http://onlinelibrary.wiley.com/doi/10.1002/eqe.2720/full>.

29. Maffei J., Yuen N. (2007). Seismic Performance and Design Requirements for High-Rise Buildings. *Struct. Magazine*, pp. 28–32.
30. Mander J, Priestley M, Park R. (1988a). Theoretical Stress-strain Model for Confined Concrete. *Journal of Structural Engineering*; 114 (8): 1804–1826. DOI: 10.1061/(ASCE)0733-9445(1988)114:8(1804).
31. Mander J, Priestley M, Park R. (1988b). Observed Stress-strain Behavior of Confined Concrete. *Journal of Structural Engineering*; 114 (8): 1827–1849.
32. McKenna F, Fenves GL, Scott MH. Open System for Earthquake Engineering Simulation (OpenSees) version 2.4.3 [Software]. Available from <http://opensees.berkeley.edu/>.
33. Mestyanek JM (1986). The Earthquake Resistance of Reinforced Concrete Structural Walls of Limited Ductility, Master of Engineering Thesis, Department of Civil and Natural Resources, University of Canterbury, Christchurch, NZ.
34. Moharrami M, Koutromanos I, Panagiotou ., Girgin SC (2014). Analysis of Shear-Dominated RC Columns Using the Nonlinear Truss Analogy. *Earthq. Eng. Struct. Dyn.*, 44(5): 677–694, <http://dx.doi.org/10.1002/eqe.2480>
35. Moharrami M., Koutromanos I., Panagiotou M. (2015). Nonlinear Truss Modeling Method for the Analysis of Shear Failures in Reinforced Concrete and Masonry Structures. *Proceedings, ATC&SEI 2nd Conference on Improving the Seismic Performance of Existing Buildings and Other Structures*, December, San Francisco. CA.
36. Oesterle RG, Fiorato AE, Johal LS, Carpenter LS, Russell HG, Corley WG. (1976). *Earthquake Resistant Structural Walls – Test of Isolated walls – Phase I1*. Report to the U.S. National Science Foundation, Construction Technology Laboratories, Portland Cement Association, Skokie, IL.
37. Oesterle RG, Aristizabal-Ochoa JD, Fiorato AE, Russell HG, Corley WG (1979). *Earthquake Resistant Structural Walls – Test of Isolated walls – Phase II*. Report to the U.S. National Science Foundation, Construction Technology Laboratories, Portland Cement Association, Skokie, IL.
38. Panagiotou M., Restrepo JI (2011). A Displacement-Based Method of Analysis for Regular Reinforced Concrete Wall Buildings: Application to a Full-Scale 7-Story Building Slice Tested at UC San Diego. *ASCE. J. Struct. Eng.*, 137(6). **2012 Alfred Noble Prize**.
39. Panagiotou M., Restrepo JI, Conte JP (2011). Shake Table Test of a 7-Story Full Scale Reinforced Concrete Wall Building Slice, Phase I: Rectangular Wall. *ASCE, J. Struct. Eng.*, 137(6).
40. Panagiotou M., Restrepo JI, Schoettler M, Geonwoo K (2012). Nonlinear Truss Model for Reinforced Concrete Walls. *ACI Struct. J.*, 109(2): 205–214. <http://dx.doi.org/10.14359/51683631>

41. Panagiotou M., Visnjic T., Antonellis G., Galanis P., Moehle JP (2013). Effect of Hoop Reinforcement Spacing on the Cyclic Response of Large Reinforced Concrete Special Moment Frame Beams. *PEER Report No. 2013/16*, Pacific Earthquake Engineering Research Center, University of California, Berkeley, CA.
42. Panagiotou M (2017). Seismic Response of Medium-rise and Tall RC Core-Wall Buildings at Near-fault Regions and Simplified Calculation of Design Demands. *Proceedings, Annual Conference of Los Angeles Tall Buildings Seismic Design Council*. [Link](#)
43. Paulay T, Priestley MJN (1992). *Seismic Design of Reinforced Concrete and Masonry Buildings*. John Wiley & Sons, Inc., Hoboken, NJ.
44. Paulay T, Santhakumar AR (1976) Ductile behavior of coupled shear walls. *J. Struct. Div.* 102(1):93–108.
45. Priestley MJN, Calvi GM, Kowalsky MJ (2007). *Displacement Based Seismic Design of Structures*. IUSS Press, Pavia, Italy.
46. Santhakumar AR (1974) *The Ductility of Coupled Shear Walls*. Ph.D. Dissertation, Department of Civil and Natural Resources, University of Canterbury, Christchurch, NZ.
47. Segura CL, Wallace JW. (2018). Seismic Performance Limitations and Detailing of Slender Reinforced Concrete Walls. *ACI Structural Journal*; 115(3): 849-860.
48. Tall Buildings Initiative (2017). *Guidelines for Performance-Based Seismic Design of Tall Buildings*. Version 2.03. [Link](#)
49. Tran TA, Wallace JW. (2015). Cyclic Testing of Moderate-Aspect-Ratio Reinforced Concrete Structural Walls. *ACI Structural Journal* 2015; 112(6): 653-666.
50. Visnjic, T., Antonellis G., Panagiotou M., Moehle, J.P. (2016). Experimental Cyclic Response of Large Reinforced Concrete Special Moment Frame Beams. *ACI Struct. J.*, 113(3).
51. Zhang P, Restrepo JI, Conte JP, Ou J. (2017). Nonlinear Finite Element Modeling and Response Analysis of the Collapsed Alto Rio Building in the 2010 Chile Maule Earthquake. *Struct. Des. Tall Spec. Build.*, 207;26. doi:10.1002/tal.1364.

18. Appendix A: Online Tutorials

A series of video tutorials on pre-processing, analysis, and post-processing using the computational framework described herein can be found [here](#). The tutorials include two examples: one for the analysis of RC walls using BTM-shells and another for the analysis of a column using fiber-section three-dimensional nonlinear beams (BEAM2). The table below summarizes the topical coverage and duration of the three tutorials.

Table 4. Contents of the online video tutorials.

| Tutorial # | Overall Content | Tutorial subpart # | Specific Content | Duration, minutes | Total duration, minutes |
|-------------------|--|---------------------------|--|--------------------------|--------------------------------|
| 1 | Pre-processing in LSPP, input for FE-MultiPhys, nonlinear static analysis, and basic post processing of RC wall modeled using BTM-shells | 1.1 | Define/draw shell elements mesh in LSPP | 15 | 144 |
| | | 1.2 | Define section <i>PARTS</i> in LSPP | 15 | |
| | | 1.3 | Boundary conditions, applied forces, and <i>PRESCRIBED MOTION</i> in LSPP | 20 | |
| | | 1.4 | Define MATERIALS, BTM-shell SECTIONS, fiber sections, nonlinear static analysis parameters in <i>FE-MultiPhys</i> | 46 | |
| | | 1.5 | Basic post-processing in LSPP: forces, displacements, strain contours | 48 | |
| 2 | Pre-processing in LSP, input for FE-MultiPhys, nonlinear static and dynamic , and post processing of RC column using fiber-section beam elements (BEAM2) | 2.1 | Define/draw beam elements mesh, boundary conditions, apply loads, <i>PRESCRIBED MOTION</i> in LSPP | 26 | 109 |
| | | 2.2 | Define MATERIALS, BEAM2 SECTIONS, fiber sections, dynamic analysis parameters in <i>FE-MultiPhys</i> | 33 | |
| | | 2.3 | Post-processing in LSPP and comparison of nonlinear static and dynamic analysis: displacements, forces, fiber stresses and strains, section cuts | 50 | |
| 3 | Advanced pre-processing with LSPP | 3.1 | Copy, replicate, transform nodes, elements, and mesh in LSPP | 25 | 25 |